

**UNIVERSIDAD DE CONCEPCION
DIRECCION DE POSTGRADO
CONCEPCION-CHILE**



**MODELAMIENTO NUMERICO DE PROBLEMAS
DE ELECTROMAGNETISMO EN METALURGIA**

*Tesis para optar al grado de Doctor
en Ciencias Aplicadas con mención en Ingeniería Matemática*

Carlos Alberto Reales Martínez

**FACULTAD DE CIENCIAS FISICAS Y MATEMATICAS
DEPARTAMENTO DE INGENIERIA MATEMATICA**

2010

MODELAMIENTO DE PROBLEMAS DE METALURGIA

Carlos Alberto Reales Martínez

Directores de Tesis: Rodolfo Rodríguez, Universidad de Concepción, Chile.

Pilar Salgado, Universidad de Santiago de Compostela, España.

Alfredo Bermúdez, Universidad de Santiago de Compostela, España.

Director de Programa: Raimund Bürger, Universidad de Concepción, Chile.

COMISION EVALUADORA

Salim Meddahi, Universidad de Oviedo, España.

Alberto Valli, Università degli Studi di Trento, Italia.

COMISION EXAMINADORA

Firma: _____

Ricardo Durán

Universidad de Buenos Aires, Argentina.

Firma: _____

Gabriel N. Gatica

Universidad de Concepción, Chile.

Firma: _____

Norbert Heuer

Pontificia Universidad Católica de Chile, Chile.

Firma: _____

Rodolfo Rodríguez

Universidad de Concepción, Chile.

Fecha Examen de Grado: _____

Calificación: _____

Concepción–Marzo de 2010

AGRADECIMIENTOS

En primer lugar quiero expresar mi agradecimiento y admiración a mi director de tesis Rodolfo Rodríguez. Su permanente ayuda, paciencia y motivación hicieron que este trabajo llegara a buen puerto. Cada reunión y cada conversación fueron importantes para mi formación académica y personal.

A mis codirectores Pilar Salgado y Alfredo Bermúdez quienes a pesar de la distancia siempre estuvieron prestos a ayudarme y animarme. Les agradezco también su hospitalidad en mis dos estadías en la Universidad de Santiago de Compostela.

Al profesor Rafael Muñoz Sola de la Universidad de Santiago de Compostela por sus valiosas sugerencias.

A mi esposa Danis, por todo su amor y comprensión a lo largo de estos años. Es mucho el tiempo que te debo a ti y a *nosotros*.

A mi familia, quienes siempre estuvieron *cerca* de mi alentándome en cada momento. No importaron las distancias ni las situaciones, siempre estuvieron *ahí*.

A todos los compañeros y amigos de la cabina 6. En especial a quienes fueron *mi familia en Chile*: Ramiro Acevedo, Verónica Anaya, Bibiana López, David Mora, Ricardo Oyarzúa, René Quintrel (Q.E.P.D), Ricardo Ruiz, Hector Torres y Carlos Vega. Los momentos vividos con ustedes, buenos y malos, estarán siempre en mi recuerdo. Gracias Don Rene por compartir su *felicidad* con nosotros.

A los profesores del doctorado que participaron en mi formación: Gabriel Barrenechea, Fernando Concha, Gabriel Gatica, Rodolfo Araya, Raimund Burger y Romel Bustinza. También quiero agradecer a Mauricio Sepúlveda quien siendo director del programa de doctorado fue de gran ayuda para iniciar mis estudios.

Al proyecto MECESUP UCO0406, a CONICYT, a la dirección de postgrado de la Universidad de Concepción, al Departamento de Matemática Aplicada de la Universidad de Santiago de Compostela y a la Universidad de Córdoba (Colombia), por el financiamiento de todas las actividades relacionadas con mi estudios de doctorado.

Finalmente quiero agradecerle a Dios por toda la gente y situaciones que ha puesto en mi camino.

A Dios por la vida que me dio.

A mis padres por su amor y constante apoyo.

A mi esposa Danis por ser mi soporte...compuesto.

Resumen

El objetivo principal de esta tesis es resolver problemas de corrientes inducidas axisimétricos derivados del modelado de diversos problemas metalúrgicos. En particular, la simulación numérica de un horno de inducción y procesos de conformado electromagnético han motivado los modelos estudiados.

Inicialmente se estudia una formulación en términos de un potencial vectorial para un problema de corrientes inducidas en régimen armónico en un dominio axisimétrico acotado. Se realiza un análisis matemático de dicha formulación en el que se demuestra que la formulación variacional correspondiente conduce a un problema bien planteado cuya solución posee regularidad adicional. Además, se demuestran estimaciones del error para la discretización por elementos finitos estándar.

Posteriormente se abordan dos problemas elíptico-parabólicos. Uno de ellos involucra términos de velocidad que afecta la elipticidad de una de las formas bilineales del problema. El otro involucra un dominio de la parte parabólica que cambia con el tiempo. Para ambos se estudian formulaciones en potenciales magnéticos en dominios axisimétricos acotados. Dichas formulaciones resultan degeneradas, por lo que se deben aplicar teorías diferentes a la clásica para probar existencia y unicidad de la solución. Para la discretización se usan elementos finitos estándar para la variable espacial y un método de Euler implícito para la variable temporal. Se demuestran estimaciones del error para los problemas semi-discreto y completamente discreto.

En cada caso, se muestran ensayos numéricos que prueban la convergencia de los métodos propuestos. Como los problemas abordados en esta tesis provienen de la meta-

lurgia, se muestran aplicaciones de los métodos numéricos a este tipo problemas.

Contents

Resumen	9
1 Introducción	13
1.1 Motivación	13
1.1.1 Hornos de inducción	14
1.1.2 El conformado electromagnético	15
1.2 Preliminares y Notación	17
1.2.1 Coordenadas cilíndricas y espacios de Sobolev	17
1.2.2 Ecuaciones de Maxwell. Modelo de corrientes inducidas	19
1.3 Organización de la tesis	22
1.3.1 Análisis de un método de elementos finitos para un modelo de corrientes inducidas axisimétrico de un horno de inducción	23
1.3.2 Análisis matemático y numérico de un problema de corrientes inducidas evolutivo axisimétrico que involucra términos de velocidad .	24
1.3.3 Análisis numérico de un modelo evolutivo de corrientes inducidas que surge en la simulación numérica de conformado electromagnético	26
2 Numerical analysis of a finite element method for the axisymmetric eddy current model of an induction furnace	29
2.1 Introduction	29
2.2 Statement of the problem	31
2.3 Weighted Sobolev spaces	37
2.4 Variational formulation	39
2.5 Finite element discretization	44
2.6 Numerical experiments	49

2.6.1	Test 1: An example with analytical solution	49
2.6.2	Test 2: Simulation of an industrial furnace	51
3	Mathematical and numerical analysis of a transient eddy current axi-symmetric problem involving velocity terms	57
3.1	Introduction	57
3.2	Statement of the problem	58
3.3	Weak Formulation	62
3.4	Semi-discrete problem	65
3.5	Fully Discrete Problem	73
3.6	Numerical experiments	79
3.6.1	Test with analytical solution	80
3.6.2	Simulation of an induction heating furnace including a moving fluid	83
3.6.3	Simulation of an industrial application: An electromagnetic forming process	86
4	Numerical analysis of a transient eddy current problem arising from electromagnetic forming	89
4.1	Introduction	89
4.2	Statement of the problem	91
4.3	Weak formulation	94
4.4	Semi-discrete problem. Finite element approximation	104
4.5	Fully discrete problem	109
4.6	Numerical tests	114
4.6.1	Test 1: An example with analytical solution	115
4.6.2	Test 2: Numerical solution of an EMF process	117
5	Conclusiones y trabajo futuro	123
5.1	Conclusiones	123
5.2	Trabajo futuro	124
	Bibliography	126

Chapter 1

Introducción

1.1 Motivación

El modelado matemático de fenómenos electromagnéticos es de gran interés para la industria y la comunidad científica en general. En la literatura resalta una gran cantidad de libros y de artículos científicos donde se proponen estos modelos así como métodos numéricos para su resolución; en particular, el método de los elementos finitos es uno de los más empleados para la obtención de soluciones (ver por ejemplo, [17, 31, 37, 41, 45]).

Uno de los fenómenos más estudiados, tanto en el ámbito de la ingeniería como en el de la matemática, es el fenómeno de las corrientes inducidas (“eddy current”). Una corriente inducida (también conocida como corriente de Foucault) aparece cuando un conductor se expone a un campo magnético variable, debido, por ejemplo, al movimiento de la fuente o del conductor o a la variación del campo con el tiempo. El nombre de “eddy current” proviene de las corrientes análogas que se observan en el agua cuando se arrastra un remo: áreas localizadas de turbulencia conocidas como remolinos dan origen a vórtices persistentes. Las corrientes inducidas, como toda corriente eléctrica, generan calor así como fuerzas electromagnéticas. El calor puede ser utilizado en hornos de inducción y las fuerzas electromagnéticas pueden ser usadas para levitación, crear movimiento, deformar o para dar un fuerte efecto de frenado. Por ello, los fenómenos de inducción aparecen asociados a problemas físicos muy diversos y su modelado es de gran importancia en la optimización de procesos industriales complejos.

El modelo matemático que permite estudiar el fenómeno de inducción electromagnética, se conoce en general como “modelo de eddy currents” y se obtiene a partir de las ecuacio-

nes de Maxwell despreciando las corrientes de desplazamiento en la ley de Ampère (ver sección 1.2.2).

En esta tesis, abordaremos el modelo de eddy currents que tiene lugar en un horno de inducción y en procesos de conformado electromagnético. A continuación se dá una breve descripción de estos problemas físicos destacando los aspectos más relevantes que se tendrán en cuenta en la tesis.

1.1.1 Hornos de inducción

Un horno de inducción consiste, básicamente, en uno o varios inductores y una pieza metálica a ser calentada. A los inductores se les suministra corriente alterna, la cual induce corrientes dentro del componente a calentar debido a la Ley de Faraday. Esta técnica es ampliamente usada en la industria metalúrgica en un número importante de aplicaciones tales como la fundición de metales, el precalentamiento para operaciones de soldadura, sistemas de purificación, y en general, procesos que necesiten un rápido calentamiento en zonas de una pieza conductora. En particular, en fundición de metales se utiliza para fundir hierro, acero, cobre, aluminio, metales preciosos y puede usarse para la fundición de cantidades que van desde el kilogramo hasta las 100 toneladas. El rango de frecuencias de operación va desde la frecuencia de red domiciliaria (50 ó 60 Hz) hasta los 10 KHz, en función del metal que se quiere fundir, la capacidad del horno y la velocidad de fundición deseada. De hecho, la frecuencia o intensidad de corriente óptimas son parámetros importantes en el diseño de un horno de inducción; para determinar estos y otros parámetros, la simulación numérica juega un papel importante.

El proceso que tiene lugar en un horno de inducción es muy complejo ya que involucra diferentes fenómenos físicos tales como fenómenos térmicos, mecánicos, electromagnéticos e hidrodinámicos todos ellos acoplados entre sí, (ver por ejemplo [10, 12, 54] para una descripción más detallada de este proceso multifísico). Dada la importancia del proceso en la metalurgia, existe una gran cantidad de artículos donde se proponen métodos numéricos para resolver los distintos modelos matemáticos que surgen en la simulación numérica del proceso. Así, por ejemplo, podemos citar la referencia [35], donde se hace una revisión detallada de los avances recientes en la simulación numérica de fenómenos de calentamiento por inducción y los papers [10, 11, 12, 20, 22, 40, 53] donde se resuelven distintos modelos acoplados en el horno (termoeléctrico, termo-magneto-hidrodinámico); en muchos de estos trabajos, se aborda el problema en geometrías que presentan simetría cilíndrica

[10, 11, 12, 20] y se combinan métodos de elementos finitos (FEM) y combinaciones de éste con el método de elementos de frontera (FEM/BEM).

En particular, el modelo electromagnético propuesto en [10] para resolver el problema termoeléctrico es el punto de partida del Capítulo 2 de esta tesis que se ocupa del análisis matemático y numérico del mismo.

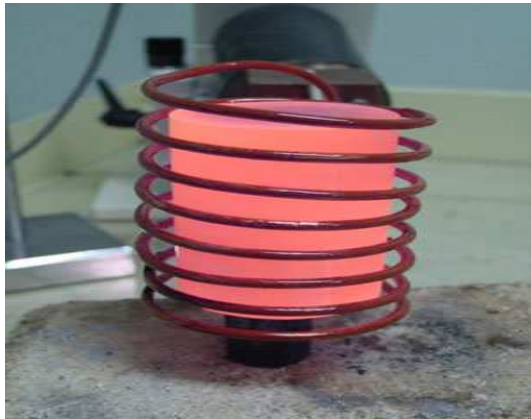


Figure 1.1: Ejemplos de Hornos de Inducción. Fotografías tomadas de www.rdoinduction.com.

1.1.2 El conformado electromagnético

El conformado electromagnético es un proceso de conformado de metales a alta velocidad, que se usa especialmente en la industria del aluminio y del cobre. Las piezas son deformadas usando campos magnéticos de alta intensidad. El campo magnético induce una corriente en la pieza, lo que a su vez genera un campo magnético que da origen a una fuerza de Lorentz repulsiva, que deforma rápidamente la placa de manera permanente.

La técnica es usualmente llamada conformado de alta velocidad porque el proceso ocurre de manera extremadamente rápida (típicamente decenas de microsegundos) y porque, debido a las grandes fuerzas, partes de las piezas alcanzan importantes aceleraciones obteniendo velocidades por encima de los 300 m/s.

En el conformado electromagnético la pieza metálica puede ser deformada sin entrar en contacto con herramienta alguna, por ejemplo cuando se usa para encoger o expandir tubos cilíndricos, pero también puede ser usado para darle forma a hojas metálicas al hacerlas chocar contra moldes a altas velocidades (ver, por ejemplo, [24]).

El conformado electromagnético es una tecnología en desarrollo por lo que necesita de la simulación numérica para diseñar sistemas de conformado eficientes. Es un proceso multifísico, por lo que su resolución numérica requiere el estudio de modelos electromagnéticos, térmicos y mecánicos, todos ellos acoplados entre si. En particular, destaca el acoplamiento magneto-mecánico debido a que la fuerza de Lorentz calculada en el modelo electromagnético es la fuerza volumétrica que deforma la pieza y la deformación de ésta, modifica el dominio del submodelo electromagnético con el tiempo.

En [24] se puede encontrar, además de una descripción del método del conformado electromagnético y sus aplicaciones, el marco matemático que se debe tener en cuenta a la hora de desarrollar métodos numéricos para la simulación numérica del proceso.

Existe una extensa lista de artículos que se ocupan de estudiar distintos modelos que simulan el conformado electromagnético. En general, estos trabajos se ocupan de la resolución numérica del problema magneto-mecánico mediante métodos de elementos finitos [7, 8, 26, 32, 38, 42, 46, 47, 48, 50, 51, 52] y aprovechando en muchos casos la simetría cilíndrica del sistema [7, 26, 32, 47, 48, 50]. El Capítulo 4 de esta tesis pretende ser una primera aproximación del análisis matemático y numérico de modelos electromagnéticos axisimétricos que surgen en conformado electromagnético.

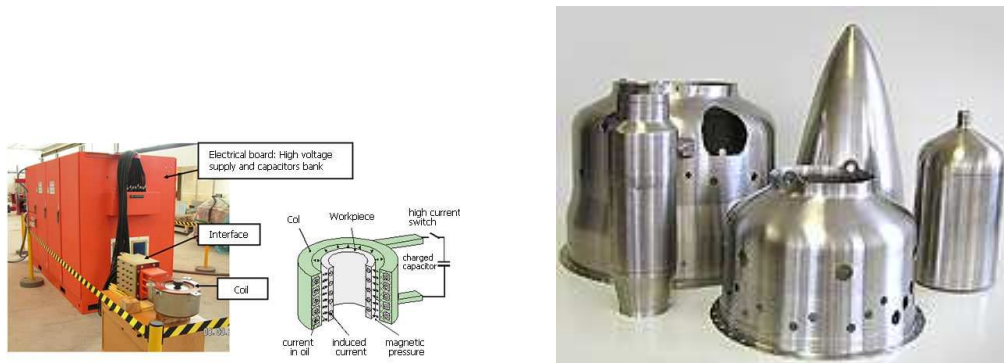


Figure 1.2: Sistema de conformado electromagnético (izquierda) y productos del conformado electromagnético (derecha). Fotos tomadas de www.proform-ip.org/ y www.pmfnd.com respectivamente.

1.2 Preliminares y Notación

1.2.1 Coordenadas cilíndricas y espacios de Sobolev

La mayoría de los problemas físicos se formulan de manera natural como problemas de valores en la frontera en dominios espaciales tridimensionales. Sin embargo, los cálculos en estos dominios son muy costosos en términos computacionales por el elevado número de incógnitas que estos problemas pueden tener. Por ello, en muchas ocasiones se proponen modelos simplificados que permiten reducir el problema a un dominio computacional bidimensional. Esto se puede hacer en algunos casos luego de asumir que la dependencia de los parámetros, los datos y la solución del problema con respecto a una variable puede ser eliminada. En particular, la hipótesis de simetría cilíndrica permite formular muchos problemas de la física en una sección meridional del dominio; así, tal y como se ha avanzado previamente, esta hipótesis es muy utilizada en la simulación numérica de hornos de inducción o procesos de conformado electromagnético. En esta tesis, se estudiarán esencialmente problemas axisimétricos, por ello se introduce a continuación la notación necesaria y los espacios funcionales más relevantes.

Existen varias referencias que tratan el análisis matemático y numérico de problemas axisimétricos. Por ejemplo, la estrategia de reducción de dimensión en el método de elementos finitos fue usado en las ecuaciones de Laplace y Stokes axisimétricas en [36] y [9], respectivamente. Una buena referencia para el estudio de problemas axisimétricos es [16].

En adelante $\tilde{\Omega}$ denotará un dominio general 3D. Asumiremos que en coordenadas cilíndricas (r, θ, z) el dominio $\tilde{\Omega}$ es axisimétrico, es decir, es simétrico con respecto al eje z y los coeficientes y los datos de los problemas son independientes de la variable angular θ . Bajo estas hipótesis, la solución de los problemas resultarán axisimétricas y sus derivadas con respecto a θ serán nulas. Por lo anterior, es suficiente calcular las soluciones en la sección meridional $\Omega = \{(r, z) : (r, 0, z) \in \tilde{\Omega}\}$. En este trabajo, supondremos además que $\partial\Omega$ siempre se interseca con el eje de simetría.

Como nuestros métodos calcularán funciones axisimétricas es importante expresar dichas funciones en términos de las coordenadas (r, θ, z) . Los vectores unitarios en coordenadas cilíndricas se denotan \mathbf{e}_r , \mathbf{e}_θ y \mathbf{e}_z (ver Figura 1.2.1). Así, dada una función vectorial $\mathbf{F} = F_r(r, \theta, z)\mathbf{e}_r + F_\theta(r, \theta, z)\mathbf{e}_\theta + F_z(r, \theta, z)\mathbf{e}_z$ y una función escalar $f = f(r, \theta, z)$, recor-

damos que

$$\begin{aligned}\operatorname{curl} \mathbf{F} &= \left(\frac{1}{r} \frac{\partial F_z}{\partial \theta} - \frac{\partial F_\theta}{\partial z} \right) \mathbf{e}_r + \left(\frac{\partial F_r}{\partial z} - \frac{\partial F_z}{\partial r} \right) \mathbf{e}_\theta + \left(\frac{1}{r} \frac{\partial(rF_\theta)}{\partial r} - \frac{1}{r} \frac{\partial F_r}{\partial \theta} \right) \mathbf{e}_z, \\ \operatorname{div} \mathbf{F} &= \frac{1}{r} \frac{\partial(rF_r)}{\partial r} + \frac{1}{r} \frac{\partial F_\theta}{\partial \theta} + \frac{\partial F_z}{\partial z}, \\ \nabla f &= \frac{\partial f}{\partial r} \mathbf{e}_r + \frac{1}{r} \frac{\partial f}{\partial \theta} \mathbf{e}_\theta + \frac{\partial f}{\partial z} \mathbf{e}_z.\end{aligned}$$

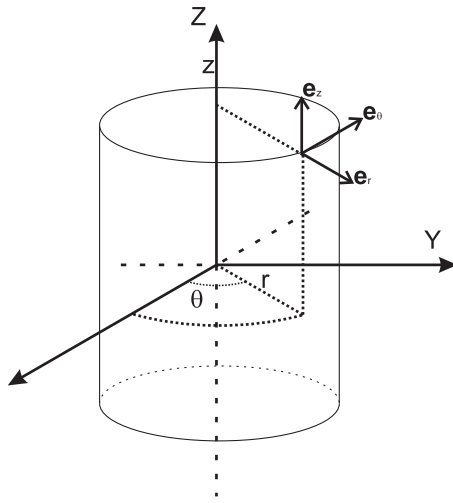


Figure 1.3: Sistema de coordenadas cilíndricas.

A continuación introducimos los espacios de funciones en Ω que contienen las trazas de funciones axisimétricas de espacios de Sobolev definidos en $\tilde{\Omega}$. Sea $L_r^2(\Omega)$ el espacio de Lebesgue ponderado de todas las funciones medibles A definidas en Ω tales que:

$$\|A\|_{L_r^2(\Omega)}^2 := \int_{\Omega} |A|^2 r dr dz < \infty.$$

El correspondiente producto interno está definido por

$$(A, Z)_{L_r^2(\Omega)} := \int_{\Omega} AZr dr dz.$$

El espacio de Sobolev ponderado $H_r^k(\Omega)$ consiste de todas las funciones en $L_r^2(\Omega)$ cuyas derivadas débiles hasta el orden k también están en $L_r^2(\Omega)$. Definimos la norma y la semi-norma en la forma usual; en particular

$$|A|_{H_r^1(\Omega)}^2 := \int_{\Omega} (|\partial_r A|^2 + |\partial_z A|^2) r dr dz.$$

Sea $L_{1/r}^2(\Omega)$ el espacio de Lebesgue ponderado de todas las funciones medibles A definidas en Ω tales que

$$\|A\|_{L_{1/r}^2(\Omega)}^2 := \int_{\Omega} \frac{|A|^2}{r} dr dz < \infty.$$

Definamos el espacio de Hilbert $\tilde{H}_r^1(\Omega)$ por

$$\tilde{H}_r^1(\Omega) := \{ A \in H_r^1(\Omega) : A \in L_{1/r}^2(\Omega) \}$$

con la norma

$$\|A\|_{\tilde{H}_r^1(\Omega)} := \left(\|A\|_{H_r^1(\Omega)}^2 + \|A\|_{L_{1/r}^2(\Omega)}^2 \right)^{1/2}.$$

Para hacernos una idea de la relación de estos espacios y los espacios de Sobolev usuales recordemos la forma del gradiente de una función vectorial \mathbf{F}

$$\nabla \mathbf{F} = \begin{bmatrix} \frac{\partial F_r}{\partial r} & \frac{1}{r} \frac{\partial F_r}{\partial \theta} - \frac{F_\theta}{r} & \frac{\partial F_r}{\partial z} \\ \frac{\partial F_\theta}{\partial r} & \frac{1}{r} \frac{\partial F_\theta}{\partial \theta} + \frac{F_r}{r} & \frac{\partial F_\theta}{\partial z} \\ \frac{\partial F_z}{\partial r} & \frac{1}{r} \frac{\partial F_z}{\partial \theta} & \frac{\partial F_z}{\partial z} \end{bmatrix}.$$

Si consideramos que todas las derivadas con respecto a la variable θ son cero, entonces es fácil ver que: $\mathbf{F}(x, y, z) = (F_x, F_y, F_z) \in H^1(\tilde{\Omega})^3$ si y solo si $\mathbf{F}(r, \theta, z) = (F_r, F_\theta, F_z) \in \tilde{H}_r^1(\Omega) \times \tilde{H}_r^1(\Omega) \times H_r^1(\Omega)$. Un resultado mas general que éste es el Teorema II.2.6 de [16].

1.2.2 Ecuaciones de Maxwell. Modelo de corrientes inducidas

Las ecuaciones de Maxwell son un conjunto de cuatro ecuaciones que describen los fenómenos electromagnéticos. La gran contribución de James Clerk Maxwell fue reunir en estas ecuaciones largos años de resultados experimentales, debidos a Coulomb, Gauss, Ampère, Faraday y otros, introduciendo los conceptos de campo y corriente de desplazamiento. El conjunto de ecuaciones de Maxwell esta conformado por las siguientes:

$$\frac{\partial \mathbf{D}}{\partial t} + \text{curl } \mathbf{H} = \mathbf{J}, \quad (1.1)$$

$$\frac{\partial \mathbf{B}}{\partial t} + \text{curl } \mathbf{E} = \mathbf{0}, \quad (1.2)$$

$$\text{div } \mathbf{B} = 0, \quad (1.3)$$

$$\text{div } \mathbf{D} = \rho. \quad (1.4)$$

Este sistema debe ser completado con leyes constitutivas,

$$\mathbf{B} = \mu \mathbf{H}, \quad (1.5)$$

$$\mathbf{D} = \epsilon \mathbf{E}, \quad (1.6)$$

$$\mathbf{J} = \sigma \mathbf{E}, \quad (1.7)$$

donde:

- \mathbf{H} es el campo magnético,
- \mathbf{B} es la inducción magnética,
- \mathbf{J} es la densidad de corriente,
- \mathbf{D} es el campo de desplazamiento eléctrico,
- \mathbf{E} es el campo eléctrico,
- ρ es la densidad de carga libre,
- ϵ es la permitividad eléctrica,
- μ es la permeabilidad magnética,
- σ es la conductividad eléctrica.

La ecuación (1.1) es conocida como Ecuación de Maxwell-Ampère y en su formulación integral en combinación con (1.5) muestra que la circulación de un campo magnético a lo largo de una línea cerrada es igual al producto de la permitividad magnética, μ , por la intensidad neta que atraviesa el área limitada por la trayectoria. El aspecto más importante del trabajo de Maxwell en el electromagnetismo es el término que introdujo en la ley de Ampère; la derivada temporal de un campo eléctrico, conocido como corriente de desplazamiento. La ley de inducción de Faraday, ecuación (1.2), establece que la corriente inducida en un circuito es directamente proporcional a la rapidez con que cambia el flujo magnético que lo atraviesa. La inducción electromagnética fue descubierta casi simultáneamente y de forma independiente por Michael Faraday y Joseph Henry en 1830. La inducción electromagnética es el principio sobre el que se basa el funcionamiento del generador eléctrico, el transformador y muchos otros dispositivos.

La ley de Gauss, ecuación (1.4), en combinación con (1.5) dice que el flujo del campo eléctrico a través de una superficie cerrada es igual al cociente entre la suma de las cargas (q) encerradas por la superficie y la permitividad eléctrica (ϵ). Por otro lado, la ley de Gauss magnética, ecuación (1.3), muestra una diferencia notable entre los campos magnéticos y los campos eléctricos: los campos magnéticos no comienzan y terminan en cargas diferentes. En otras palabras, las líneas de los campos magnéticos deben ser cerradas.

Los parámetros, ϵ , μ y σ dependen de las características del material. En el caso de materiales isótropos, es decir, en los que las propiedades de los materiales no dependen de la dirección del campo, ϵ , μ y σ son funciones escalares. Si además el material es lineal, estos parámetros solo dependen de la variable espacial. Además, ϵ y μ son estrictamente positivos, mientras que σ es estrictamente positiva en los conductores y nula en el dieléctrico.

La Ley de Ohm (1.7) establece que, en un conductor en reposo, la densidad de corriente generada por un campo eléctrico es proporcional al mismo. Cuando el conductor está en movimiento a esta ley se le agrega otro término, quedando de la siguiente forma:

$$\mathbf{J} = \sigma \mathbf{E} + \sigma \mathbf{v} \times \mathbf{B}. \quad (1.8)$$

donde \mathbf{v} es la velocidad del conductor.

Muchos problemas de electromagnetismo no requieren de la resolución completa de las ecuaciones de Maxwell debido a que, en algunos casos, ciertos términos son muy pequeños con respecto a otros. Este es el caso del modelo de las corrientes inducidas, que resulta de despreciar el término del desplazamiento eléctrico en la ley de Ampère [3, 45], obteniéndose el siguiente sistema de ecuaciones:

$$\operatorname{curl} \mathbf{H} = \mathbf{J}, \quad (1.9)$$

$$\frac{\partial \mathbf{B}}{\partial t} + \operatorname{curl} \mathbf{E} = \mathbf{0}, \quad (1.10)$$

$$\operatorname{div} \mathbf{B} = 0. \quad (1.11)$$

Este sistema, denominado frecuentemente “eddy currents model” es adecuado en hornos de inducción y en conformado electromagnético.

Nótese que se trata de un sistema evolutivo; en el caso particular de que las leyes constitutivas muestren un comportamiento lineal (1.5)-(1.7)), si las fuentes son sinusoidales

(como en corriente alterna), todos los campos se pueden considerar de la forma

$$\mathbf{F}(t, x) = \operatorname{Re} \left[e^{i\omega t} \widehat{\mathbf{F}}(\mathbf{x}) \right],$$

donde ω es la frecuencia angular, $\omega = 2\pi f$, siendo f la frecuencia de la corriente y $\widehat{\mathbf{F}}$ es la amplitud compleja asociada a \mathbf{F} que solo depende de \mathbf{x} .

En estos casos, el modelo de corrientes inducidas se escribe de la siguiente manera

$$\operatorname{curl} \widehat{\mathbf{H}} = \widehat{\mathbf{J}}, \quad (1.12)$$

$$i\omega \widehat{\mathbf{B}} + \operatorname{curl} \widehat{\mathbf{E}} = \mathbf{0}, \quad (1.13)$$

$$\operatorname{div} \widehat{\mathbf{B}} = 0, \quad (1.14)$$

$$\widehat{\mathbf{B}} = \mu \widehat{\mathbf{H}}, \quad (1.15)$$

$$\widehat{\mathbf{J}} = \sigma \widehat{\mathbf{E}}. \quad (1.16)$$

A pesar que las ecuaciones anteriormente descritas están definidas en todo \mathbb{R}^3 , existe una gran cantidad de trabajos que abordan problemas en régimen armónico y transitorio en dominios acotados tridimensionales (ver, por ejemplo, la revisión bibliográfica realizada en [1, 2, 15]). En esta tesis nos centraremos en el modelo de eddy currents en régimen armónico y transitorio en dominios axisimétricos acotados.

1.3 Organización de la tesis

Como se adelantó en las secciones anteriores, el estudio y resolución numérica de modelos electromagnéticos axisimétricos está muy desarrollado. Debido a que no pasa lo mismo con el análisis matemático y numérico de este tipo de problemas, en esta tesis se aborda el análisis de problemas axisimétricos en régimen armónico o transitorio considerando distintos aspectos del modelado. Los principales resultados se recogen en los Capítulos 2, 3 y 4, cuyos objetivos se describen brevemente a continuación. La tesis finaliza con las conclusiones y con una breve descripción del camino a seguir en el análisis matemático y numérico para el modelamiento del conformado electromagnético.

1.3.1 Análisis de un método de elementos finitos para un modelo de corrientes inducidas axisimétrico de un horno de inducción

El problema abordado en el Capítulo 2 es el modelo axisimétrico de corrientes inducidas introducido en [10] para simular el comportamiento de un horno de inducción.

El propósito de este trabajo es analizar un método de elementos finitos para resolver dicho problema. Aunque el modelo se escribe con detalle en el capítulo correspondiente, aquí se resaltan las características más relevantes.

Tomando ventaja de la simetría cilíndrica, el problema tridimensional se reduce a uno definido en la sección meridional donde la densidad de corriente, escrita en coordenadas cilíndricas, tiene solo componente azimutal, esto es,

$$\hat{\mathbf{J}}(r, z) = J(r, 0, z)\mathbf{e}_\theta.$$

A partir de (1.14), se introduce un potencial magnético vectorial \mathbf{A} tal que

$$\hat{\mathbf{B}} = \operatorname{curl} \mathbf{A} \quad (1.17)$$

de la forma

$$\mathbf{A} = A(r, z)\mathbf{e}_\theta.$$

De (1.13), (1.16) y (1.17) se obtiene

$$\operatorname{curl} ((i\omega A + \sigma^{-1} J_\theta) \mathbf{e}_\theta) = \mathbf{0} \quad (\text{en el material conductor}).$$

De la ecuación anterior puede deducirse que existen constantes $V_k \in \mathbb{C}$, $k = 0, \dots, m$, tales que

$$i\omega A + \sigma^{-1} J_\theta = \frac{V_k}{r} \quad \text{en } \Omega_k,$$

donde los Ω_k representan las componentes conexas del material conductor. Así, se obtienen las ecuaciones

$$-\left(\frac{\partial}{\partial r}\left(\frac{1}{\mu r}\frac{\partial(rA)}{\partial r}\right) + \frac{\partial}{\partial z}\left(\frac{1}{\mu}\frac{\partial A}{\partial z}\right)\right) + i\omega\sigma A = \frac{\sigma}{r}V_k \quad \text{en } \Omega_k,$$

$$-\left(\frac{\partial}{\partial r}\left(\frac{1}{\mu r}\frac{\partial(rA)}{\partial r}\right) + \frac{\partial}{\partial z}\left(\frac{1}{\mu}\frac{\partial A}{\partial z}\right)\right) = 0 \quad \text{en el aire.}$$

En general, los datos conocidos en la práctica son las intensidades de corriente, I_k , que atraviesan cada sección de la bobina, por ello, a estas ecuaciones hay que añadir las condiciones:

$$\int_{\Omega_k} J_\theta dr dz = I_k, \quad k = 1, \dots, m.$$

Para resolver este problema, damos una formulación mixta en espacios de Sobolev ponderados, cuya solución es el potencial vectorial magnético, A , y multiplicadores de Lagrange que son constantes en cada componente conexa de la sección meridional del inductor, V_k . La existencia y unicidad de la solución se demuestra a través del análisis de una formulación débil equivalente. Además, se demuestra regularidad adicional de la solución bajo hipótesis convenientes de los coeficientes físicos. El problema se discretiza usando elementos finitos estándar y se demuestran estimaciones del error *a priori*. Finalmente, se presentan algunos experimentos numéricos que permiten evaluar la convergencia del método. Este trabajo está contenido en el artículo:

- A. BERMÚDEZ, C. REALES, R. RODRÍGUEZ AND P. SALGADO, *Numerical analysis of a finite element method to solve the axisymmetric eddy current model of an induction furnace*. IMA Journal of Numerical Analysis (doi:10.1093/imanum/drn063).

1.3.2 Análisis matemático y numérico de un problema de corrientes inducidas evolutivo axisimétrico que involucra términos de velocidad

En problemas de magneto-hidrodinámica y en problemas de conformado electromagnético, el modelo de eddy currents involucra términos de velocidad, a través de la ley de Ohm (1.8) o bien a través del movimiento de una parte del dominio conductor.

En general, los términos convectivos en la ley de Ohm son despreciados en el modelado de conformado (ver, por ejemplo, [46]); sin embargo, la inclusión de este término puede ser importante en problemas de magneto-hidrodinámica. En esta tesis, en los Capítulos 3 y 4 se separarán las dificultades de estos términos convectivos. Además, a diferencia del Capítulo 2, la densidad de corriente se supondrá uniformemente distribuida en la bobina y se considerarán fuentes transitorias generales, por lo que los problemas serán evolutivos.

Así, en un primer paso, en el Capítulo 3 se estudia el problema electromagnético bajo la hipótesis de que las partículas de conductor poseen velocidad, pero están con-

finadas en un recinto en reposo. Este modelo se presenta, por ejemplo, en la magneto-hidrodinámica donde el término $\mathbf{v} \times \mathbf{B}$ puede ser importante (ver por ejemplo, confinamiento de plasma, enfriamiento por metales líquidos de los reactores nucleares y el moldeado electromagnético). Igual que en el Capítulo 2, se toma ventaja de la simetría cilíndrica y el problema se reduce a uno bidimensional en la sección meridional, donde la densidad de corriente, que ahora depende del tiempo, escrita en coordenadas cilíndricas tiene solo componente azimutal:

$$\mathbf{J}(t, r, \theta, z) = J(t, r, z)\mathbf{e}_\theta.$$

A partir de (1.11), se introduce un potencial magnético vectorial \mathbf{A} de la forma

$$\mathbf{A} = A(t, r, z)\mathbf{e}_\theta,$$

de manera que

$$\mathbf{B} = \operatorname{curl} \mathbf{A}$$

y $\mathbf{E} = E\mathbf{e}_\theta$. Por tanto,

$$\frac{\partial A}{\partial t} + E = 0 \quad \text{en el material conductor.}$$

Para resolver este problema consideramos términos de velocidad en la Ley de Ohm y un dominio fijo de la pieza. En consecuencia, se tiene que

$$\mathbf{J} = \begin{cases} \sigma\mathbf{E} + \sigma\mathbf{v} \times \mathbf{B} & \text{en el material conductor,} \\ \mathbf{J}_S & \text{en la bobina (dato),} \\ \mathbf{0} & \text{en el aire.} \end{cases}$$

Con lo que obtenemos el siguiente problema elíptico-parabólico:

$$\left\{ \begin{array}{ll} \sigma \frac{\partial A}{\partial t} \mathbf{e}_\theta + \operatorname{curl} \left(\frac{1}{\mu} \operatorname{curl} (A\mathbf{e}_\theta) \right) + \mathbf{v} \times \operatorname{curl} (A\mathbf{e}_\theta) = \mathbf{0} & \text{en el conductor,} \\ \operatorname{curl} \left(\frac{1}{\mu} \operatorname{curl} (A\mathbf{e}_\theta) \right) = J_S \mathbf{e}_\theta & \text{en la bobina,} \\ \operatorname{curl} \left(\frac{1}{\mu} \operatorname{curl} (A\mathbf{e}_\theta) \right) = \mathbf{0} & \text{en el aire.} \end{array} \right.$$

Este problema conduce a una formulación variacional dependiente del tiempo degenerada y cuya forma bilineal asociada no es elíptica. Se establece la existencia y unicidad del problema continuo y de los correspondientes problemas semi-discreto y totalmente

discreto. Para resolver el problema débil, desarrollamos un código computacional que usa elementos finitos estándar para la variable espacial y discretización temporal implícita. Además, se prueban estimaciones del error *a priori* para los problemas semi-discreto discreto y totalmente discreto. Se presentan algunos experimentos numéricos que permiten evaluar la convergencia del método. El método numérico propuesto permite estudiar diversos problemas metalúrgicos; en particular, aplicamos este método a un problema de magnetohidrodinámica y a un problema de conformado electromagnético simplificado, donde se desprecia el movimiento de la pieza a deformar.

Los resultados de este capítulo se recogen en el trabajo

- A. BERMÚDEZ, C. REALES, R. RODRÍGUEZ AND P. SALGADO, *Mathematical and numerical analysis of a transient eddy current axisymmetric problem involving velocity terms*. Preprint Departamento de Ingeniería Matemática de la Universidad de Concepción.

1.3.3 Análisis numérico de un modelo evolutivo de corrientes inducidas que surge en la simulación numérica de conformado electromagnético

La tercera parte de esta tesis se dedica al estudio de un modelo electromagnético donde el dominio conductor cambia con el tiempo. Nótese que en un problema de conformado es necesario modelar este movimiento, debido a la deformación que sufre parte del dominio conductor. Para tener en cuenta este movimiento, el modelo de corrientes inducidas se plantea teniendo en cuenta que la conductividad eléctrica σ varía con el tiempo. Por otra parte, dado que en problemas de conformado la corriente inducida por la velocidad de la pieza es poco significativa, se desprecia este término en la ley de Ohm. Así, utilizaremos la siguiente ley constitutiva

$$\mathbf{J} = \begin{cases} \sigma(t)\mathbf{E} & \text{en el conductor en movimiento,} \\ \mathbf{J}_S(\text{dato}) & \text{en la bobina,} \\ \mathbf{0} & \text{en el aire} \end{cases}$$

obteniendo el siguiente problema elíptico-parabólico:

$$\left\{ \begin{array}{ll} \sigma(t) \frac{\partial A}{\partial t} \mathbf{e}_\theta + \operatorname{curl} \left(\frac{1}{\mu} \operatorname{curl} (A \mathbf{e}_\theta) \right) = \mathbf{0} & \text{en el conductor en movimiento,} \\ \operatorname{curl} \left(\frac{1}{\mu} \operatorname{curl} (A \mathbf{e}_\theta) \right) = J_S \mathbf{e}_\theta & \text{en la bobina,} \\ \operatorname{curl} \left(\frac{1}{\mu} \operatorname{curl} (A \mathbf{e}_\theta) \right) = \mathbf{0} & \text{en el aire.} \end{array} \right.$$

Como en el Capítulo 3, consideramos una formulación variacional donde la derivada temporal sólo está definida en una parte del dominio, que además, cambia con el tiempo. La existencia y unicidad de los problemas continuo y semidiscreto se estudia a través de argumentos de regularización.

El esquema numérico propuesto combina el método de elementos finitos con un método de Euler implícito. Para todo el proceso usamos una malla fija mas refinada en la zona por la que atraviesa la pieza. Las integrales en el dominio ocupado por la pieza se calculan con métodos numéricos de bajo orden y usando un gran número de puntos de integración. Se prueban estimaciones del error cuando existe regularidad adicional de la densidad de corriente y del dato inicial. Los resultados de este capítulo forman parte del siguiente trabajo:

- A. BERMÚDEZ, C. REALES, R. RODRÍGUEZ AND P. SALGADO, *Numerical analysis of a transient eddy current problem arising from electromagnetic forming (en preparación)*.

Chapter 2

Numerical analysis of a finite element method for the axisymmetric eddy current model of an induction furnace

2.1 Introduction

An induction heating system consists basically of one or several inductors and metallic workpieces to be heated. The inductors are supplied with alternating current which induces eddy currents inside the component being heated due to Faraday's law. This technique is widely used in the metallurgical industry in an important number of applications such as metal smelting, preheating for operations of welding, purification systems and, in general, processes needing a high speed of heating in particular zones of a piece of a conductive material. The overall process is highly complex and involves different physical phenomena: electromagnetics, heat transfer with phase change and hydrodynamics in the liquid metal.

Cylindrical symmetry allows reducing very often the original three-dimensional problem to a two-dimensional one. This approach has been followed in some recent papers ([10, 11, 12]), where numerical tools for solving this kind of problems have been proposed and tested. The aim of this paper is to provide a rigorous mathematical analysis of the finite element method used to solve the underlying electromagnetic model: an eddy current

problem in a two-dimensional meridional domain.

There exist several references dealing with the mathematical and numerical analysis of axisymmetric problems. For instance, the strategy of reducing the dimension in finite element methods was used for the axisymmetric Laplace and Stokes equations in [36] and [9], respectively. The time-dependent and static Maxwell equations in axisymmetric singular domains were studied in [5, 6] by introducing a method based on a splitting of the space of solutions into a regular subspace and a singular one. In [34], a method was introduced to solve a time-harmonic Maxwell equation in an axisymmetric domain using a Fourier decomposition. Fourier decomposition in axisymmetric problems was used in [36] for the Laplace equation, too.

We consider a formulation of the eddy current problem arising from the modeling of an induction furnace, which is based on introducing a vector potential for the magnetic field. This vector potential is shown to have only azimuthal component in meridional coordinates. We introduce suitable weighted Sobolev spaces in this two-dimensional setting and consider a mixed formulation, whose solution is the magnetic vector potential and Lagrange multipliers which are constant on each connected component of the two-dimensional section of the inductor. To prove well-posedness, we also introduce an equivalent direct formulation. Then, the existence and uniqueness of the solution of this problem follows from the Lax-Milgram lemma.

We discretize the mixed formulation by using piecewise linear finite elements on triangular meshes. We study the convergence of the method by introducing an equivalent direct discrete problem, too. Due to Cea's lemma, this study reduces to the existence of a suitable interpolation operator. A Clément operator introduced in [9] is used in the general case. A regularity result of the solution is proved when the magnetic permeability is constant in the whole domain. This allows using a Lagrange interpolant and to prove optimal order error estimates in such a case. Moreover, a duality argument allows improving the order of convergence for the current density, which is typically the variable of main interest.

The outline of this paper is as follows: In Section 2.2, we introduce the eddy current problem in induction furnaces and the geometric assumptions. Then, we derive a vector potential formulation under axisymmetric assumptions and introduce adequate boundary conditions. In Section 2.3, we recall the definitions of some weighted Sobolev spaces and some of their properties. This allows us to obtain, in Section 2.4, equivalent variational

formulations in mixed and direct forms of the problem. We prove that the problem has a unique solution. At the end of the section, we prove an additional regularity result. In Section 2.5, we introduce the finite element method and prove the error estimates. Finally, in Section 2.6, we report some numerical tests which allow us to asses the performance of the proposed method.

2.2 Statement of the problem

We consider an induction furnace consisting of an induction coil surrounding a workpiece, as sketched in Figure 2.1. The workpiece consists of a crucible containing the metal to be heated. The current flowing through the coil produces an electromagnetic field. This, in turn, induces eddy currents in the workpiece which, due to the Joule effect, produce heat that melts the metal. The domain of the problem is in principle the whole space; however, for computational purposes, we will take an artificial bounded domain $\tilde{\Omega}$ “sufficiently large” and suitable conditions on its boundary.

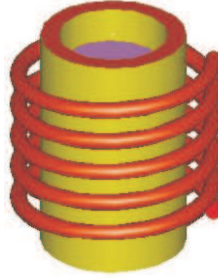


Figure 2.1: Sketch of the induction furnace.

To take advantage of the symmetry of the problem, we will use a cylindrical coordinate system (r, θ, z) . Accordingly, the artificial domain $\tilde{\Omega}$ will be chosen as a cylinder of radius R and height L . We denote by e_r , e_θ and e_z the unit vectors of the local orthonormal basis corresponding to this coordinate system. We assume cylindrical symmetry, i.e., we suppose that no field depends on the angular variable θ . We denote by $\Omega := (0, R) \times (0, L)$ a meridional section ($\theta = \text{constant}$) of $\tilde{\Omega}$. The boundary of Ω consists of the union of Γ_N , Γ_R and Γ_D , as shown in Figure 2.2: Γ_D lies on the revolution axis, Γ_R is parallel to this axis and Γ_N is perpendicular. We denote by Ω_0 the section of the workpiece to be heated and

by $\Omega_1, \dots, \Omega_m$ the sections of the turns of the coil (see Figure 2.2). We assume $\overline{\Omega}_0, \dots, \overline{\Omega}_m$ are connected and mutually disjoint. Moreover, we assume $\Omega_k \cap \Gamma_D = \emptyset$, $k = 1, \dots, m$. Let $\Omega_c := \Omega_0 \cup \Omega_1 \cup \dots \cup \Omega_m$ denote the section of the domain occupied by all the conductors and $\Omega_A := \Omega \setminus \overline{\Omega}_c$ that of the surrounding air.

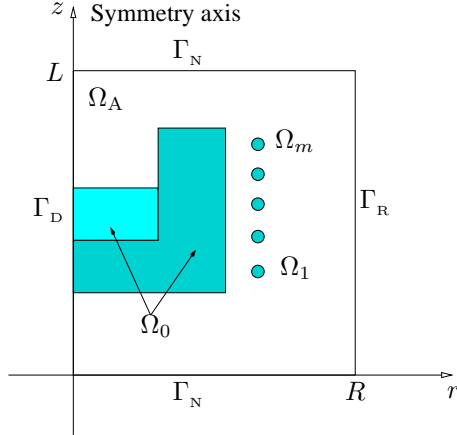


Figure 2.2: Sketch of the domain Ω .

Eddy currents are usually modeled by the low-frequency harmonic Maxwell equations. We will use standard notation in electromagnetism:

- \mathbf{E} is the electric field,
- \mathbf{B} is the magnetic induction,
- \mathbf{H} is the magnetic field,
- \mathbf{J} is the current density,
- ρ is the electric charge density,
- μ is the magnetic permeability,
- ε is the electric permittivity,
- σ is the electric conductivity.

We use boldface letters to denote vector fields and variables, as well as vector-valued operators, throughout the paper.

In the low-frequency harmonic regime, the electric displacement can be neglected in

Ampère's law, leading to the so-called eddy current model:

$$\operatorname{curl} \mathbf{H} = \mathbf{J}, \quad (2.1)$$

$$i\omega \mathbf{B} + \operatorname{curl} \mathbf{E} = \mathbf{0}, \quad (2.2)$$

$$\operatorname{div} \mathbf{B} = 0, \quad (2.3)$$

$$\operatorname{div} \mathbf{D} = \varrho. \quad (2.4)$$

The system (2.1)–(2.4) above needs to be completed by the constitutive relations

$$\mathbf{B} = \mu \mathbf{H}, \quad (2.5)$$

$$\mathbf{D} = \varepsilon \mathbf{E}, \quad (2.6)$$

and the Ohm's law

$$\mathbf{J} = \sigma \mathbf{E}. \quad (2.7)$$

The electric conductivity satisfies

$$0 < \underline{\sigma} \leq \sigma \leq \bar{\sigma} \quad \text{in conductors,} \quad (2.8)$$

$$\sigma \equiv 0 \quad \text{in air,} \quad (2.9)$$

whereas the other physical parameters are bounded above and below:

$$0 < \underline{\mu} \leq \mu \leq \bar{\mu}, \quad (2.10)$$

$$0 < \underline{\varepsilon} \leq \varepsilon \leq \bar{\varepsilon}. \quad (2.11)$$

These parameters may take different values at different points of the conductors, but are assumed not to depend on the magnetic or the electric fields. Therefore, the whole problem is assumed to be linear.

We notice that, since $\omega \neq 0$, equation (2.3) follows from (2.2). As will be shown below, equations (2.1) and (2.2) can be solved independently of (2.4) leading to \mathbf{H} in the whole domain and \mathbf{J} in conductors.

In [5, Proposition 2.2], it was shown that the eddy current equations in cylindrical coordinates lead to two decoupled problems, one for the azimuthal component (\mathbf{e}_θ) of \mathbf{J} and the other for the meridional component ($\mathbf{e}_r, \mathbf{e}_z$). In our case, the induction furnace has been modeled in [10] by assuming that all the physical quantities are independent of the angular coordinate θ and that the current density field has only azimuthal non-zero component, i.e,

$$\mathbf{J}(r, \theta, z) = J_\theta(r, z) \mathbf{e}_\theta. \quad (2.12)$$

Given a vector field $\mathbf{F} = F_r(r, \theta, z)\mathbf{e}_r + F_\theta(r, \theta, z)\mathbf{e}_\theta + F_z(r, \theta, z)\mathbf{e}_z$ and a scalar field $f = f(r, \theta, z)$, we recall that

$$\operatorname{curl} \mathbf{F} = \left(\frac{1}{r} \frac{\partial F_z}{\partial \theta} - \frac{\partial F_\theta}{\partial z} \right) \mathbf{e}_r + \left(\frac{\partial F_r}{\partial z} - \frac{\partial F_z}{\partial r} \right) \mathbf{e}_\theta + \left(\frac{1}{r} \frac{\partial(rF_\theta)}{\partial r} - \frac{1}{r} \frac{\partial F_r}{\partial \theta} \right) \mathbf{e}_z, \quad (2.13)$$

$$\operatorname{div} \mathbf{F} = \frac{1}{r} \frac{\partial(rF_r)}{\partial r} + \frac{1}{r} \frac{\partial F_\theta}{\partial \theta} + \frac{\partial F_z}{\partial z}, \quad (2.14)$$

$$\nabla f = \frac{\partial f}{\partial r} \mathbf{e}_r + \frac{1}{r} \frac{\partial f}{\partial \theta} \mathbf{e}_\theta + \frac{\partial f}{\partial z} \mathbf{e}_z. \quad (2.15)$$

Notice that from the assumption that \mathbf{H} does not depend on θ , (2.1), (2.13) and (2.12) lead to

$$-\frac{\partial H_\theta}{\partial z} = \frac{1}{r} \frac{\partial(rH_\theta)}{\partial r} = 0,$$

which in its turn implies that rH_θ has to be constant in $\tilde{\Omega}$. Now, if $\mathbf{H} \in L^2(\tilde{\Omega})^3$, then $H_\theta \mathbf{e}_\theta \in L^2(\tilde{\Omega})^3$, too. However, rH_θ being constant, this could happen only if this constant is zero. Therefore, H_θ has to vanish and, from (2.5), B_θ will vanish as well. Moreover, from (2.7), (2.8) and (2.12), E_r and E_z also vanish in conductors. Therefore, we have

$$\mathbf{H}(r, \theta, z) = H_r(r, z)\mathbf{e}_r + H_z(r, z)\mathbf{e}_z, \quad (2.16)$$

$$\mathbf{B}(r, \theta, z) = B_r(r, z)\mathbf{e}_r + B_z(r, z)\mathbf{e}_z, \quad (2.17)$$

$$\mathbf{E}(r, \theta, z) = E_\theta(r, z)\mathbf{e}_\theta \quad (\text{in conductors}). \quad (2.18)$$

Since \mathbf{B} is divergence-free (cf. (2.3)), there exists a so-called magnetic vector potential \mathbf{A} such that $\mathbf{B} = \operatorname{curl} \mathbf{A}$. For the sake of uniqueness, we take \mathbf{A} to be divergence-free, too, and satisfying $\mathbf{A} \cdot \mathbf{n} = 0$ on $\partial\tilde{\Omega}$. Thus, we have

$$\operatorname{curl} \mathbf{A} = \mathbf{B} \quad \text{in } \tilde{\Omega}, \quad (2.19)$$

$$\operatorname{div} \mathbf{A} = 0 \quad \text{in } \tilde{\Omega}, \quad (2.20)$$

$$\mathbf{A} \cdot \mathbf{n} = 0 \quad \text{on } \partial\tilde{\Omega}. \quad (2.21)$$

According to our axisymmetric assumption, we will look for \mathbf{A} independent of the angular variable. Next, from (2.19), (2.17) and (2.13), we obtain

$$\frac{\partial A_r}{\partial z} - \frac{\partial A_z}{\partial r} = 0 \quad \text{in } \Omega.$$

Therefore, since Ω is simply connected, there exists $\varphi \in H^1(\Omega)$ such that $A_r = \frac{\partial \varphi}{\partial r}$ and $A_z = \frac{\partial \varphi}{\partial z}$. On the other hand, from (2.20), (2.14) and (2.15),

$$0 = \operatorname{div} \mathbf{A} = \frac{1}{r} \frac{\partial(rA_r)}{\partial r} + \frac{\partial A_z}{\partial z} = \Delta \tilde{\varphi} \quad \text{in } \tilde{\Omega},$$

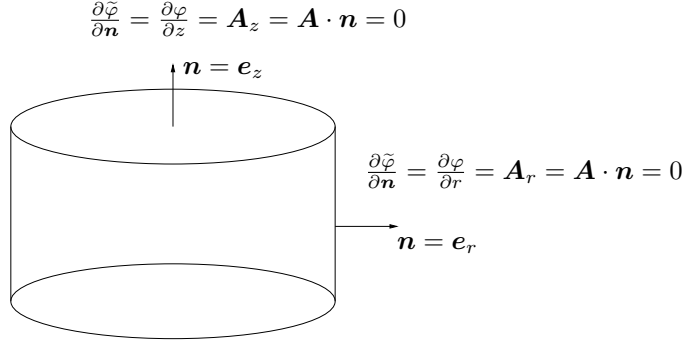


Figure 2.3: Boundary conditions for $\tilde{\varphi}$ in the domain $\tilde{\Omega}$.

where $\tilde{\varphi}(r, \theta, z) := \varphi(r, z)$. Thus, we have

$$\begin{aligned}\Delta \tilde{\varphi} &= 0 && \text{in } \tilde{\Omega}, \\ \frac{\partial \tilde{\varphi}}{\partial \mathbf{n}} &= 0 && \text{on } \partial \tilde{\Omega}\end{aligned}$$

(for the deduction of the boundary condition, see Figure 2.3). Hence $\tilde{\varphi}$ is constant and, consequently, $A_r = A_z = 0$. Therefore, we conclude that

$$\mathbf{A}(r, \theta, z) = A(r, z)\mathbf{e}_\theta \quad \text{in } \tilde{\Omega}$$

and, hence, from (2.19) and (2.13),

$$B_r(r, z) = -\frac{\partial A}{\partial z} \quad \text{and} \quad B_z(r, z) = \frac{1}{r} \frac{\partial(rA)}{\partial r} \quad \text{in } \Omega. \quad (2.22)$$

On the other hand, taking into account again (2.19), we deduce from (2.2) and (2.7) that

$$\operatorname{curl}((i\omega A + \sigma^{-1}J_\theta)\mathbf{e}_\theta) = \mathbf{0} \quad (\text{in conductors}),$$

from which it follows from (2.13) that

$$\begin{aligned}\frac{\partial}{\partial z}(i\omega A + \sigma^{-1}J_\theta) &= 0 && \text{in } \Omega_c, \\ \frac{\partial}{\partial r}(r(i\omega A + \sigma^{-1}J_\theta)) &= 0 && \text{in } \Omega_c.\end{aligned}$$

Hence, we deduce that there exist constants $V_k \in \mathbb{C}$, $k = 0, \dots, m$, such that

$$i\omega A + \sigma^{-1}J_\theta = \frac{V_k}{r} \quad \text{in } \Omega_k \quad (2.23)$$

(recall that Ω_k are the connected components of Ω_c).

Next, from (2.1), (2.5), (2.17), (2.22) and (2.12),

$$\operatorname{curl} \left(-\frac{1}{\mu} \frac{\partial A}{\partial z} \mathbf{e}_r + \frac{1}{\mu r} \frac{\partial(rA)}{\partial r} \mathbf{e}_z \right) = J_\theta \mathbf{e}_\theta.$$

Thus, taking into account (2.13) and (2.23), we obtain for $k = 0, \dots, m$,

$$-\left(\frac{\partial}{\partial r} \left(\frac{1}{\mu r} \frac{\partial(rA)}{\partial r} \right) + \frac{\partial}{\partial z} \left(\frac{1}{\mu} \frac{\partial A}{\partial z} \right) \right) + i\omega\sigma A = \frac{\sigma}{r} V_k \quad \text{in } \Omega_k, \quad (2.24)$$

whereas using that J_θ vanishes outside the conductors (cf. (2.7), (2.9) and (2.12)),

$$-\left(\frac{\partial}{\partial r} \left(\frac{1}{\mu r} \frac{\partial(rA)}{\partial r} \right) + \frac{\partial}{\partial z} \left(\frac{1}{\mu} \frac{\partial A}{\partial z} \right) \right) = 0 \quad \text{in } \Omega_A. \quad (2.25)$$

In order to solve equations (2.24) and (2.25), we assume that the intensities going through each cylindrical ring are given data. Thus we add to the model the equations

$$\int_{\Omega_k} J_\theta dr dz = I_k, \quad k = 1, \dots, m,$$

I_k being the intensity traversing Ω_k . Hence, from (2.23), we have for $k = 1, \dots, m$,

$$V_k = \frac{1}{d_k} \left(I_k + i\omega \int_{\Omega_k} \sigma A dr dz \right), \quad (2.26)$$

where

$$d_k := \int_{\Omega_k} \frac{\sigma}{r} dr dz.$$

Additional physical considerations (see [20]) allow us to impose

$$V_0 = 0. \quad (2.27)$$

Notice that, as a consequence of (2.23), this condition has to hold true for \mathbf{A} and \mathbf{E} to belong to $L^2(\tilde{\Omega})^3$, whenever $\operatorname{meas}(\partial\Omega_0 \cap \Gamma_D) > 0$ (as is the case for the problem sketched in Figure 2.2).

Equations (2.24)–(2.27) must be completed with suitable boundary conditions. Following [20], we impose on Γ_R the Robin condition

$$\frac{\partial(rA)}{\partial r} + A = 0 \quad \text{on } \Gamma_R \quad (2.28)$$

and on Γ_N the homogeneous Neumann condition

$$\frac{\partial A}{\partial z} = 0 \quad \text{on } \Gamma_N; \quad (2.29)$$

the latter stems from the fact that the radial component of the magnetic induction is close to zero on this boundary. Finally, the natural symmetry condition along the revolution axis leads to

$$A = 0 \quad \text{on } \Gamma_D. \quad (2.30)$$

2.3 Weighted Sobolev spaces

In this section we define appropriate weighted Sobolev spaces that will be used in the sequel and establish some of their properties; the corresponding proofs can be found in [9, 29, 36, 33]. More general results about weighted Sobolev spaces can be found in the last reference. To simplify the notation, we will denote the partial derivatives by ∂_r and ∂_z .

Let $L_r^2(\Omega)$ denote the weighted Lebesgue space of all measurable functions u defined in Ω for which

$$\|u\|_{L_r^2(\Omega)} := \int_{\Omega} |u|^2 r dr dz < \infty.$$

The weighted Sobolev space $H_r^k(\Omega)$ consists of all functions in $L_r^2(\Omega)$ whose derivatives up to order k are also in $L_r^2(\Omega)$. We define the norms and semi-norms in the standard way; in particular,

$$\begin{aligned} |u|_{H_r^1(\Omega)}^2 &:= \int_{\Omega} (|\partial_r u|^2 + |\partial_z u|^2) r dr dz, \\ |u|_{H_r^2(\Omega)}^2 &:= \int_{\Omega} (|\partial_{rr} u|^2 + |\partial_{rz} u|^2 + |\partial_{zz} u|^2) r dr dz. \end{aligned}$$

Let $\tilde{H}_r^1(\Omega) := H_r^1(\Omega) \cap L_{1/r}^2(\Omega)$, where $L_{1/r}^2(\Omega)$ denotes the set of all measurable functions u defined in Ω for which

$$\|u\|_{L_{1/r}^2(\Omega)}^2 := \int_{\Omega} \frac{|u|^2}{r} dr dz < \infty.$$

$\tilde{H}_r^1(\Omega)$ is a Hilbert space with the norm

$$\|u\|_{\tilde{H}_r^1(\Omega)} := \left(\|u\|_{H_r^1(\Omega)}^2 + \|u\|_{L_{1/r}^2(\Omega)}^2 \right)^{1/2}.$$

Let $\tilde{H}_r^2(\Omega) := \left\{ u \in \tilde{H}_r^1(\Omega) : \|u\|_{\tilde{H}_r^2(\Omega)} < \infty \right\}$, where

$$\|u\|_{\tilde{H}_r^2(\Omega)}^2 := |u|_{\tilde{H}_r^2(\Omega)}^2 + \|u\|_{\tilde{H}_r^1(\Omega)}^2 + \|\partial_z u\|_{L_{1/r}^2(\Omega)}^2,$$

with

$$|u|_{\tilde{H}_r^2(\Omega)}^2 := \left| \frac{1}{r} \partial_r(ru) \right|_{H_r^1(\Omega)}^2 + |\partial_z u|_{H_r^1(\Omega)}^2.$$

The proof of the following three lemmas can be found in [29, Section 3.1].

Lemma 2.3.1 *The set of $\mathcal{C}^\infty(\overline{\Omega})$ functions which vanish in a neighborhood of Γ_D is dense in $\tilde{H}_r^1(\Omega)$.*

Lemma 2.3.2 *Consider the notation of Figure 2.4, with $0 \leq r_0 < r_1$ and $a \in [r_0, r_1]$. For all $u \in \tilde{H}_r^1(S)$, $u|_{\gamma_a} \in L^2(\gamma_a)$ and there holds*

$$\|u\|_{L^2(\gamma_a)}^2 \leq \|\partial_r u\|_{L_r^2(S)}^2 + \frac{2r_1 - r_0}{r_1 - r_0} \|u\|_{L_{1/r}^2(S)}.$$

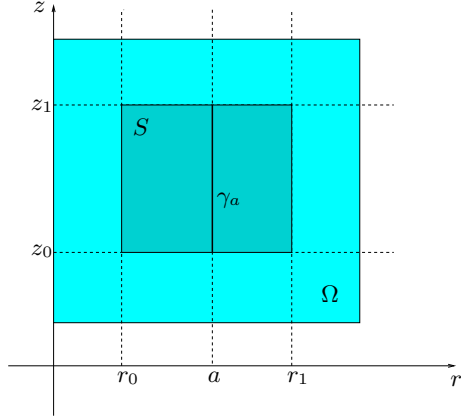


Figure 2.4: Sketch of S .

The preceding result implies that the functions in $\tilde{H}_r^1(\Omega)$ have traces on Γ_D ($r = 0$). Moreover, since the set of the functions in $\mathcal{C}^\infty(\overline{\Omega})$ vanishing in a neighborhood of Γ_D is dense in $\tilde{H}_r^1(\Omega)$ (cf. Lemma 2.3.1), the functions in $\tilde{H}_r^1(\Omega)$ have vanishing traces on Γ_D .

Lemma 2.3.3 *For all $u \in \tilde{H}_r^1(\Omega)$, $\partial_r(ru) \in L_{1/r}^2(\Omega)$ and there holds*

$$\|\partial_r u\|_{L_r^2(\Omega)}^2 + \|u\|_{L_{1/r}^2(\Omega)}^2 \leq \|\partial_r(ru)\|_{L_{1/r}^2(\Omega)}^2 \leq 2 \|\partial_r u\|_{L_r^2(\Omega)}^2 + 2 \|u\|_{L_{1/r}^2(\Omega)}^2.$$

The following result has been proved in [36, Theorem 4.7].

Lemma 2.3.4 *The injection $H_r^2(\Omega) \hookrightarrow \mathcal{C}^0(\overline{\Omega})$ is continuous.*

Finally, the next lemma is a variation of a result from [25].

Lemma 2.3.5 *Let Ω be a Lipschitz bounded connected open set. Let f be a continuous linear functional on $H_r^1(\Omega)$ whose restriction to constant functions is not zero. Then, there exist $\alpha > 0$ such that*

$$\alpha \|u\|_{H_r^1(\Omega)} \leq \|\nabla u\|_{L_r^2(\Omega)} + |f(u)| \quad \forall u \in H_r^1(\Omega).$$

Proof. We repeat the steps of the proof of Lemma B.63 from [25] with $X := H_r^1(\Omega)$, $Y := L_r^2(\Omega) \times \mathbb{C}$ and $Z := L_r^2(\Omega)$, and use that the injection $X \hookrightarrow Z$ is compact due to Theorem 4.5 from [36]. \square

2.4 Variational formulation

In this section we establish a variational formulation of problem (2.24)–(2.30) for which we will prove the existence and uniqueness of the solution. With this aim, we multiply (2.24) and (2.25) by a test function in $\tilde{H}_r^1(\Omega)$, integrate by parts, use that the functions in this space have a vanishing trace on Γ_D , the boundary conditions (2.28) and (2.29), (2.27) and rewrite (2.26) in a convenient way, to obtain the following problem:

Problem 2.4.1 *Given $\mathbf{I} := (I_1, \dots, I_m) \in \mathbb{C}^m$, find $(A, \mathbf{V}) \in \tilde{H}_r^1(\Omega) \times \mathbb{C}^m$ such that*

$$\begin{aligned} & \int_{\Omega} \frac{1}{\mu} \left(\frac{1}{r} \frac{\partial(rA)}{\partial r} \frac{1}{r} \frac{\partial(r\bar{Z})}{\partial r} + \frac{\partial A}{\partial z} \frac{\partial \bar{Z}}{\partial z} \right) r dr dz + \int_{\Gamma_R} \frac{1}{\mu} A \bar{Z} dz \\ & + i\omega \int_{\Omega_c} \sigma A \bar{Z} r dr dz - \sum_{k=1}^m \int_{\Omega_k} \sigma V_k \bar{Z} dr dz = 0 \quad \forall Z \in \tilde{H}_r^1(\Omega), \\ & \sum_{k=1}^m \int_{\Omega_k} \sigma \bar{W}_k A dr dz + \frac{i}{\omega} \sum_{k=1}^m \int_{\Omega_k} \frac{\sigma \bar{W}_k V_k}{r} dr dz = \frac{i}{\omega} \sum_{k=1}^m \bar{W}_k I_k \quad \forall \mathbf{W} \in \mathbb{C}^m. \end{aligned}$$

Let a be the sesquilinear form defined in $\tilde{H}_r^1(\Omega)$ by

$$\begin{aligned} a(A, Z) := & \int_{\Omega} \frac{1}{\mu} \left(\frac{1}{r} \frac{\partial(rA)}{\partial r} \frac{1}{r} \frac{\partial(r\bar{Z})}{\partial r} + \frac{\partial A}{\partial z} \frac{\partial \bar{Z}}{\partial z} \right) r dr dz + \int_{\Gamma_R} \frac{1}{\mu} A \bar{Z} dz \\ & + i\omega \left(\int_{\Omega_c} \sigma A \bar{Z} r dr dz - \sum_{k=1}^m \frac{1}{d_k} \int_{\Omega_k} \sigma A dr dz \int_{\Omega_k} \sigma \bar{Z} dr dz \right). \end{aligned}$$

For the analysis, we will use the following problem:

Problem 2.4.2 Given $\mathbf{I} \in \mathbb{C}^m$, find $A \in \tilde{H}_r^1(\Omega)$ such that

$$a(A, Z) = \sum_{k=1}^m \frac{I_k}{d_k} \int_{\Omega_k} \sigma \bar{Z} dr dz \quad \forall Z \in \tilde{H}_r^1(\Omega).$$

The following lemma shows that Problems 2.4.1 and 2.4.2 are equivalent. We do not include its proof which is straightforward.

Lemma 2.4.1 Let $\mathbf{I} \in \mathbb{C}^m$. If (A, \mathbf{V}) is a solution of Problem 2.4.1, then A is a solution of Problem 2.4.2. Conversely, if A is a solution of Problem 2.4.2 and V_k , $k = 1, \dots, m$, are defined by (2.26), then (A, \mathbf{V}) is a solution of Problem 2.4.1.

Remark 2.4.1 Problem 2.4.2 will be used to prove the existence and uniqueness of the solution and error estimates, but not for the actual numerical approximation, because the term $\int_{\Omega_k} \sigma A dr dz \int_{\Omega_k} \sigma \bar{Z} dr dz$ would lead to a fully dense matrix. In fact, for the numerical computations we will use a discretization of Problem 2.4.1, since it leads to matrices in which only the last m rows and columns of the matrix will be dense.

In the following lemma and thereafter C will denote a generic constant, not necessarily the same at each occurrence.

Lemma 2.4.2 There holds

$$\|u\|_{H_r^1(\Omega)} \leq C \left(|u|_{H_r^1(\Omega)} + \|u\|_{L^2(\Gamma_R)} \right) \quad \forall u \in H_r^1(\Omega).$$

Proof. Let $f(u) := \int_{\Gamma_R} \frac{1}{\mu} u dz$, $u \in H_r^1(\Omega)$. Because of Lemma 2.3.5,

$$\alpha \|u\|_{H_r^1(\Omega)} \leq \|\nabla u\|_{L_r^2(\Omega)} + |f(u)| \leq |u|_{H_r^1(\Omega)} + \frac{\sqrt{L}}{\mu} \|u\|_{L^2(\Gamma_R)} \quad \forall u \in H_r^1(\Omega),$$

which allows us to conclude the proof. \square

Remark 2.4.2 The lemma above holds true for any Lipschitz bounded connected domain Ω and any subset $\Gamma_R \subset \partial\Omega \setminus \Gamma_D$ with positive measure.

Lemma 2.4.3 The sesquilinear form a is $\tilde{H}_r^1(\Omega)$ -elliptic and continuous.

Proof. The ellipticity arises from the definition of a and (2.10) as follows:

$$\begin{aligned} \operatorname{Re}(a(A, A)) &\geq \frac{1}{\underline{\mu}} \left(\|\partial_r(rA)\|_{L^2_{1/r}(\Omega)}^2 + \|\partial_z A\|_{L^2_r(\Omega)}^2 + \|A\|_{L^2(\Gamma_R)}^2 \right) \\ &\geq \frac{1}{\underline{\mu}} \left(\|\partial_r A\|_{L^2_r(\Omega)}^2 + \|A\|_{L^2_{1/r}(\Omega)}^2 + \|\partial_z A\|_{L^2_r(\Omega)}^2 + \|A\|_{L^2(\Gamma_R)}^2 \right) \\ &\geq C \left(\|A\|_{H^1_r(\Omega)}^2 + \|A\|_{L^2_{1/r}(\Omega)}^2 \right) \\ &= C \|A\|_{\tilde{H}_r^1(\Omega)}^2, \end{aligned}$$

where we have used Lemma 2.3.3 for the second inequality and Lemma 2.4.2 for the third one. The continuity follows directly from Lemmas 2.3.2 and 2.3.3. \square

Now we are in a position to prove that Problem 2.4.1 is well posed. Here and thereafter $\|\mathbf{I}\|_{\mathbb{C}^m} := (\sum_{k=1}^m |I_k|^2)^{1/2}$ denotes the standard Euclidean norm in \mathbb{C}^m .

Theorem 2.4.1 *Problem 2.4.1 has a unique solution which satisfies*

$$\|A\|_{\tilde{H}_r^1(\Omega)} \leq C \|\mathbf{I}\|_{\mathbb{C}^m}.$$

Proof. Since Problems 2.4.1 and 2.4.2 are equivalent, it is enough to show that the latter is well posed. The right-hand side of Problem 2.4.2 satisfies

$$\left| \sum_{k=1}^m \frac{I_k}{d_k} \int_{\Omega_k} \sigma \bar{Z} dr dz \right| \leq C \|\mathbf{I}\|_{\mathbb{C}^m} \|Z\|_{L^2_r(\Omega_k)}.$$

Hence, the theorem follows from Lemma 2.4.3 and the Lax-Milgram Lemma. \square

To end this section we will prove a regularity result for the solution of Problem 2.4.1, valid at least when the magnetic permeability is constant in the whole domain. With this aim, we will consider a slightly more general framework, which will be also used to prove a double order of convergence in $L^2_r(\Omega)$ of the numerical method proposed in the following section. Consider the following auxiliary problem:

Problem 2.4.3 *Given $g \in L^2_r(\Omega)$, find $Y_\theta \in \tilde{H}_r^1(\Omega)$ such that*

$$\int_{\Omega} \frac{1}{\mu} \left(\frac{1}{r} \frac{\partial(rY_\theta)}{\partial r} \frac{1}{r} \frac{\partial(r\bar{Z})}{\partial r} + \frac{\partial Y_\theta}{\partial z} \frac{\partial \bar{Z}}{\partial z} \right) r dr dz + \int_{\Gamma_R} \frac{1}{\mu} Y_\theta \bar{Z} dz = \int_{\Omega} g \bar{Z} r dr dz \quad \forall Z \in \tilde{H}_r^1(\Omega),$$

Lemma 2.4.4 *If μ is constant in Ω , then the solution of Problem 2.4.3 satisfies $Y_\theta \in \tilde{H}_r^2(\Omega)$ and*

$$\|Y_\theta\|_{\tilde{H}_r^2(\Omega)} \leq C \|g\|_{L^2_r(\Omega)}.$$

Proof. The arguments in the proof of Lemma 2.4.3 show that the sesquilinear form on the left-hand side of Problem 2.4.3 is $\tilde{H}_r^1(\Omega)$ -elliptic, as well. Hence the problem is well posed and its solution satisfies $\|Y_\theta\|_{\tilde{H}_r^1(\Omega)} \leq C \|g\|_{L_r^2(\Omega)}$.

Let $\mathbf{Y}(r, \theta, z) := Y_\theta(r, z)\mathbf{e}_\theta$. Using (2.13) and Lemma 2.3.3, it is easy to show that $\mathbf{curl} \mathbf{Y} \in L^2(\tilde{\Omega})^3$ and

$$\|\mathbf{Y}\|_{H(\mathbf{curl}, \tilde{\Omega})} \leq C \|Y_\theta\|_{\tilde{H}_r^1(\Omega)} \leq C \|g\|_{L_r^2(\Omega)}. \quad (2.31)$$

To prove additional regularity we test Problem 2.4.3 with $Z \in \mathcal{D}(\Omega)$. Hence, using (2.13), (2.14) and the fact that \mathbf{e}_θ is orthogonal to \mathbf{n} throughout the whole boundary of Ω , we have that

$$\mathbf{curl} \left(\frac{1}{\mu} \mathbf{curl} \mathbf{Y} \right) = g\mathbf{e}_\theta \quad \text{in } \tilde{\Omega}, \quad (2.32)$$

$$\operatorname{div} \mathbf{Y} = 0 \quad \text{in } \tilde{\Omega}, \quad (2.33)$$

$$\mathbf{Y} \cdot \mathbf{n} = 0 \quad \text{on } \partial\tilde{\Omega}. \quad (2.34)$$

Thus, from (2.31), (2.33) and (2.34), we have that $\mathbf{Y} \in H(\mathbf{curl}, \tilde{\Omega}) \cap H_0(\operatorname{div}, \tilde{\Omega})$. Hence, since $\tilde{\Omega}$ is convex, $\mathbf{Y} \in H^1(\tilde{\Omega})^3$ (cf. [4, Theorem 2.17]) and

$$\|\mathbf{Y}\|_{H^1(\tilde{\Omega})^3} \leq C \|\mathbf{Y}\|_{H(\mathbf{curl}, \tilde{\Omega})} \leq C \|g\|_{L_r^2(\Omega)}. \quad (2.35)$$

Next, we prove that $\mathbf{curl} \mathbf{Y}$ is also in $H^1(\tilde{\Omega})^3$. In this case the results from [4] cannot be directly applied, because neither $\mathbf{curl} \mathbf{Y} \cdot \mathbf{n}$ nor $\mathbf{curl} \mathbf{Y} \times \mathbf{n}$ vanish on $\partial\tilde{\Omega}$. This is the reason for making a translation by using the function Φ defined below. Let $0 < r_1 < r_2 < R$ (recall that Γ_R lies on the line $r = R$) and let $\varphi \in \mathcal{C}^\infty([0, R])$ be such that $\varphi(r) \equiv 0$ in $[0, r_1]$ and $\varphi(r) \equiv 1$ in $[r_2, R]$. Let

$$\Phi(r, \theta, z) := -\frac{1}{R} \mathbf{Y}(r, \theta, z) \times \varphi(r) \mathbf{e}_r = \frac{1}{R} \varphi(r) Y_\theta(r, z) \mathbf{e}_z,$$

and $\Psi := \mathbf{curl} \mathbf{Y} + \Phi$. We will show that $\Psi \in H_0(\mathbf{curl}, \tilde{\Omega}) \cap H(\operatorname{div}, \tilde{\Omega})$. To prove this, we split $\partial\tilde{\Omega}$ into two parts, $\tilde{\Gamma}_R$ and $\tilde{\Gamma}_N$, which correspond to the Robin (Γ_R) and the Neumann (Γ_N) boundaries of the two-dimensional domain Ω , respectively. From (2.13), we have

$$\Psi \times \mathbf{n} = (\mathbf{curl} \mathbf{Y} + \Phi) \times \mathbf{e}_r = \frac{1}{r} \frac{\partial(r Y_\theta)}{\partial r} \mathbf{e}_\theta + \frac{1}{R} \varphi(r) Y_\theta(r, z) \mathbf{e}_\theta = \mathbf{0} \quad \text{on } \tilde{\Gamma}_R,$$

where for the last equality we have used the boundary condition

$$\frac{1}{r} \frac{\partial(r Y_\theta)}{\partial r} + Y_\theta = 0 \quad \text{on } \tilde{\Gamma}_R,$$

which in its turn is obtained by testing Problem 2.4.3 with $Z \in \mathcal{C}^\infty(\bar{\Omega})$ such that $\text{supp}(Z) \cap (\Gamma_D \cup \Gamma_N) = \emptyset$. On the other hand,

$$\Psi \times \mathbf{n} = (\mathbf{curl} \mathbf{Y} + \Phi) \times \mathbf{e}_z = \frac{\partial Y_\theta}{\partial z} \mathbf{e}_\theta = \mathbf{0} \quad \text{on } \tilde{\Gamma}_N,$$

where now the last equality follows by testing Problem 2.4.3 with $Z \in \mathcal{C}^\infty(\bar{\Omega})$ such that $\text{supp}(Z) \cap (\Gamma_D \cup \Gamma_R) = \emptyset$. Therefore, by using (2.32) and the regularity of Φ , we conclude that $\Psi \in H_0(\mathbf{curl}, \tilde{\Omega}) \cap H(\text{div}, \tilde{\Omega})$. Hence $\Psi \in H^1(\tilde{\Omega})^3$ (cf. [4, Theorem 2.17], again) and

$$\|\Psi\|_{H^1(\tilde{\Omega})^3} \leq \|\mathbf{curl} \mathbf{Y}\|_{H(\mathbf{curl}, \tilde{\Omega})} + \|\Phi\|_{H^1(\tilde{\Omega})^3} \leq C \|g\|_{L_r^2(\Omega)},$$

where we have used (2.31), (2.32) and (2.35) for the last inequality. Consequently, $\mathbf{curl} \mathbf{Y} = \Psi - \Phi \in H^1(\tilde{\Omega})^3$ and

$$\|\mathbf{curl} \mathbf{Y}\|_{H^1(\tilde{\Omega})^3} \leq C \|g\|_{L_r^2(\Omega)}. \quad (2.36)$$

Finally, from [6, Proposition 3.17] we have that $\|\mathbf{Y}\|_{H^1(\tilde{\Omega})^3}^2 = 2\pi \|Y_\theta\|_{\tilde{H}_r^1(\Omega)}^2$ and

$$\|\mathbf{curl} \mathbf{Y}\|_{H^1(\tilde{\Omega})^3}^2 = 2\pi \|\partial_z Y_\theta\|_{\tilde{H}_r^1(\Omega)}^2 + 2\pi \left\| \frac{1}{r} \partial_r(r Y_\theta) \right\|_{H_r^1(\Omega)}^2.$$

Consequently, the definition of the $\tilde{H}_r^2(\Omega)$ -norm, (2.35) and (2.36) lead to

$$\|Y_\theta\|_{\tilde{H}_r^2(\Omega)}^2 \leq \frac{1}{2\pi} \left(\|\mathbf{curl} \mathbf{Y}\|_{H^1(\tilde{\Omega})^3}^2 + \|\mathbf{Y}\|_{H^1(\tilde{\Omega})^3}^2 \right) \leq C \|g\|_{L_r^2(\Omega)}^2.$$

Thus, we conclude the proof. \square

Theorem 2.4.2 *If μ is constant in Ω , then the solution of Problem 2.4.3 satisfies $Y_\theta \in H_r^2(\Omega)$ and*

$$\|Y_\theta\|_{H_r^2(\Omega)} \leq C \|g\|_{L_r^2(\Omega)}.$$

Proof. Let J_1 denote the first-order Bessel function of the first kind. Define

$$j_m(r) := \frac{\sqrt{2}}{|J_2(\beta_m R)|} J_1(\beta_m r), \quad m = 1, 2, \dots$$

where $\beta_m := \alpha_m/R$, with α_m being the m th positive zero of the equation

$$2 J_1(x) + x J_1'(x) = 0,$$

and

$$s_n(z) := \sqrt{2} \cos \left(\frac{n\pi z}{L} \right), \quad n = 0, 1, 2, \dots$$

Then by classical completeness results for Bessel functions (see [28, Sections 10.7–8] and [30]), the set of functions $e_{mn}(r, z) = j_m(r)s_n(z)$, $m = 1, 2, \dots$, $n = 0, 1, 2, \dots$, is a complete orthogonal system of $L_r^2(\Omega)$. From this fact and Lemma 2.4.4, the rest of the proof runs essentially as those of Proposition 4.1 and Theorem 4.1 from [29]. \square

Corollary 2.4.1 *If μ is constant in Ω , then the solution of Problem 2.4.1 satisfies $A \in H_r^2(\Omega)$ and*

$$\|A\|_{H_r^2(\Omega)} \leq C \|\mathbf{I}\|_{\mathbb{C}^m}.$$

Proof. It follows from the first equation of Problem 2.4.1 and Theorem 2.4.2 applied to Problem 2.4.3 with

$$g := -i\omega\sigma A + \sum_{k=1}^m \sigma \frac{V_k}{r} \chi_{\Omega_k},$$

χ_{Ω_k} being the characteristic function of Ω_k , $k = 1, \dots, m$. In its turn, $\|g\|_{L_r^2(\Omega)} \leq C \|\mathbf{I}\|_{\mathbb{C}^m}$, by virtue of Theorem 2.4.1 and (2.26). \square

2.5 Finite element discretization

In this section we introduce a discretization of Problem 2.4.1 and prove error estimates. Let $\{\mathcal{T}_h\}_{h>0}$ be a regular family of triangulations of Ω with h being the mesh-size (see [21]). Let us remark that there is no need of assuming that the meshes are compatible with the geometry of the conductor domain (i.e., that each element of \mathcal{T}_h is contained either in Ω_c or in Ω_A), although, of course, this kind of meshes make easier the implementation of the method. From now on, the generic constant C will always be independent of the mesh-size.

Let

$$\mathcal{V}_h := \left\{ u_h \in \tilde{H}_r^1(\Omega) : u_h|_T \in \mathbb{P}_1 \ \forall T \in \mathcal{T}_h \right\},$$

with \mathbb{P}_1 being the complex-valued linear functions in the coordinates r and z :

$$\mathbb{P}_1 := \{p(r, z) = c_0 + c_1 r + c_2 z : c_0, c_1, c_2 \in \mathbb{C}\}.$$

The finite element approximation of Problem 2.4.1 is defined as the solution (A^h, \mathbf{V}^h) of the following problem:

Problem 2.5.1 Given $\mathbf{I} := (I_1, \dots, I_m) \in \mathbb{C}^m$, find $(A^h, \mathbf{V}^h) \in \mathcal{V}_h \times \mathbb{C}^m$ such that

$$\begin{aligned} & \int_{\Omega} \frac{1}{\mu} \left(\frac{1}{r} \frac{\partial(rA^h)}{\partial r} \frac{1}{r} \frac{\partial(r\bar{Z}^h)}{\partial r} + \frac{\partial A^h}{\partial z} \frac{\partial \bar{Z}^h}{\partial z} \right) r dr dz + \int_{\Gamma_R} \frac{1}{\mu} A^h \bar{Z}^h dz \\ & + i\omega \int_{\Omega_c} \sigma A^h \bar{Z}^h r dr dz - \sum_{k=1}^m \int_{\Omega_k} \sigma V_k^h \bar{Z}^h dr dz = 0 \quad \forall Z^h \in \mathcal{V}_h, \\ & \sum_{k=1}^m \int_{\Omega_k} \sigma \bar{W}_k^h A^h dr dz + \frac{i}{\omega} \sum_{k=1}^m \int_{\Omega_k} \frac{\sigma \bar{W}_k^h V_k^h}{r} dr dz = \frac{i}{\omega} \sum_{k=1}^m \bar{W}_k^h I_k \quad \forall \mathbf{W}^h \in \mathbb{C}^m. \end{aligned}$$

It is straightforward to see that Problem 2.5.1 is equivalent to the following one, with $\mathbf{V}^h := (V_1^h, \dots, V_m^h)$ given by

$$V_k^h = \frac{1}{d_k} \left(I_k + i\omega \int_{\Omega_k} \sigma A^h dr dz \right), \quad k = 1, \dots, m. \quad (2.37)$$

Problem 2.5.2 Given $\mathbf{I} \in \mathbb{C}^m$, find $A^h \in \mathcal{V}_h$ such that

$$a(A^h, Z^h) = \sum_{k=1}^m \frac{I_k}{d_k} \int_{\Omega_k} \sigma \bar{Z}^h dr dz \quad \forall Z^h \in \mathcal{V}_h.$$

We will use Problem 2.5.2 to prove well-posedness and error estimates. However, as stated in Remark 2.4.1, for the computer implementation of this approach we will use Problem 2.5.1 to avoid dense matrices.

Theorem 2.5.1 Problem 2.5.1 has a unique solution (A^h, \mathbf{V}^h) . Moreover, there exists a constant $C > 0$, independent of h , such that if (A, \mathbf{V}) is the solution of Problem 2.4.1, then

$$\|A - A^h\|_{\tilde{H}_r^1(\Omega)} + \sum_{k=1}^m |V_k - V_k^h| \leq C \inf_{Z^h \in \mathcal{V}_h} \|A - Z^h\|_{\tilde{H}_r^1(\Omega)}.$$

Proof. Since Problems 2.5.1 and 2.5.2 are equivalent, we use the latter for the estimate for A , which follows immediately from Cea's lemma (see for instance [21]). The estimate for V_k , $k = 1, \dots, m$, follows from the latter, (2.26) and (2.37). \square

According to the theorem above, there only remains to prove that A can be conveniently approximated by a function in \mathcal{V}_h . With this purpose, in the most general case, we resort to a Clément operator stable for functions in $\tilde{H}_r^1(\Omega)$ (which, recall, vanish on Γ_D). Such operators have been studied for weighted Sobolev spaces in [9] and [36].

In particular, we consider the Clément operator $\tilde{\Pi}_h : \tilde{H}_r^1(\Omega) \rightarrow \mathcal{V}_h$ defined in [9, Eq. (36)]. The proof of the following lemma can be found in [9, Theorem 2].

Lemma 2.5.1 *If $1 \leq l \leq 2$, then there exists a constant $C > 0$, independent of h , such that for all $u \in H_r^l(\Omega) \cap \tilde{H}_r^1(\Omega)$,*

$$\|u - \tilde{\Pi}_h u\|_{\tilde{H}_r^1(\Omega)} \leq Ch^{l-1} \|u\|_{H_r^l(\Omega) \cap \tilde{H}_r^1(\Omega)}.$$

On the other hand, when the solution A is sufficiently smooth, we are able to use the Lagrange interpolation operator Π_h . In fact, according to Lemma 2.3.4, such interpolant is well defined for functions in $\tilde{H}_r^2(\Omega)$. Moreover, for functions in $H_r^2(\Omega)$, there holds the following error estimate, whose proof can be found in [36, Lemma 6.3].

Lemma 2.5.2 *There exists constants $C > 0$, independent of h , such that for all $u \in \tilde{H}_r^1(\Omega) \cap H_r^2(\Omega)$,*

$$\|u - \Pi_h u\|_{\tilde{H}_r^1(\Omega)} \leq Ch \|u\|_{H_r^2(\Omega)}.$$

Now we are in a position to establish the main result of this paper.

Theorem 2.5.2 *Let (A, \mathbf{V}) be the solution of Problem 2.4.1 and (A^h, \mathbf{V}^h) the solution of Problem 2.5.1. There exists a constant $C > 0$, independent of h , such that if $A \in H_r^2(\Omega)$, then*

$$\|A - A^h\|_{\tilde{H}_r^1(\Omega)} + \sum_{k=1}^m |V_k - V_k^h| \leq Ch \|A\|_{H_r^2(\Omega)}.$$

Proof. It follows from Theorem 2.5.1 and Lemma 2.5.2. \square

The solution (A^h, \mathbf{V}^h) of Problem 2.5.1 allows us to compute the three-dimensional electromagnetic quantities. In fact, recalling (2.17) and (2.22), we define the computed magnetic induction by

$$\mathbf{B}^h := -\frac{\partial A^h}{\partial z} \mathbf{e}_r + \frac{1}{r} \frac{\partial(rA^h)}{\partial r} \mathbf{e}_z.$$

Analogously, from (2.12) and (2.23), the computed current density is given by

$$\mathbf{J}^h := J_\theta^h \mathbf{e}_\theta,$$

with J_θ^h vanishing in the dielectric and defined in the conductors as follows:

$$J_\theta^h|_{\Omega_k} := \sigma \left(\frac{V_k^h}{r} - i\omega A^h \right), \quad k = 0, 1, \dots, m,$$

where $V_0^h := V_0 = 0$ (cf. (2.27)). Notice that, in particular, the current density in the workpiece to be heated, which is typically the quantity of main interest, is given by $\mathbf{J}^h = -i\sigma\omega A^h \mathbf{e}_\theta$.

In what follows we obtain error estimates for these three-dimensional quantities.

Corollary 2.5.1 *Under the same hypotheses as in Theorem 2.5.2, we have*

$$\|\mathbf{B} - \mathbf{B}^h\|_{L^2(\tilde{\Omega})^3} \leq Ch \|A\|_{H_r^2(\Omega)}.$$

Proof. Recalling (2.17) and (2.22), we have

$$\begin{aligned} \|\mathbf{B} - \mathbf{B}^h\|_{L^2(\tilde{\Omega})^3}^2 &= \|\partial_z(A - A^h)\|_{L_r^2(\Omega)}^2 + \|\partial_r(r(A - A^h))\|_{L_{1/r}^2(\Omega)}^2 \\ &\leq \|\partial_z(A - A^h)\|_{L_r^2(\Omega)}^2 + 2\|\partial_r(A - A^h)\|_{L_r^2(\Omega)}^2 + 2\|A - A^h\|_{L_{1/r}^2(\Omega)}^2 \\ &\leq C\|A - A^h\|_{\tilde{H}_r^1(\Omega)}^2 \\ &\leq Ch \|A\|_{H_r^2(\Omega)}^2, \end{aligned}$$

where we have used Lemma 2.3.3 for the first inequality and Theorem 2.5.2 for the last one. \square

Corollary 2.5.2 *Under the same hypotheses as in Theorem 2.5.2, if for all $g \in L_r^2(\Omega)$ the solution Y_θ of Problem 2.4.3 satisfies $\|Y_\theta\|_{H_r^2(\Omega)} \leq C \|g\|_{L_r^2(\Omega)}$, then*

$$\|\mathbf{J} - \mathbf{J}^h\|_{L^2(\tilde{\Omega})^3} \leq Ch^2 \|A\|_{H_r^2(\Omega)}.$$

Proof. Since \mathbf{J} and \mathbf{J}^h vanish in the dielectric, we have

$$\|\mathbf{J} - \mathbf{J}^h\|_{L^2(\tilde{\Omega})^3}^2 = 2\pi \sum_{k=0}^m \|J_\theta - J_\theta^h\|_{L_r^2(\Omega_k)}^2.$$

Now, from (2.23) and the definition of J_θ^h , we have

$$\|J_\theta - J_\theta^h\|_{L_r^2(\Omega_k)} \leq C (|V_k - V_k^h| + \|A - A^h\|_{L_r^2(\Omega_k)}), \quad k = 0, 1, \dots, m$$

(recall $V_0^h = V_0 = 0$).

In what follows, we will use a duality argument to estimate $\|A - A^h\|_{L_r^2(\Omega)}$. With this end, for each $f \in L_r^2(\Omega)$, let $Y_\theta \in \tilde{H}_r^1(\Omega)$ denote the solution of the problem

$$a(Z, Y_\theta) = \int_{\Omega} Z \bar{f} r dr dz \quad \forall Z \in \tilde{H}_r^1(\Omega).$$

Because of Lemma 2.4.3 and the Lax-Milgram Lemma, this problem has a unique solution, which satisfies

$$\|Y_\theta\|_{\tilde{H}_r^1(\Omega)} \lambda^* C \|f\|_{L_r^2(\Omega)}.$$

Moreover, proceeding as was done to prove the equivalence of Problems 2.4.1 and 2.4.2, we have that Y_θ also solves Problem 2.4.3 with

$$g := f - i\omega\sigma Y_\theta + \sum_{k=1}^m \sigma \frac{W_k}{r} \chi_{\Omega_k},$$

where

$$W_k := \frac{i\omega}{d_k} \int_{\Omega_k} \sigma Y_\theta \, dr \, dz, \quad k = 1, \dots, m.$$

Therefore, according to the hypothesis of this corollary, the expression of g and the estimate for Y_θ above, there holds

$$\|Y_\theta\|_{\tilde{H}_r^1(\Omega)} \leq C \|g\|_{L_r^2(\Omega)} \leq C \|f\|_{L_r^2(\Omega)}. \quad (2.38)$$

Now we proceed with the duality argument:

$$\begin{aligned} \|A - A^h\|_{L_r^2(\Omega)} &= \sup_{f \in L_r^2(\Omega)} \frac{\left| \int_{\Omega} (A - A^h) \bar{f} r \, dr \, dz \right|}{\|f\|_{L_r^2(\Omega)}} \\ &= \sup_{f \in L_r^2(\Omega)} \frac{|a(A - A^h, Y_\theta)|}{\|f\|_{L_r^2(\Omega)}} \\ &= \sup_{f \in L_r^2(\Omega)} \frac{|a(A - A^h, Y_\theta - \Pi_h Y_\theta)|}{\|f\|_{L_r^2(\Omega)}} \\ &\leq \sup_{f \in L_r^2(\Omega)} \frac{Ch \|A\|_{H_r^2(\Omega)} h \|Y_\theta\|_{H_r^2(\Omega)}}{\|f\|_{L_r^2(\Omega)}} \\ &\leq Ch^2 \|A\|_{H_r^2(\Omega)}, \end{aligned}$$

where we have used the Galerkin orthogonality, Theorem 2.5.2, Lemma 2.5.2 and the estimate (2.38).

On the other hand, to estimate $|V_k - V_k^h|$, $k = 1, \dots, m$, we use (2.26), (2.37) and the estimate above, to write

$$|V_k - V_k^h| = \left| \frac{i\omega}{d_k} \int_{\Omega_k} \sigma (A - A^h) \, dr \, dz \right| \leq C \|A - A^h\|_{L_r^2(\Omega_k)} \leq Ch^2 \|A\|_{H_r^2(\Omega)}.$$

Thus, we conclude the proof. \square

Remark 2.5.1 As shown in the proof above, under the assumptions of this corollary, the computed constants V_k^h also converge quadratically.

Corollary 2.5.3 *If μ is constant in Ω , then*

$$\|\mathbf{B} - \mathbf{B}^h\|_{L^2(\tilde{\Omega})^3} \leq Ch \|\mathbf{I}\|_{\mathbb{C}^m} \quad \text{and} \quad \|\mathbf{J}^h - \mathbf{J}\|_{L^2(\tilde{\Omega})^3} \leq Ch^2 \|\mathbf{I}\|_{\mathbb{C}^m}.$$

Proof. It is a direct consequence of Corollaries 2.4.1, 2.5.1 and 2.5.2 and Theorem 2.4.2.

□

2.6 Numerical experiments

The numerical method analyzed above has been implemented in a FORTRAN code; several numerical tests have been already reported in [10]. In this section, we will apply this code to a couple of problems, to assess the orders of convergence proved for the physical quantities \mathbf{B} and \mathbf{J} . First, we will consider a problem with known analytical solution, which does not fit exactly in the theoretical framework considered in the previous sections. We will also apply the code to another problem lying in this framework: the simulation of an industrial furnace. Since no analytical solution is available in this case, we will assess the orders of convergence by comparing the obtained results with those obtained with the same method on extremely refined meshes.

2.6.1 Test 1: An example with analytical solution

Let us consider an infinite cylinder consisting of a core metal surrounded by a crucible and an extremely thin coil. The multi-turn coil is modeled as a continuous single coil with a uniform surface current density (see Figure 2.5). The solution of the electromagnetic problem can be obtained in the whole space, even for an axisymmetric crucible composed by different materials, provided the physical properties are constants in each material. We refer the reader to the appendix from [10] for further details.

In particular, for the problem described in Figure 2.5, the azimuthal component of the vector potential reads as follows:

$$A(r, z) = \begin{cases} \alpha_1 I_1(r\sqrt{i\omega\mu\sigma}), & 0 < r < R_1, \\ \alpha_2 I_1(r\sqrt{i\omega\mu\sigma}) + \beta_1 K_1(r\sqrt{i\omega\mu\sigma}), & R_1 < r < R_2, \\ \alpha_3 \mu_0 \frac{r}{2} + \frac{\beta_2}{r}, & R_2 < r < R_3, \\ \frac{\beta_{\text{ext}}}{r}, & r > R_3, \end{cases}$$

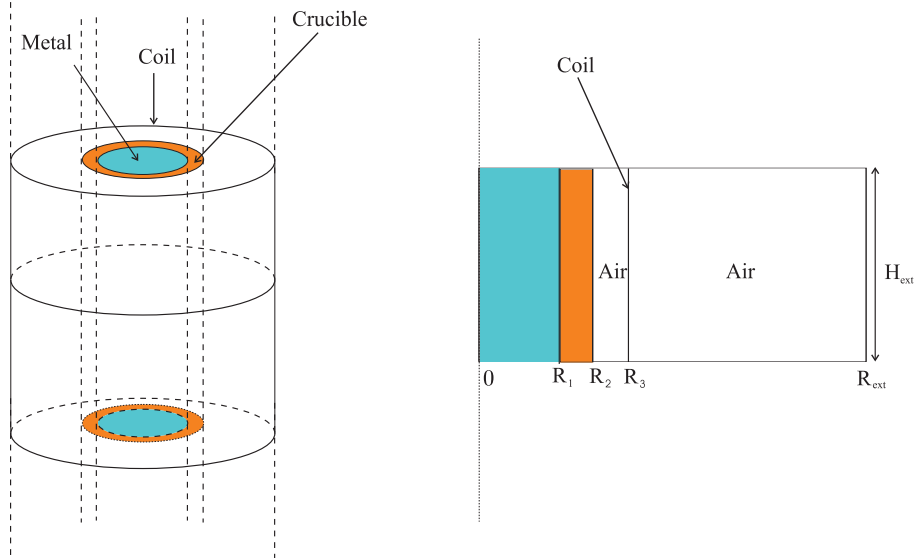


Figure 2.5: Test 1. Sketch of the domain.

with I_1 and K_1 being the first-order modified Bessel functions of the first and second kind, respectively. The coefficients μ and σ are constant in each material and the constants α_1 , α_2 , α_3 , β_1 , β_2 and β_{ext} are chosen so that A and $\frac{1}{\mu r} \frac{\partial(rA)}{\partial r}$ are continuous at $r = R_1$, $r = R_2$ and $r = R_3$.

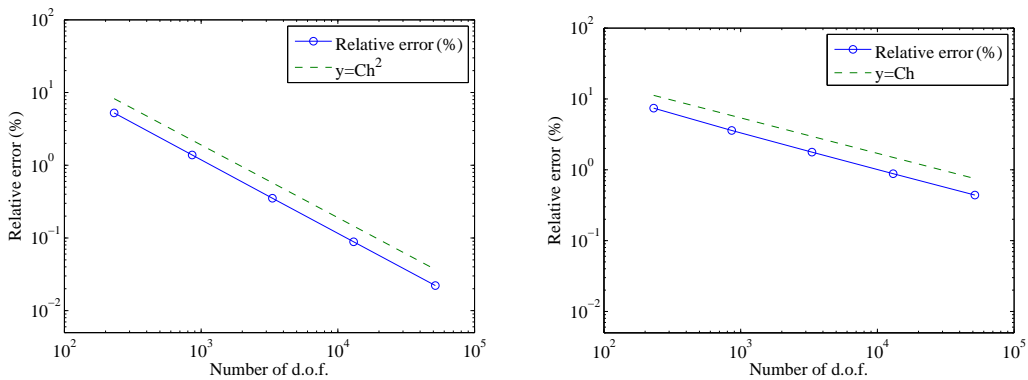
We denote by R_{ext} and H_{ext} the width and height of the rectangular box enclosing the domain for the finite element computations (see Figure 2.5, again). We remark that, in this case, due to the infinite height of the domain, the Robin condition (2.28) is not valid. For validation purposes, we will use exact Dirichlet boundary conditions, $A = \beta_{\text{ext}}/r$ at $r = R_{\text{ext}}$ and $A = 0$ at $r = 0$, and homogeneous Neumann conditions on the horizontal edges.

The geometrical data and physical parameters used for this problem are displayed in Table 2.1.

The numerical method has been used on several successively refined meshes and the obtained numerical approximations have been compared with the analytical solution. Figure 2.6 shows log-log plots of the errors in $L^2(\tilde{\Omega})^3$ -norm for the computed current density \mathbf{J} and the magnetic induction \mathbf{B} versus the number of degrees of freedom (d.o.f.). We can observe a quadratic dependence on the mesh-size h for \mathbf{J} and a linear dependence for \mathbf{B} , which agree with the theoretically predicted orders of convergence.

Table 2.1: Test 1. Geometrical data and physical parameters

Inner radius of crucible (R_1):	0.05 m
Outer radius of crucible (R_2):	0.07 m
Radius of the induction coil (R_3):	0.09 m
R_{ext} :	0.2 m
H_{ext} :	0.1 m
Frequency:	3700 Hz
RMS intensity/unit of length:	30460 Am^{-1}
Electrical conductivity of metal:	$1234568 (\text{Ohm m})^{-1}$
Electrical conductivity of crucible:	$240000 (\text{Ohm m})^{-1}$
Magnetic permeability of all materials:	$4\pi 10^{-7} \text{ Hm}^{-1}$

Figure 2.6: Test 1. Relative errors $\|\mathbf{J}^h - \mathbf{J}\|_{L^2(\tilde{\Omega})^3}/\|\mathbf{J}^h\|_{L^2(\tilde{\Omega})^3}$ (left) and $\|\mathbf{B}^h - \mathbf{B}\|_{L^2(\tilde{\Omega})^3}/\|\mathbf{B}^h\|_{L^2(\tilde{\Omega})^3}$ (right) versus number of d.o.f. (log-log scale).

2.6.2 Test 2: Simulation of an industrial furnace

Our next goal is to study the convergence behavior of the method applied to a problem lying in the framework of the theoretical results. With this aim, we have considered the simulation of an industrial problem: a small furnace composed of a graphite crucible containing silicon in its interior and a 4-turns coil (see Figure 2.7). The geometrical and physical data are displayed in Table 2.2.

Since in this case there is no analytical solution to compare with, we have used a reference solution \mathbf{J}_{ref} and \mathbf{B}_{ref} computed with the same finite element method over an

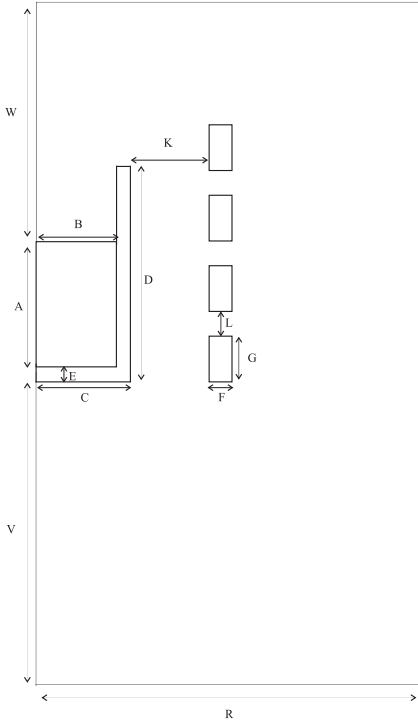


Figure 2.7: Test 2. Sketch of the geometry of the industrial furnace.

extremely fine mesh. The numerical approximations \mathbf{J}^h and \mathbf{B}^h obtained with several successively refined meshes have been compared with the reference ones. Figure 2.8 shows the coarsest used mesh. Figure 2.9 shows log-log plots of the corresponding errors measured in $L^2(\tilde{\Omega})^3$ -norm versus the number of degrees of freedom for different meshes. Notice that a quadratic dependence for \mathbf{J} and a linear dependence for \mathbf{B} can be observed again.

We have also compared the computed constants V_1^h, \dots, V_4^h with those corresponding to the reference solution. Figure 2.10 shows log-log plots of the errors for each constant versus the number of degrees of freedom for the different meshes. In this case, a quadratic order of convergence can be clearly appreciated, in agreement with Remark 2.5.1.

Finally, let us remark that the method proposed in this paper has an additional source of error which cannot be appreciated from Figure 2.9: the effect of truncating the domain and imposing homogeneous Robin and Neumann conditions (2.28) and (2.29), respectively. In principle, these boundary conditions are approximately fulfilled by the physical solution, as long as the artificial boundaries Γ_R and Γ_N are sufficiently far from the conductors. To test this effect, we have also solved the problem in two other domains, Ω_1 and Ω_2 , larger than Ω . We denote now $\Omega_0 := \Omega$ and \mathbf{J}_i and \mathbf{B}_i the current density and the

Table 2.2: Test 2. Geometrical data and physical parameters

Height of silicon (A):	0.046 m
Inner radius of crucible (B):	0.021 m
Outer radius of crucible (C):	0.025 m
Crucible height (D):	0.08 m
Crucible width (E):	0.004 m
Coil diameter (F):	0.005 m
Coil height (G):	0.02 m
Distance coil-crucible (K):	0.035 m
Distance between coil turns (L):	0.006 m
Vertical distance from crucible to the bottom (V):	0.5 m
Vertical distance from silicon to the top (W):	0.45 m
Width of the rectangular box (R):	0.5 m
Number of coil turns:	4
Frequency:	3700 Hz
RMS coil current (in each turn):	3000 A
Electrical conductivity of silicon:	$1234568 \text{ (Ohm m)}^{-1}$
Electrical conductivity of crucible (graphite):	$240000 \text{ (Ohm m)}^{-1}$
Electrical conductivity of coil (copper):	$2 \times 10^7 \text{ (Ohm m)}^{-1}$
Magnetic permeability of all materials:	$4\pi 10^{-7} \text{ Hm}^{-1}$

magnetic induction computed using the artificial domains Ω_i , $i = 0, 1, 2$. Table 2.3 shows the geometrical data and relative errors of these quantities computed on each domain with meshes which coincide in Ω_c . It can be seen from this table that the errors arising from truncating the domain are smaller than the discretization error.

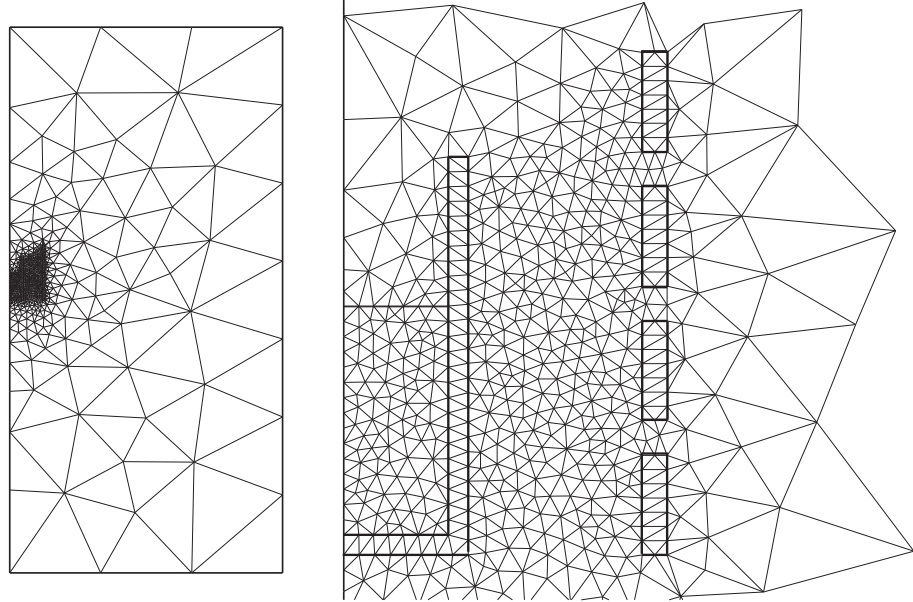


Figure 2.8: Test 2. Initial mesh: global view (left) and detail near the workpiece (right).

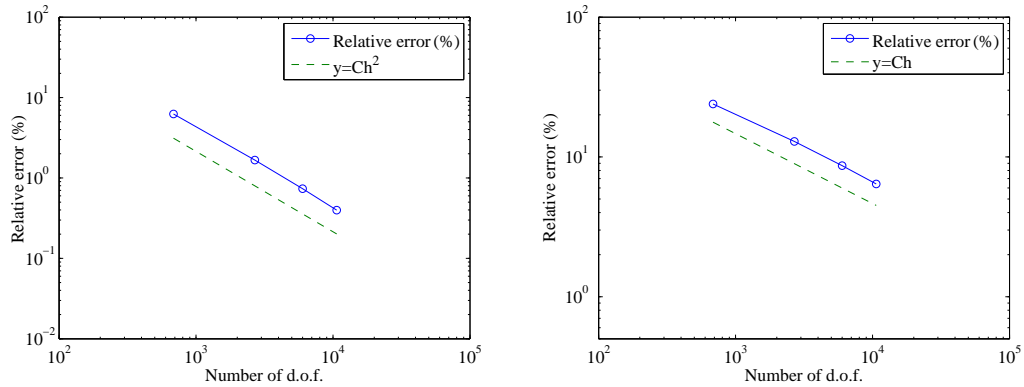


Figure 2.9: Test 2. Relative errors $\|\mathbf{J}^h - \mathbf{J}_{\text{ref}}\|_{L^2(\tilde{\Omega})^3}/\|\mathbf{J}^h\|_{L^2(\tilde{\Omega})^3}$ (left) and $\|\mathbf{B}^h - \mathbf{B}_{\text{ref}}\|_{L^2(\tilde{\Omega})^3}/\|\mathbf{B}^h\|_{L^2(\tilde{\Omega})^3}$ (right) versus number of d.o.f. (log-log scale).

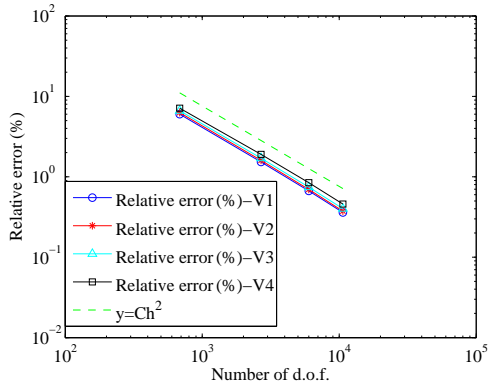


Figure 2.10: Test 2. Relative errors versus number of d.o.f. (log-log scale) for V_1 , V_2 , V_3 and V_4 .

Table 2.3: Test 2. Comparison on different artificial domains

Domain	V	W	R	Errors in $\mathbf{J} _{\Omega_c}$		Errors in $\mathbf{B} _{\Omega_c}$	
				$\frac{\ \mathbf{J}_0 - \mathbf{J}_{\text{ref}}\ _{\Omega_c}}{\ \mathbf{J}_0\ _{\Omega_0}} = 0.73\%$	$\frac{\ \mathbf{B}_0 - \mathbf{B}_{\text{ref}}\ _{\Omega_c}}{\ \mathbf{B}_0\ _{\Omega_0}} = 5.45\%$	$\frac{\ \mathbf{B}_1 - \mathbf{B}_0\ _{\Omega_c}}{\ \mathbf{B}_0\ _{\Omega_0}} = 0.44\%$	$\frac{\ \mathbf{B}_2 - \mathbf{B}_0\ _{\Omega_c}}{\ \mathbf{B}_0\ _{\Omega_0}} = 0.56\%$
Ω_0	0.50 m	0.45 m	0.50 m	$\frac{\ \mathbf{J}_0 - \mathbf{J}_{\text{ref}}\ _{\Omega_c}}{\ \mathbf{J}_0\ _{\Omega_0}} = 0.73\%$	$\frac{\ \mathbf{B}_0 - \mathbf{B}_{\text{ref}}\ _{\Omega_c}}{\ \mathbf{B}_0\ _{\Omega_0}} = 5.45\%$		
Ω_1	0.75 m	0.70 m	0.75 m	$\frac{\ \mathbf{J}_1 - \mathbf{J}_0\ _{\Omega_c}}{\ \mathbf{J}_0\ _{\Omega_0}} = 0.22\%$		$\frac{\ \mathbf{B}_1 - \mathbf{B}_0\ _{\Omega_c}}{\ \mathbf{B}_0\ _{\Omega_0}} = 0.44\%$	
Ω_2	1.00 m	0.95 m	1.00 m	$\frac{\ \mathbf{J}_2 - \mathbf{J}_0\ _{\Omega_c}}{\ \mathbf{J}_0\ _{\Omega_0}} = 0.25\%$		$\frac{\ \mathbf{B}_2 - \mathbf{B}_0\ _{\Omega_c}}{\ \mathbf{B}_0\ _{\Omega_0}} = 0.56\%$	

Chapter 3

Mathematical and numerical analysis of a transient eddy current axisymmetric problem involving velocity terms

3.1 Introduction

The main goal of this paper is to analyze a numerical method to solve a transient eddy current axisymmetric problem. We consider the case of a coil supplied with a source current generating a magnetic field which induces eddy currents in a nearby workpiece. This classical model appears in many physical phenomena such as induction heating, electromagnetic stirring, magnetohydrodynamics or electromagnetic forming. In each case the induced currents in the workpiece have different roles (moving a fluid, heating or deforming the workpiece, etc); see for instance [7, 12, 24, 35, 46].

The cylindrical symmetry allows stating the eddy current problem in terms of the azimuthal component of a magnetic vector potential defined in a meridional section of the domain (see, for instance, [13]). We consider transient problems and assume a more general Ohm's law including velocity terms, which can be relevant in some industrial applications. As a consequence, we obtain a degenerate parabolic problem including convective terms which introduce interesting aspects in its mathematical and numerical analysis.

From a mathematical point of view, we cannot use the classical theory for abstract

parabolic problems (see, for instance, [25]) because our formulation is degenerate. More precisely, the term involving the time derivative appears only in a part of the domain. Thus, in order to prove well-posedness, we resort to the theory for degenerate evolution problems proposed in [56]. On the other hand, the velocity term in the Ohm's law introduces a non-symmetric term which destroys the elliptic character of the bilinear form associated with the parabolic problem. However, we prove that a Gårding-like inequality holds, which allows us to use the theory from [56] by means of an exponential shift.

For the numerical solution of the problem, we discretize first in space by finite elements. This leads to a singular differential algebraic system (see [18]) which is proved to be well posed. We prove error estimates for this semi-discrete approximation. To do this, we adapt the classical theory (see [25]) to the degenerate character of the parabolic problem and the fact that the bilinear form is no longer elliptic. Then, we combine the finite element discretization with a backward Euler time-discretization. We prove error estimates for this fully discretized scheme by adapting once more the classical theory to the non-elliptic character of the bilinear form. Because of this, the error estimates are valid provided the time step is sufficiently small with respect to the physical data of the problem.

The outline of the paper is as follows: In Section 3.2, we describe the transient eddy current model and introduce a magnetic vector potential formulation under axisymmetric assumptions. In Section 3.3, we state the weak formulation and prove its well-posedness. In Section 3.4, we introduce the finite element space discretization and prove error estimates. In Section 3.5, we propose a backward Euler scheme for time discretization and prove error estimates for the fully discretized problem. Finally, in Section 3.6, we report some numerical tests which allow us to asses the performance of the proposed method.

3.2 Statement of the problem

We are interested in computing the eddy currents induced in a cylindrical workpiece by a nearby helical coil (see Figure 3.1 for possible configurations). The material on the workpiece is allowed to move, although without changing its domain.

In order to have a domain with cylindrical symmetry, we replace the coil by several superimposed rings with toroidal geometry. On the other hand, to solve the electromagnetic model in a bounded domain, we introduce a sufficiently large three dimensional cylinder $\tilde{\Omega}$ of radius R and height L containing the coil and the workpiece.

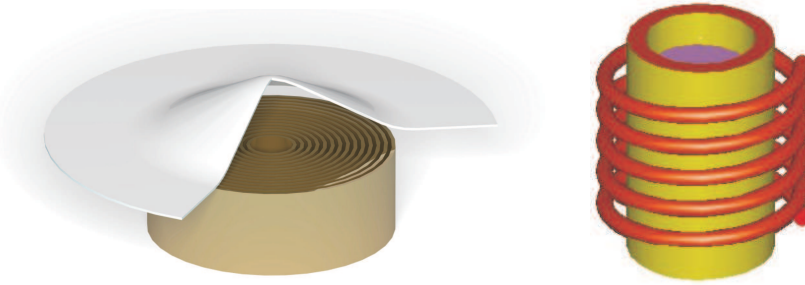


Figure 3.1: Sketch of the 3D-domain in some industrial applications.

Because of the cylindrical symmetry, we can work on a meridional section of $\tilde{\Omega}$, which we denote by Ω . Let $\Omega_S := \Omega_1 \cup \dots \cup \Omega_m$, where Ω_k ($k = 1, \dots, m$) are the meridional sections of the turns of the coil. Let Ω_0 be the corresponding section of the workpiece and $\Omega_A := \Omega \setminus (\overline{\Omega}_S \cup \overline{\Omega}_0)$ the section of the domain occupied by the air. Let Γ_0 be the intersection between $\partial\Omega$ and the symmetry axis ($r = 0$) and $\Gamma_D := \partial\Omega \setminus \Gamma_0$ (see Figure 3.2).

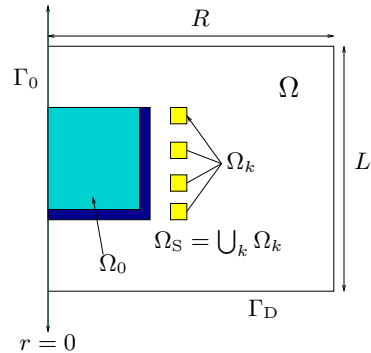


Figure 3.2: Sketch of the meridional section.

We will use standard notation:

- \mathbf{E} is the electric field,
- \mathbf{B} is the magnetic induction,
- \mathbf{H} is the magnetic field,
- \mathbf{J} is the current density,
- μ is the magnetic permeability,

- σ is the electric conductivity.

The physical parameters are supposed to satisfy:

$$0 < \underline{\mu} \leq \mu \leq \bar{\mu}, \quad (3.1)$$

$$0 < \underline{\sigma} \leq \sigma \leq \bar{\sigma} \quad \text{in conductors,} \quad (3.2)$$

$$\sigma = 0 \quad \text{in dielectrics.} \quad (3.3)$$

These parameters are assumed not to vary with time. This implies that the part of the workpiece subjected to motion has to be homogeneous (i.e., the parameters σ and μ are assumed to be constant on that part).

In this kind of problem, the electric displacement can be neglected in Ampère's law leading to the so called eddy current model:

$$\operatorname{curl} \mathbf{H} = \mathbf{J}, \quad (3.4)$$

$$\frac{\partial \mathbf{B}}{\partial t} + \operatorname{curl} \mathbf{E} = \mathbf{0}, \quad (3.5)$$

$$\operatorname{div} \mathbf{B} = 0. \quad (3.6)$$

This system must be completed with the following relations:

$$\mathbf{B} = \mu \mathbf{H}, \quad (3.7)$$

and

$$\mathbf{J} = \begin{cases} \sigma \mathbf{E} + \sigma \mathbf{v} \times \mathbf{B} & \text{in the workpiece,} \\ \mathbf{J}_S & \text{in the coil (data),} \\ \mathbf{0} & \text{in the air.} \end{cases} \quad (3.8)$$

The vector field \mathbf{v} in (3.8) represents the velocity of the material in the workpiece, which in the present analysis is taken as a data. The current density is taken as data in the coil (\mathbf{J}_S) and unknown in the workpiece Ω_0 . In the latter, \mathbf{J} results from the eddy currents ($\sigma \mathbf{E}$) and the currents due to the motion of the workpiece ($\sigma \mathbf{v} \times \mathbf{B}$).

We assume that all the physical quantities are independent of the angular coordinate θ and that the current density field has only azimuthal non-zero component, i.e.,

$$\mathbf{J}(r, \theta, z) = J(r, z) \mathbf{e}_\theta. \quad (3.9)$$

We also assume that the velocity has only meridional components, $\mathbf{v} = v_r(r, z) \mathbf{e}_r + v_z(r, z) \mathbf{e}_z$, as corresponds to an axisymmetric problem.

Proceeding as in [13], it can be shown that

$$\mathbf{H}(r, \theta, z) = H_r(r, z)\mathbf{e}_r + H_z(r, z)\mathbf{e}_z, \quad (3.10)$$

$$\mathbf{B}(r, \theta, z) = B_r(r, z)\mathbf{e}_r + B_z(r, z)\mathbf{e}_z, \quad (3.11)$$

$$\mathbf{E}(r, \theta, z) = E(r, z)\mathbf{e}_\theta \quad \text{in the workpiece.} \quad (3.12)$$

Moreover, from (3.6), the arguments in [13] allow us to introduce a vector potential \mathbf{A} for \mathbf{B} ,

$$\mathbf{B} = \mathbf{curl} \mathbf{A}, \quad (3.13)$$

of the form

$$\mathbf{A}(r, \theta, z) = A(r, z)\mathbf{e}_\theta. \quad (3.14)$$

Using (3.13) in (3.5), we obtain $\mathbf{curl}(\frac{\partial \mathbf{A}}{\partial t} + \mathbf{E}) = \mathbf{0}$ in the workpiece. On the other hand, using (3.12) and (3.14), from the expression of the **curl** in cylindrical coordinates we obtain

$$\frac{1}{r} \left\{ \frac{\partial}{\partial z} \left[r \left(\frac{\partial A}{\partial t} + E \right) \right] \mathbf{e}_r + \frac{\partial}{\partial r} \left[r \left(\frac{\partial A}{\partial t} + E \right) \right] \mathbf{e}_z \right\} = \mathbf{0}.$$

Hence we deduce that

$$r \left(\frac{\partial A}{\partial t} + E \right) = C,$$

with C an arbitrary constant. This constant has to vanish in most cases of interest. In fact, typically $\partial\Omega_0$ intersects Γ_0 in a set with a non vanishing 1D measure (for instance in the cases depicted in Figure 3.1). In such a case, it is immediate to show that for $\frac{\partial A}{\partial t} + E = \frac{C}{r}$ to be square integrable in the workpiece, C has to vanish. Hence, we write

$$\frac{\partial A}{\partial t} + E = 0 \quad \text{in } \Omega_0.$$

Therefore, substituting this expression in (3.8), we obtain

$$J\mathbf{e}_\theta = \begin{cases} -\sigma \frac{\partial A}{\partial t} \mathbf{e}_\theta + \sigma \mathbf{v} \times \mathbf{curl}(A\mathbf{e}_\theta) & \text{in } \Omega_0, \\ J_S \mathbf{e}_\theta & \text{in } \Omega_S, \\ \mathbf{0} & \text{in } \Omega_A. \end{cases} \quad (3.15)$$

On the other hand, using (3.4), (3.7), (3.9), (3.13), and (3.14), we have

$$\mathbf{curl} \left[\frac{1}{\mu} \mathbf{curl}(A\mathbf{e}_\theta) \right] = J\mathbf{e}_\theta,$$

Thus, we are led to the following parabolic-elliptic problem:

$$\left\{ \begin{array}{ll} \sigma \frac{\partial A}{\partial t} \mathbf{e}_\theta + \mathbf{curl} \left[\frac{1}{\mu} \mathbf{curl} (A \mathbf{e}_\theta) \right] - \mathbf{v} \times \mathbf{curl} (A \mathbf{e}_\theta) = \mathbf{0} & \text{in } \Omega_0, \\ \mathbf{curl} \left[\frac{1}{\mu} \mathbf{curl} (A \mathbf{e}_\theta) \right] = J_S \mathbf{e}_\theta & \text{in } \Omega_S, \\ \mathbf{curl} \left[\frac{1}{\mu} \mathbf{curl} (A \mathbf{e}_\theta) \right] = \mathbf{0} & \text{in } \Omega_A. \end{array} \right. \quad (3.16)$$

Finally we impose homogeneous Dirichlet boundary conditions for the vector potential A on Γ_D , which makes sense provided Γ_D has been chosen sufficiently far away from Ω_0 and Ω_S .

3.3 Weak Formulation

In this section we will obtain a weak formulation of the electromagnetic model given above and prove its well-posedness. Let $L_r^2(\Omega)$ be the weighted Lebesgue space of all measurable functions Z defined in Ω such that

$$\|Z\|_{L_r^2(\Omega)}^2 := \int_{\Omega} |Z|^2 r dr dz < \infty.$$

Clearly, $Z \mathbf{e}_\theta \in L^2(\tilde{\Omega})^3$ if and only if $Z \in L_r^2(\Omega)$. We will use $(\cdot, \cdot)_{L_r^2(\Omega)}$ to denote the corresponding inner product. The weighted Sobolev space $H_r^k(\Omega)$ consists of all functions in $L_r^2(\Omega)$ whose derivatives up to the order k are also in $L_r^2(\Omega)$. We define the norms and seminorms in the standard way; in particular

$$|Z|_{H_r^1(\Omega)}^2 := \int_{\Omega} (|\partial_r Z|^2 + |\partial_z Z|^2) r dr dz.$$

Let $L_{1/r}^2(\Omega)$ be the weighted Lebesgue space of all measurable functions Z defined in Ω such that

$$\|Z\|_{L_{1/r}^2(\Omega)}^2 := \int_{\Omega} \frac{|Z|^2}{r} dr dz < \infty.$$

Let us define the Hilbert space

$$\tilde{H}_r^1(\Omega) := \{Z \in H_r^1(\Omega) : Z \in L_{1/r}^2(\Omega)\},$$

with the norm

$$\|Z\|_{\tilde{H}_r^1(\Omega)} := \left[\|Z\|_{H_r^1(\Omega)}^2 + \|Z\|_{L_{1/r}^2(\Omega)}^2 \right]^{1/2}.$$

It is well known (see [16, 36]) that $Z\mathbf{e}_\theta \in H^1(\tilde{\Omega})^3$ if and only if $Z \in \tilde{H}_r^1(\Omega)$. Finally, let

$$\mathcal{V} := \{Z \in \tilde{H}_r^1(\Omega) : Z = 0 \text{ on } \Gamma_D\}$$

and

$$\mathcal{V}_0 := \tilde{H}_r^1(\Omega_0).$$

Regarding the data of our problem we assume that \mathbf{v} is bounded, i.e.,

$$|\mathbf{v}(t, r, z)| \leq \|\mathbf{v}\|_\infty \quad \forall t \in [0, T] \quad \forall (r, z) \in \Omega_0,$$

and $J_S \in L^2(0, T; L_r^2(\Omega_S))$.

By testing (3.16) with $Z\mathbf{e}_\theta$, $Z \in \mathcal{V}$, we obtain

$$\begin{aligned} & \int_{\Omega_0} \sigma \partial_t A Z r dr dz + \int_{\Omega} \frac{1}{\mu} \operatorname{curl}(A \mathbf{e}_\theta) \cdot \operatorname{curl}(Z \mathbf{e}_\theta) r dr dz \\ & - \int_{\Omega_0} \sigma \mathbf{v} \times \operatorname{curl}(A \mathbf{e}_\theta) \cdot (Z \mathbf{e}_\theta) r dr dz = \int_{\Omega_S} J_S Z r dr dz. \end{aligned} \quad (3.17)$$

We have to add to this equation an initial condition $A(0) = A^0$ in Ω_0 .

We define the bilinear forms

$$\begin{aligned} \tilde{a}(Y, Z) &:= \int_{\Omega} \frac{1}{\mu} \operatorname{curl}(Y \mathbf{e}_\theta) \cdot \operatorname{curl}(Z \mathbf{e}_\theta) r dr dz, \quad Y, Z \in \mathcal{V}, \\ c(t, Y, Z) &:= - \int_{\Omega_0} \sigma \mathbf{v}(t) \times \operatorname{curl}(Y \mathbf{e}_\theta) \cdot (Z \mathbf{e}_\theta) r dr dz, \quad Y, Z \in \mathcal{V}, \end{aligned}$$

and

$$a(t, Y, Z) := \tilde{a}(Y, Z) + c(t, Y, Z). \quad (3.18)$$

Let \mathcal{V}'_0 be the dual space of \mathcal{V}_0 with respect to the pivot space $L_r^2(\Omega_0)$ with measure $\sigma r dr dz$ (which according to (3.2) is topologically equivalent to $L_r^2(\Omega_0)$ with measure $r dr dz$). Let us define the space

$$\mathcal{W}_0 := \{Y \in L^2(0, T; \mathcal{V}) : \partial_t Y \in L^2(0, T; \mathcal{V}'_0)\}.$$

Thus, from (3.17), we arrive at the following problem:

Problem 3.3.1 Find $A \in \mathcal{W}_0$ such that

$$\begin{cases} \langle \partial_t A, Z \rangle_{\mathcal{V}'_0 \times \mathcal{V}_0} + a(t, A, Z) = (J_S, Z)_{L_r^2(\Omega_S)} & \forall Z \in \mathcal{V}, \\ A(0)|_{\Omega_0} = A^0. \end{cases}$$

The initial data A^0 is taken in $L_r^2(\Omega_0)$. Let us remark that this initial condition makes sense because $\mathcal{W}_0 \hookrightarrow \mathcal{C}^0(0, T; L_r^2(\Omega_0))$ (see [55], for instance).

It is simple to show that \tilde{a} is \mathcal{V} -elliptic (see [29, Prop. 2.1]); namely, there exists $\alpha > 0$ such that

$$\tilde{a}(Z, Z) \geq \alpha \|Z\|_{\tilde{H}_r^1(\Omega)}^2 \quad \forall Z \in \mathcal{V}. \quad (3.19)$$

Our next step is to prove a Gårding-like inequality for the bilinear form a .

Lemma 3.3.1 *Let $\lambda^* := \|\mathbf{v}\|_\infty^2 \bar{\sigma}/\alpha$. For all $\lambda \geq \lambda^*$ and for all $Z \in \mathcal{V}$,*

$$a(t, Z, Z) + \lambda (\sigma Z, Z)_{L_r^2(\Omega_0)} \geq \frac{\alpha}{2} \|Z\|_{\tilde{H}_r^1(\Omega)}^2 \quad \forall t \in [0, T].$$

Proof. First, we estimate the term $c(t, Z, Z)$. With this aim, we use the expression of $\operatorname{curl}(Ze_\theta)$ in cylindrical coordinates to write

$$c(t, Z, Z) = \int_{\Omega_0} \sigma v_r \frac{1}{r} \frac{\partial(rZ)}{\partial r} Z r dr dz - \int_{\Omega_0} \sigma v_z \frac{\partial Z}{\partial z} Z r dr dz.$$

Then, we use a weighted Cauchy-Schwartz inequality to obtain for all $\epsilon > 0$ and all $t \in [0, T]$

$$\begin{aligned} & \left| \int_{\Omega_0} \sigma v_r \frac{1}{r} \frac{\partial(rZ)}{\partial r} Z r dr dz \right| \\ & \leq \epsilon \left[\|\partial_r Z\|_{L_r^2(\Omega_0)}^2 + \|Z\|_{L_{1/r}^2(\Omega_0)}^2 \right] + \frac{\bar{\sigma} \|v_r\|_\infty^2}{4\epsilon} \|\sigma^{1/2} Z\|_{L_r^2(\Omega_0)}^2 \end{aligned}$$

and

$$\left| \int_{\Omega_0} \sigma v_z \frac{\partial Z}{\partial z} Z r dr dz \right| \leq \epsilon \|\partial_z Z\|_{L_r^2(\Omega_0)}^2 + \frac{\|v_z\|_\infty^2 \bar{\sigma}}{4\epsilon} \|\sigma^{1/2} Z\|_{L_r^2(\Omega_0)}^2.$$

Hence

$$|c(t, Z, Z)| \leq 2\epsilon \|Z\|_{\tilde{H}_r^1(\Omega)}^2 + \frac{\|\mathbf{v}\|_\infty^2 \bar{\sigma}}{4\epsilon} \|\sigma^{1/2} Z\|_{L_r^2(\Omega_0)}^2.$$

Therefore, from this inequality and (3.19),

$$\begin{aligned} a(t, Z, Z) + \lambda (\sigma Z, Z)_{L_r^2(\Omega_0)} &= \tilde{a}(Z, Z) + c(t, Z, Z) + \lambda \|\sigma^{1/2} Z\|_{L_r^2(\Omega_0)}^2 \\ &\geq (\alpha - 2\epsilon) \|Z\|_{\tilde{H}_r^1(\Omega)}^2 + \left(\lambda - \frac{\|\mathbf{v}\|_\infty^2 \bar{\sigma}}{4\epsilon} \right) \|\sigma^{1/2} Z\|_{L_r^2(\Omega_0)}^2. \end{aligned}$$

Thus, the lemma holds by taking $\epsilon = \alpha/4$. \square

Now, we are in a position to prove the main theorem of this section. In its proof and throughout the paper C will denote a constant not necessarily the same at each occurrence.

Theorem 3.3.1 *Problem 3.3.1 has a unique solution $A \in \mathcal{W}_0$ and there exists a positive constant C independent of the data of the problem, J_S and A^0 , such that*

$$\|A\|_{L^2(0,T;\tilde{H}_r^1(\Omega))} \leq C \left[\|J_S\|_{L^2(0,T;L_r^2(\Omega_S))}^2 + \|A^0\|_{L_r^2(\Omega_0)}^2 \right]^{1/2}.$$

Proof. Let $\lambda \geq \lambda^*$, with λ^* as in Lemma 3.3.1, and $\hat{A} := e^{-\lambda t} A$. Then, A is a solution of Problem 3.3.1 if and only if $\hat{A} \in \mathcal{W}_0$ is a solution of the following problem:

$$\begin{cases} \langle \partial_t \hat{A}, Z \rangle_{\mathcal{V}_0' \times \mathcal{V}_0} + \hat{a}(t, \hat{A}, Z) = (J_S, Z)_{L_r^2(\Omega_S)} & \forall Z \in \mathcal{V}, \\ \hat{A}(0)|_{\Omega_0} = A^0, \end{cases} \quad (3.20)$$

where

$$\hat{a}(t, \hat{A}, Z) := a(t, \hat{A}, Z) + \lambda(\sigma \hat{A}, Z)_{L_r^2(\Omega_0)}.$$

Lemma 3.3.1 guarantees that $\hat{a}(t, \hat{A}, \hat{A}) \geq \frac{\alpha}{2} \|\hat{A}\|_{\tilde{H}_r^1(\Omega)}^2$. Hence, the existence of a unique solution of problem (3.20) follows from [56, Theorem 2] (see also [57]).

Next, testing the first equation of (3.20) with $Z = \hat{A}$ and integrating with respect to time, we obtain (see [44, Prop. 1.2])

$$\frac{1}{2} \int_0^T \frac{d}{dt} (\sigma \hat{A}, \hat{A})_{L_r^2(\Omega_0)} dt + \int_0^T \hat{a}(t, \hat{A}, \hat{A}) dt = \int_0^T (J_S, \hat{A})_{L_r^2(\Omega_S)} dt.$$

Consequently,

$$\begin{aligned} \|\sigma^{1/2} \hat{A}(T)\|_{L_r^2(\Omega_0)}^2 - \|\sigma^{1/2} \hat{A}(0)\|_{L_r^2(\Omega_0)}^2 + \frac{\alpha}{2} \|\hat{A}\|_{L^2(0,T;\tilde{H}_r^1(\Omega))}^2 \\ \leq \|J_S\|_{L^2(0,T;L_r^2(\Omega_S))} \|\hat{A}\|_{L^2(0,T;\tilde{H}_r^1(\Omega))} \end{aligned}$$

and hence

$$\|\hat{A}\|_{L^2(0,T;\tilde{H}_r^1(\Omega))}^2 \leq C \left[\|J_S\|_{L^2(0,T;L_r^2(\Omega_S))}^2 + \|\hat{A}(0)\|_{L_r^2(\Omega_0)}^2 \right].$$

Therefore, by using that $A = e^{\lambda t} \hat{A}$ and the initial condition of problem (3.20), we conclude the proof. \square

3.4 Semi-discrete problem

From now on we assume that Ω_0 is a polygonal domain. Let $\{\mathcal{T}_h\}_{h>0}$ be a regular family of triangulations of Ω such that each element $T \in \mathcal{T}_h$ is contained either in $\overline{\Omega}_0$ or in $\overline{\Omega \setminus \Omega_0}$. Therefore

$$\mathcal{T}_h^0 := \{T \in \mathcal{T}_h : T \subset \Omega_0\}$$

is a triangulation of Ω_0 . The parameter h stands for the mesh-size. Let

$$\mathcal{V}_h := \{A_h \in \mathcal{V} : A_h|_T \in \mathbb{P}_1 \forall T \in \mathcal{T}_h\}$$

and

$$\mathcal{V}_h^0 := \{A_h \in \mathcal{V}_0 : A_h|_T \in \mathbb{P}_1 \forall T \in \mathcal{T}_h^0\},$$

where

$$\mathbb{P}_1 := \{p(r, z) = c_0 + c_1 r + c_2 z, c_0, c_1, c_2 \in \mathbb{R}\}.$$

We consider the Lagrange interpolation operator $\mathcal{I}_h \in \mathcal{L}(H_r^2(\Omega), \mathcal{V}_h)$. The proof of the following estimate can be found in [36, Prop. 6.1].

Theorem 3.4.1 *There exists a positive constant C , independent of h , such that for all $Z \in \mathcal{V} \cap H_r^2(\Omega)$*

$$\|Z - \mathcal{I}_h Z\|_{\tilde{H}_r^1(\Omega)} \leq Ch \|Z\|_{H_r^2(\Omega)}.$$

By using this finite element space we are led to the following discretization of Problem 3.3.1:

Problem 3.4.1 *Find $A_h \in H^1(0, T; \mathcal{V}_h)$ such that*

$$\begin{cases} (\sigma \partial_t A_h, Z_h)_{L_r^2(\Omega_0)} + a(t, A_h, Z_h) = (J_S, Z_h)_{L_r^2(\Omega_S)} & \forall Z_h \in \mathcal{V}_h, \\ A_h(0)|_{\Omega_0} = A_h^0. \end{cases}$$

The initial data A_h^0 has to belong to \mathcal{V}_h^0 and should be a reasonable approximation to A^0 . Provided the latter is sufficiently smooth, a natural choice is $A_h^0 = \mathcal{I}_h A^0$, for instance. Moreover, because of the degenerate character of the problem, for its solution to lie in $H^1(0, T; \mathcal{V}_h)$, we will have to assume additional regularity in time of the source current. In fact, from now on we assume

$$J_S \in H^1(0, T; L_r^2(\Omega_S)). \quad (3.21)$$

We note that Problem 3.4.1 is a linear system of ordinary differential-algebraic equations. To prove that this system has a unique solution, we will write it in matrix form.

With this aim, let $\{\phi_1, \dots, \phi_N\}$ be the nodal basis of \mathcal{V}_h ordered in such a way that $\{\phi_1|_{\Omega_0}, \dots, \phi_M|_{\Omega_0}\}$ ($M < N$) is a basis of \mathcal{V}_h^0 . For all $t \in [0, T]$, a solution A_h to Problem 3.4.1 can be written as follows:

$$A_h(t, r, z) = \sum_{i=1}^N A_i(t) \phi_i(r, z).$$

Analogously we write

$$A_h^0 = \sum_{i=1}^M A_i^0 \phi_i|_{\Omega_0}.$$

For all $t \in [0, T]$, we set $\mathcal{A}(t) := (A_i(t))_{1 \leq i \leq N}$ and $\mathcal{F}(t) := ((J_S(t), \phi_i)_{L_r^2(\Omega_S)})_{1 \leq i \leq N}$. We also set $\mathcal{A}^0 := (A_i^0)_{1 \leq i \leq M}$.

We introduce the matrices $\mathcal{K}(t) := (K_{ij}(t))_{1 \leq i, j \leq N}$ and $\mathcal{M} := (M_{ij})_{1 \leq i, j \leq N}$, with

$$K_{ij}(t) := a(t, \phi_i, \phi_j), \quad M_{ij} := (\sigma \phi_i, \phi_j)_{L_r^2(\Omega_0)}, \quad 1 \leq i, j \leq N.$$

Since the initial condition in Problem 3.4.1 involves only the components of $A_h(0)$ which correspond to the nodes in the conducting domain Ω_0 , we decompose $\mathcal{A}(t)$ as follows:

$$\mathcal{A}(t) = \begin{bmatrix} \mathcal{A}_C(t) \\ \mathcal{A}_D(t) \end{bmatrix},$$

with $\mathcal{A}_C(t) = (A_i(t))_{1 \leq i \leq M}$ and $\mathcal{A}_D(t) = (A_i(t))_{M+1 \leq i \leq N}$. Therefore, Problem 3.4.1 can be written in the following form:

$$\begin{cases} \mathcal{M}\mathcal{A}'(t) + \mathcal{K}(t)\mathcal{A}(t) = \mathcal{F}(t), \\ \mathcal{A}_C(0) = \mathcal{A}^0. \end{cases}$$

This is a degenerate problem, because the matrix \mathcal{M} is singular. Hence, to prove its well-posedness, we write it in block matrix form:

$$\begin{cases} \begin{bmatrix} \mathcal{M}_{CC} & \mathbf{0} \\ \mathbf{0} & \mathbf{0} \end{bmatrix} \begin{bmatrix} \mathcal{A}'_C(t) \\ \mathcal{A}'_D(t) \end{bmatrix} + \begin{bmatrix} \mathcal{K}_{CC}(t) & \mathcal{K}_{CD} \\ \mathcal{K}_{DC} & \mathcal{K}_{DD} \end{bmatrix} \begin{bmatrix} \mathcal{A}_C(t) \\ \mathcal{A}_D(t) \end{bmatrix} = \begin{bmatrix} \mathbf{0} \\ \mathcal{F}_D(t) \end{bmatrix}, \\ \mathcal{A}_C(0) = \mathcal{A}^0. \end{cases}$$

Notice that only \mathcal{K}_{CC} depends on t . Indeed, since \mathbf{v} vanishes in $\overline{\Omega} \setminus \overline{\Omega}_0$, we have that $c(t, \phi_i, \phi_j) \neq 0$ only if ϕ_i and ϕ_j correspond to nodes in $\overline{\Omega}_0$. Moreover, from the ellipticity of \tilde{a} , \mathcal{K}_{DD} is positive definite and we can write

$$\mathcal{A}_D(t) = \mathcal{K}_{DD}^{-1} [-\mathcal{K}_{DC}\mathcal{A}_C(t) + \mathcal{F}_D(t)]. \quad (3.22)$$

Hence,

$$\begin{cases} \mathcal{M}_{CC}\mathcal{A}'_C(t) = [-\mathcal{K}_{CC}(t) + \mathcal{K}_{CD}\mathcal{K}_{DD}^{-1}\mathcal{K}_{DC}]\mathcal{A}_C(t) - \mathcal{K}_{CD}\mathcal{K}_{DD}^{-1}\mathcal{F}_D(t), \\ \mathcal{A}_C(0) = \mathcal{A}^0. \end{cases}$$

Since \mathcal{M}_{CC} is also positive definite, this linear system of ordinary differential-algebraic equations has a unique solution. Moreover, $\mathcal{K}_{\text{CC}} \in L^2(0, T; \mathbb{R}^{M \times M})$ and consequently $\mathcal{A}_{\text{C}} \in H^1(0, T; \mathbb{R}^M)$. Finally, from the assumption (3.21), we obtain from (3.22) that $\mathcal{A}_{\text{D}} \in H^1(0, T; \mathbb{R}^{N-M})$. Thus, we have proved the following result:

Theorem 3.4.2 *Problem 3.4.1 is well-posed.*

In what follows we will prove error estimates for this semi-discrete problem. Since the bilinear form a is not elliptic due to the presence of the velocity terms, we use its elliptic part \tilde{a} to define an elliptic projector. In this context, we can find in [49] some alternatives.

Let us introduce $P_h \in \mathcal{L}(\mathcal{V}, \mathcal{V}_h)$ by

$$\tilde{a}(P_h Y, Z_h) = \tilde{a}(Y, Z_h) \quad \forall Z_h \in \mathcal{V}_h, \quad Y \in \mathcal{V}.$$

Notice that, from Cea's lemma and Theorem 3.4.1, for all $Y \in H_r^2(\Omega) \cap \mathcal{V}$

$$\|Y - P_h Y\|_{\tilde{H}_r^1(\Omega)} \leq C \|Y - \mathcal{I}_h Y\|_{\tilde{H}_r^1(\Omega)} \leq Ch \|Y\|_{H_r^2(\Omega)}; \quad (3.23)$$

moreover, a standard duality argument leads to

$$\|Y - P_h Y\|_{L_r^2(\Omega)} \leq Ch^2 \|Y\|_{H_r^2(\Omega)}. \quad (3.24)$$

Let A and A_h be the solutions to Problems 3.3.1 and 3.4.1, respectively. We write

$$A(t) - A_h(t) = \delta_h(t) + \rho_h(t),$$

where

$$\delta_h(t) := P_h A(t) - A_h(t) \quad \text{and} \quad \rho_h(t) := A(t) - P_h A(t).$$

Provided A is smooth enough, $\partial_t(P_h A) = P_h(\partial_t A)$ (cf [55, Theorem P.111]) and, consequently, we have from (3.24)

$$\|\partial_t \rho_h\|_{L_r^2(\Omega)} \leq Ch^2 \|\partial_t A\|_{H_r^2(\Omega)}. \quad (3.25)$$

The following lemma is the basic tool to prove error estimates for the semi-discrete problem.

Lemma 3.4.1 *If $A \in H^1(0, T; H_r^2(\Omega) \cap \mathcal{V})$, then*

$$\|\delta_h\|_{C^0(0, T; L_r^2(\Omega_0))} \leq C \left[\|\delta_h(0)\|_{L_r^2(\Omega_0)} + h \|A\|_{H^1(0, T; H_r^2(\Omega))} \right], \quad (3.26)$$

$$\|\delta_h\|_{L^2(0, T; \tilde{H}_r^1(\Omega))} \leq C \left[\|\delta_h(0)\|_{L_r^2(\Omega_0)} + h \|A\|_{H^1(0, T; H_r^2(\Omega))} \right], \quad (3.27)$$

$$\|\partial_t \delta_h\|_{L^2(0, T; L_r^2(\Omega_0))} \leq C \left[\|\delta_h(0)\|_{\tilde{H}_r^1(\Omega)} + h \|A\|_{H^1(0, T; H_r^2(\Omega))} \right]. \quad (3.28)$$

Proof. Testing Problems 3.3.1 and 3.4.1 with $Z_h \in \mathcal{V}_h \subset \mathcal{V}$ and subtracting, we obtain

$$(\sigma \partial_t(A - A_h), Z_h)_{L_r^2(\Omega_0)} + a(t, A - A_h, Z_h) = 0 \quad \forall Z_h \in \mathcal{V}_h,$$

where we have used that $\partial_t A \in L_r^2(\Omega_0)$ (because of the assumed regularity) to write the duality pairing as an inner product. Using that $A(t) - A_h(t) = \delta_h(t) + \rho_h(t)$ and (3.18), we have

$$(\sigma \partial_t \delta_h(t), Z_h)_{L_r^2(\Omega_0)} + a(\delta_h(t), Z_h) = -(\sigma \partial_t \rho_h(t), Z_h)_{L_r^2(\Omega_0)} - c(t, \rho_h(t), Z_h). \quad (3.29)$$

By setting $Z_h = \delta_h(t)$, we obtain

$$\begin{aligned} \frac{1}{2} \frac{d}{dt} (\sigma \delta_h(t), \delta_h(t))_{L_r^2(\Omega_0)} + a(\delta_h(t), \delta_h(t)) \\ = -(\sigma \partial_t \rho_h(t), \delta_h(t))_{L_r^2(\Omega_0)} - c(t, \rho_h(t), \delta_h(t)). \end{aligned}$$

We use Lemma 3.3.1 and a weighted Cauchy-Schwartz inequality to write

$$\begin{aligned} \frac{1}{2} \frac{d}{dt} \|\sigma^{1/2} \delta_h(t)\|_{L_r^2(\Omega_0)}^2 + \frac{\alpha}{2} \|\delta_h(t)\|_{\tilde{H}_r^1(\Omega)}^2 - \lambda^* \|\sigma^{1/2} \delta_h(t)\|_{L_r^2(\Omega_0)}^2 \\ \leq \frac{\alpha}{4} \|\delta_h(t)\|_{L_r^2(\Omega_0)}^2 + C \left[\|\partial_t \rho_h(t)\|_{L_r^2(\Omega_0)}^2 + \|\rho_h(t)\|_{\tilde{H}_r^1(\Omega_0)}^2 \right], \end{aligned}$$

with C depending only on $\|\mathbf{v}\|_\infty$, $\bar{\sigma}$, and α . Then,

$$\begin{aligned} \frac{d}{dt} \|\sigma^{1/2} \delta_h(t)\|_{L_r^2(\Omega_0)}^2 + \frac{\alpha}{2} \|\delta_h(t)\|_{\tilde{H}_r^1(\Omega)}^2 \\ \leq C \left[\|\sigma^{1/2} \delta_h(t)\|_{L_r^2(\Omega_0)}^2 + \|\partial_t \rho_h(t)\|_{L_r^2(\Omega_0)}^2 + \|\rho_h(t)\|_{\tilde{H}_r^1(\Omega_0)}^2 \right]. \end{aligned} \quad (3.30)$$

The term involving $\|\delta_h(t)\|_{\tilde{H}_r^1(\Omega)}$ can be dropped out and the inequality is preserved. Hence, using Gronwall inequality we obtain

$$\begin{aligned} \|\sigma^{1/2} \delta_h(t)\|_{L_r^2(\Omega_0)}^2 \\ \leq C \left[\|\sigma^{1/2} \delta_h(0)\|_{L_r^2(\Omega_0)}^2 + \|\partial_t \rho_h\|_{L^2(0,T;L_r^2)}^2 + \|\rho_h\|_{L^2(0,T;\tilde{H}_r^1(\Omega))}^2 \right]. \end{aligned}$$

Thus, (3.26) follows from (3.23), (3.25), and the last inequality.

To prove (3.27) we integrate (3.30) with respect to time to obtain

$$\begin{aligned} \|\sigma^{1/2} \delta_h(T)\|_{L_r^2(\Omega_0)}^2 - \|\sigma^{1/2} \delta_h(0)\|_{L_r^2(\Omega_0)}^2 + \frac{\alpha}{2} \int_0^T \|\delta_h(t)\|_{\tilde{H}_r^1(\Omega)}^2 dt \\ \leq C \int_0^T \left[\|\sigma^{1/2} \delta_h(t)\|_{L_r^2(\Omega_0)}^2 + \|\partial_t \rho_h(t)\|_{L_r^2(\Omega_0)}^2 + \|\rho_h(t)\|_{\tilde{H}_r^1(\Omega_0)}^2 \right] dt. \end{aligned}$$

Hence, (3.27) follows from (3.26), (3.23), and (3.25) again.

Finally, to prove (3.28), we set $Z_h = \partial_t \delta_h(t)$ in (3.29) to write

$$\begin{aligned} & (\sigma \partial_t \delta_h(t), \partial_t \delta_h(t))_{L_r^2(\Omega_0)} + \tilde{a}(\delta_h(t), \partial_t \delta_h(t)) \\ &= -(\sigma \partial_t \rho_h(t), \partial_t \delta_h(t))_{L_r^2(\Omega_0)} - c(t, \delta_h(t), \partial_t \delta_h(t)) - c(t, \rho_h(t), \partial_t \delta_h(t)). \end{aligned}$$

We estimate the right hand side above by using a weighted Cauchy-Schwartz inequality. Then, since \tilde{a} is symmetric, we have

$$\begin{aligned} & \|\sigma^{1/2} \partial_t \delta_h(t)\|_{L_r^2(\Omega_0)}^2 + \frac{1}{2} \frac{d}{dt} \tilde{a}(\delta_h(t), \delta_h(t)) \\ & \leq \frac{1}{2} \|\sigma^{1/2} \partial_t \delta_h(t)\|_{L_r^2(\Omega_0)}^2 + C \left[\|\partial_t \rho_h(t)\|_{L_r^2(\Omega_0)}^2 + \|\delta_h(t)\|_{\tilde{H}_r^1(\Omega_0)}^2 + \|\rho_h(t)\|_{\tilde{H}_r^1(\Omega_0)}^2 \right]. \end{aligned}$$

Next, we integrate in $[0, T]$ to obtain

$$\begin{aligned} & \frac{1}{2} \int_0^T \|\sigma^{1/2} \partial_t \delta_h(t)\|_{L_r^2(\Omega_0)}^2 dt + \frac{1}{2} \tilde{a}(\delta_h(T), \delta_h(T)) - \frac{1}{2} \tilde{a}(\delta_h(0), \delta_h(0)) \\ & \leq C \int_0^T \left[\|\partial_t \rho_h(t)\|_{L_r^2(\Omega_0)}^2 + \|\delta_h(t)\|_{\tilde{H}_r^1(\Omega_0)}^2 + \|\rho_h(t)\|_{\tilde{H}_r^1(\Omega_0)}^2 \right] dt. \end{aligned}$$

Thus, (3.28) follows from the ellipticity and the continuity of \tilde{a} , (3.23), and (3.25). \square

Now we are in a position to prove error estimates for the computed vector potential A_h as well as for the approximations of the physical quantities of interest that can be derived from it. According to (3.13) and (3.14), we define

$$\mathbf{B}_h := \mathbf{curl}(A_h \mathbf{e}_\theta)$$

and, according to (3.9) and (3.15),

$$\mathbf{J}_h := -\sigma \frac{\partial A_h}{\partial t} \mathbf{e}_\theta + \sigma \mathbf{v} \times \mathbf{B}_h \quad \text{in } \Omega_0.$$

The following error estimates hold true.

Theorem 3.4.3 *Let A and A_h be the solutions to Problems 3.3.1 and 3.4.1, respectively. Let \mathbf{B} be defined by (3.13) and (3.14) and \mathbf{J} by (3.9) and (3.15). Let \mathbf{B}_h and \mathbf{J}_h be defined as above. If $A \in H^1(0, T; H_r^2(\Omega) \cap \mathcal{V})$, then there exists a positive constant C independent of h and A such that*

$$\|A - A_h\|_{C^0(0, T; L_r^2(\Omega_0))} \leq C \left[\|A^0 - A_h^0\|_{L_r^2(\Omega_0)} + h \|A\|_{H^1(0, T; H_r^2(\Omega))} \right], \quad (3.31)$$

$$\|\mathbf{B} - \mathbf{B}_h\|_{L^2(0, T; L_r^2)} \leq C \left[\|A^0 - A_h^0\|_{L_r^2(\Omega_0)} + h \|A\|_{H^1(0, T; H_r^2(\Omega))} \right], \quad (3.32)$$

$$\|\mathbf{J} - \mathbf{J}_h\|_{L^2(0, T; L_r^2(\Omega_0))} \leq C \left[\|A(0) - A_h(0)\|_{\tilde{H}_r^1(\Omega)} + h \|A\|_{H^1(0, T; H_r^2(\Omega))} \right]. \quad (3.33)$$

Proof. We use that $A(t) - A_h(t) = \delta_h(t) + \rho_h(t)$, (3.26), and (3.24), to write

$$\begin{aligned} \|A - A_h\|_{C^0(0,T;L_r^2(\Omega_0))} &\leq \sup_{t \in [0,T]} \|\delta_h(t)\|_{L_r^2(\Omega_0)} + \sup_{t \in [0,T]} \|\rho_h(t)\|_{L_r^2(\Omega_0)} \\ &\leq C \left[\|A^0 - A_h^0\|_{L_r^2(\Omega_0)} + \|\rho_h(0)\|_{L_r^2(\Omega_0)} \right. \\ &\quad \left. + h\|A\|_{H^1(0,T;H_r^2(\Omega))} \right] + \sup_{t \in [0,T]} \|\rho_h(t)\|_{L_r^2(\Omega)} \\ &\leq C \left[\|A^0 - A_h^0\|_{L_r^2(\Omega_0)} + h\|A\|_{H^1(0,T;H_r^2(\Omega))} \right. \\ &\quad \left. + h^2\|A\|_{C^0(0,T;H_r^2(\Omega))} \right], \end{aligned}$$

from which we conclude (3.31).

For the second inequality we use the definitions of \mathbf{B} and \mathbf{B}_h , (3.27), and (3.23):

$$\begin{aligned} \|\mathbf{B} - \mathbf{B}^h\|_{L^2(0,T;L_r^2)} &\leq \|\delta_h\|_{L^2(0,T;\tilde{H}_r^1(\Omega))} + \|\rho_h\|_{L^2(0,T;\tilde{H}_r^1(\Omega))} \\ &\leq C \left[\|A^0 - A_h^0\|_{L_r^2(\Omega_0)} + h\|A\|_{H^1(0,T;H_r^2(\Omega))} \right]. \end{aligned}$$

This inequality is also used to prove (3.33), together with the following one which follows from (3.28), (3.25) and (3.23):

$$\begin{aligned} \|\partial_t A - \partial_t A_h\|_{L^2(0,T;L_r^2(\Omega_0))} &\leq \|\partial_t \delta_h\|_{L^2(0,T;L_r^2(\Omega_0))} + \|\partial_t \rho_h\|_{L^2(0,T;L_r^2(\Omega_0))} \\ &\leq C \left[\|A(0) - A_h(0)\|_{\tilde{H}_r^1(\Omega)} + h\|A\|_{H^1(0,T;H_r^2(\Omega))} \right]. \end{aligned}$$

Thus, according to the definitions of \mathbf{J} and \mathbf{J}_h , (3.33) follows from the last two inequalities and we conclude the proof. \square

Notice that in the theorem above, (3.33) is not an actual a priori error estimate. In fact,

$$\|A(0) - A_h(0)\|_{\tilde{H}_r^1(\Omega)}^2 = \|A(0) - A_h(0)\|_{\tilde{H}_r^1(\Omega_0)}^2 + \|A(0) - A_h(0)\|_{H^1(0,T;\Omega \setminus \bar{\Omega}_0)}^2.$$

The first term on the right hand side above depends only on the initial data of both problems: $\|A(0) - A_h(0)\|_{\tilde{H}_r^1(\Omega_0)} = \|A^0 - A_h^0\|_{\tilde{H}_r^1(\Omega_0)}$. Instead the second one depends on the solutions of Problems 3.3.1 and 3.4.1. In what follows we prove that if we choose the initial data of the semi-discrete problem as the Lagrange interpolant of A^0 (which is well defined under the smoothness assumptions of Theorem 3.4.3), then the second term can be also conveniently bounded.

Lemma 3.4.2 *If $A \in H^1(0, T; H_r^2(\Omega) \cap \mathcal{V})$ and $A_h^0 = \mathcal{I}_h A^0$, then there exists a positive constant C independent of h such that*

$$\|A(0) - A_h(0)\|_{\tilde{H}_r^1(\Omega)} \leq Ch \|A(0)\|_{H_r^2(\Omega)}$$

Proof. By testing Problems 3.3.1 and 3.4.1 with $Z_h \in \mathcal{V}_h$ and subtracting we have

$$\int_{\Omega_0} \sigma(\partial_t A(t) - \partial_t A_h(t)) Z_h r dr dz + \tilde{a}(A(t) - A_h(t), Z_h) + c(t, A(t) - A_h(t), Z_h) = 0.$$

Hence, if $Z_h \in \mathcal{V}_h$ is such that $\text{supp } Z_h \subset \Omega \setminus \Omega_0$, we obtain

$$\tilde{a}(A(t) - A_h(t), Z_h) = 0 \quad \text{a.e. } t \in [0, T].$$

Since $A_h \in H^1(0, T; \mathcal{V}_h)$ and we have assumed $A \in H^1(0, T; \mathcal{V})$, we have that $\tilde{a}(A(t) - A_h(t), Z_h)$ is a continuous function of t in $[0, T]$. Therefore, for all $Z_h \in \mathcal{V}_h$ such that $\text{supp } Z_h \subset \Omega \setminus \Omega_0$, we can write

$$\tilde{a}(A(0) - A_h(0), Z_h) = 0.$$

Let $Z_h := A_h(0) - \mathcal{I}_h A(0) \in \mathcal{V}_h$. Notice that $\text{supp } Z_h \subset \Omega \setminus \Omega_0$, because

$$Z_h|_{\Omega_0} = A_h(0)|_{\Omega_0} - \mathcal{I}_h A(0)|_{\Omega_0} = A_h^0 - \mathcal{I}_h A^0 = 0.$$

Then,

$$\tilde{a}(A(0) - A_h(0), A(0) - A_h(0)) = \tilde{a}(A(0) - A_h(0), A(0) - \mathcal{I}_h A(0)).$$

Therefore, since \tilde{a} is elliptic, using Theorem 3.4.1 we have

$$\begin{aligned} \alpha \|A(0) - A_h(0)\|_{\tilde{H}_r^1(\Omega)}^2 &\leq \tilde{a}(A(0) - A_h(0), A(0) - \mathcal{I}_h A(0)) \\ &\leq \|A(0) - A_h(0)\|_{\tilde{H}_r^1(\Omega)} Ch \|A(0)\|_{H_r^2(\Omega)}. \end{aligned}$$

Hence we conclude the lemma. \square

Now we are in a position to conclude an $\mathcal{O}(h)$ order of convergence.

Corollary 3.4.1 *Under the assumptions of Theorem 3.4.3, if $A_h^0 = \mathcal{I}_h A^0$, then there exists a positive constant C independent of h and A such that*

$$\begin{aligned} \|A - A_h\|_{C^0(0, T; L_r^2(\Omega_0))} &\leq Ch \|A\|_{H^1(0, T; H_r^2(\Omega))}, \\ \|\mathbf{B} - \mathbf{B}_h\|_{L^2(0, T; L_r^2)} &\leq Ch \|A\|_{H^1(0, T; H_r^2(\Omega))}, \\ \|\mathbf{J} - \mathbf{J}_h\|_{L^2(0, T; L_r^2(\Omega_0))} &\leq Ch \|A\|_{H^1(0, T; H_r^2(\Omega))}. \end{aligned}$$

Proof. It is an immediate consequence of Theorem 3.4.3, Lemma 3.4.2, and Theorem 3.4.1. \square

3.5 Fully Discrete Problem

In this section we introduce a time discretization of Problem 3.4.1 by means of a backward Euler scheme and prove its stability and convergence. With this aim, we will adapt the standard theory for parabolic problems (see, for instance, [25]) taking into account that in our case the problem is degenerate and the bilinear form is non-elliptic.

We consider a uniform partition $\{t^k := k\Delta t, k = 0, \dots, N\}$ of $[0, T]$ with time step $\Delta t := \frac{T}{N}$. A fully discrete approximation of Problem 3.3.1 is defined as follows:

Problem 3.5.1 Given $A_h^0 \in \mathcal{V}_h^0$, for $k = 1, \dots, N$ find $A_h^k \in \mathcal{V}_h$ such that

$$\frac{1}{\Delta t} (\sigma A_h^k - \sigma A_h^{k-1}, Z_h)_{L_r^2(\Omega_0)} + a(t^k, A_h^k, Z_h) = (J_S(t^k), Z_h)_{L_r^2(\Omega_S)} \quad \forall Z_h \in \mathcal{V}_h.$$

First we prove that this problem is well-posed, at least for Δt sufficiently small, by means of the following stability result.

Theorem 3.5.1 Let λ^* be defined as in Lemma 3.3.1. If $\lambda^* \Delta t < 1/4$, then Problem 3.5.1 has a unique solution and there exists a positive constant C independent of h , Δt , and the data of the problem, A_h^0 and J_S , such that

$$\max_{1 \leq k \leq N} \|A_h^k\|_{L_r^2(\Omega_0)}^2 + \Delta t \sum_{k=1}^N \|A_h^k\|_{\tilde{H}_r^1(\Omega)}^2 \leq C \left[\|A_h^0\|_{L_r^2(\Omega_0)}^2 + \Delta t \sum_{k=1}^N \|J_S(t^k)\|_{L_r^2(\Omega_S)}^2 \right].$$

Proof. We only have to prove the estimate, since it implies that the fully discrete problem has a unique solution. To do this, we test Problem 3.5.1 with $Z_h = A_h^k$ to write

$$(\sigma A_h^k - \sigma A_h^{k-1}, A_h^k)_{L_r^2(\Omega_0)} + \Delta t a(t^k, A_h^k, A_h^k) = \Delta t (J_S(t^k), A_h^k)_{L_r^2(\Omega_S)}.$$

On the other hand, we note that

$$\begin{aligned} 2 (\sigma A_h^k - \sigma A_h^{k-1}, A_h^k)_{L_r^2(\Omega_0)} \\ = \|\sigma^{1/2} A_h^k\|_{L_r^2(\Omega_0)}^2 - \|\sigma^{1/2} A_h^{k-1}\|_{L_r^2(\Omega_0)}^2 + \|\sigma^{1/2} A_h^k - \sigma^{1/2} A_h^{k-1}\|_{L_r^2(\Omega_0)}^2, \end{aligned} \tag{3.34}$$

whereas from Lemma 3.3.1 we have

$$a(t^k, A_h^k, A_h^k) \geq \frac{\alpha}{2} \|A_h^k\|_{\tilde{H}_r^1(\Omega)}^2 - \lambda^* \|\sigma^{1/2} A_h^k\|_{L_r^2(\Omega_0)}^2.$$

Substituting these last two relations into the first one and using a weighted Cauchy-Schwarz inequality, we obtain

$$\begin{aligned} & \|\sigma^{1/2} A_h^k\|_{L_r^2(\Omega_0)}^2 - \|\sigma^{1/2} A_h^{k-1}\|_{L_r^2(\Omega_0)}^2 + \|\sigma^{1/2} A_h^k - \sigma^{1/2} A_h^{k-1}\|_{L_r^2(\Omega_0)}^2 \\ & + \alpha \Delta t \|A_h^k\|_{\tilde{H}_r^1(\Omega)}^2 - 2\lambda^* \Delta t \|\sigma^{1/2} A_h^k\|_{L_r^2(\Omega_0)}^2 \\ & \leq \frac{2\Delta t}{\alpha} \|J_S(t^k)\|_{L_r^2(\Omega)}^2 + \frac{\alpha \Delta t}{2} \|A_h^k\|_{\tilde{H}_r^1(\Omega)}^2. \end{aligned}$$

We add the above inequalities from $k = 1$ to n and use the assumption $\lambda^* \Delta t \leq 1/4$ to write

$$\begin{aligned} & \frac{1}{2} \|\sigma^{1/2} A_h^n\|_{L_r^2(\Omega_0)}^2 + \frac{\alpha \Delta t}{2} \sum_{k=1}^n \|A_h^k\|_{\tilde{H}_r^1(\Omega)}^2 \\ & \leq \|\sigma^{1/2} A_h^0\|_{L_r^2(\Omega_0)}^2 + \frac{2\Delta t}{\alpha} \sum_{k=1}^n \|J_S(t^k)\|_{L_r^2(\Omega)}^2 + 2\lambda^* \Delta t \sum_{k=1}^{n-1} \|\sigma^{1/2} A_h^k\|_{L_r^2(\Omega_0)}^2. \end{aligned} \quad (3.35)$$

Hence, the discrete Gronwall lemma, (see, for instance, [39, Lemma 1.4.2]) yields

$$\|\sigma^{1/2} A_h^n\|_{L_r^2(\Omega_0)}^2 \leq C \left[\|A_h^0\|_{L_r^2(\Omega_0)}^2 + \Delta t \sum_{k=1}^n \|J_S(t^k)\|_{L_r^2(\Omega)}^2 \right], \quad n = 1, \dots, N.$$

On the other hand, setting $n = N$ in (3.35) and using the previous inequality we obtain

$$\Delta t \sum_{k=1}^N \|A_h^k\|_{\tilde{H}_r^1(\Omega)}^2 \leq C \left[\|A_h^0\|_{L_r^2(\Omega_0)}^2 + \Delta t \sum_{k=1}^N \|J_S(t^k)\|_{L_r^2(\Omega)}^2 \right].$$

Thus we conclude the proof. \square

Our next goal is to prove error estimates for the solution of the fully discrete problem. To do this we introduce some notation. Given $(\phi^0, \dots, \phi^N) \in \mathbb{R}^{N+1}$, we define the backward difference quotient

$$\bar{\partial} \phi^k := \frac{\phi^k - \phi^{k-1}}{\Delta t}, \quad k = 1, \dots, N.$$

For A and A_h^k being the solutions of Problems 3.3.1 and 3.5.1, respectively, if $A \in \mathcal{C}^0(0, T; \mathcal{V})$, we write

$$A(t^k) - A_h^k = \delta_h^k + \rho_h^k \quad \text{in } \Omega.$$

with

$$\delta_h^k := P_h A(t^k) - A_h^k \quad \text{and} \quad \rho_h^k := A(t^k) - P_h A(t^k), \quad k = 1, \dots, N.$$

In the proofs that follow we will have to use $\bar{\partial}\rho_h^k$ and $\bar{\partial}\delta_h^k$, which for $k = 1$ involves δ_h^0 and ρ_h^0 . The latter is well defined in the whole Ω by the same expression as above. However, this is not the case for δ_h^0 , since the domain of the data A_h^0 is just Ω_0 . To define δ_h^0 in the whole domain Ω , we need to consider an extension of A_h^0 outside Ω_0 . In principle any arbitrary extension could be used. We resort to the solution A_h of the semi-discrete problem for reasons that will be clear below. Let

$$\rho_h^0 := A(0) - P_h A(0) \quad \text{and} \quad \delta_h^0 := P_h A(0) - A_h(0),$$

where A_h is the solution to Problem 3.4.1. Then,

$$A^0 - A_h^0 = \delta_h^0 + \rho_h^0 \quad \text{in } \Omega_0.$$

Finally, provided $A \in \mathcal{C}^1(0, T; L_r^2(\Omega_0))$, we define the truncation errors:

$$\tau^k := \bar{\partial}A(t^k) - \partial_t A(t^k) \quad \text{in } \Omega_0, \quad k = 1, \dots, N.$$

The first step is to estimate δ_h^k in terms of ρ_h^k and τ^k .

Lemma 3.5.1 *If $\lambda^* \Delta t < 1/4$ and $A \in \mathcal{C}^0(0, T; \mathcal{V}) \cap \mathcal{C}^1(0, T; L_r^2(\Omega_0))$, then*

$$\begin{aligned} & \max_{1 \leq k \leq N} \|\delta_h^k\|_{L_r^2(\Omega_0)}^2 \\ & \leq C \|\delta_h^0\|_{L_r^2(\Omega_0)}^2 + C \Delta t \sum_{k=1}^N \left[\|\bar{\partial}\rho_h^k\|_{L_r^2(\Omega_0)}^2 + \|\rho_h^k\|_{\tilde{H}_r^1(\Omega_0)}^2 + \|\tau^k\|_{L_r^2(\Omega_0)}^2 \right], \end{aligned} \tag{3.36}$$

$$\begin{aligned} & \Delta t \sum_{k=1}^N \|\delta_h^k\|_{\tilde{H}_r^1(\Omega)}^2 \\ & \leq C \|\delta_h^0\|_{L_r^2(\Omega_0)}^2 + C \Delta t \sum_{k=1}^N \left[\|\bar{\partial}\rho_h^k\|_{L_r^2(\Omega_0)}^2 + \|\rho_h^k\|_{\tilde{H}_r^1(\Omega_0)}^2 + \|\tau^k\|_{L_r^2(\Omega_0)}^2 \right], \end{aligned} \tag{3.37}$$

$$\begin{aligned} & \Delta t \sum_{k=1}^N \|\bar{\partial}\delta_h^k\|_{L_r^2(\Omega_0)}^2 \\ & \leq C \|\delta_h^0\|_{\tilde{H}_r^1(\Omega)}^2 + C \Delta t \sum_{k=1}^N \left[\|\bar{\partial}\rho_h^k\|_{L_r^2(\Omega_0)}^2 + \|\rho_h^k\|_{\tilde{H}_r^1(\Omega_0)}^2 + \|\tau^k\|_{L_r^2(\Omega_0)}^2 \right]. \end{aligned} \tag{3.38}$$

Proof. Because of the assumed regularity of A , testing Problems 3.5.1 and 3.3.1 with $Z_h \in \mathcal{V}_h \subset \mathcal{V}$ and subtracting allows us to write

$$\begin{aligned} & (\sigma \bar{\partial} \delta_h^k, Z_h)_{L_r^2(\Omega_0)} + a(t_k, \delta_h^k, Z_h) \\ & = - (\sigma \bar{\partial} \rho_h^k, Z_h)_{L_r^2(\Omega_0)} - c(t_k, \rho_h^k, Z_h) + (\sigma \tau^k, Z_h)_{L_r^2(\Omega_0)} \end{aligned} \tag{3.39}$$

for all $Z_h \in \mathcal{V}_h$ and $k = 1, \dots, N$.

On the other hand, the same argument leading to (3.34) in the proof of Theorem 3.5.1 leads to

$$\frac{1}{2\Delta t} \left[\|\sigma^{1/2} \delta_h^k\|_{L_r^2(\Omega_0)}^2 - \|\sigma^{1/2} \delta_h^{k-1}\|_{L_r^2(\Omega_0)}^2 \right] \leq (\sigma \bar{\partial} \delta_h^k, \delta_h^k)_{L_r^2(\Omega_0)}.$$

By using the above inequality and Lemma 3.3.1, we obtain from (3.39) with $Z_h = \delta_h^k$ and a weighted Cauchy-Schwarz inequality,

$$\begin{aligned} & \frac{1}{2\Delta t} \left[\|\sigma^{1/2} \delta_h^k\|_{L_r^2(\Omega_0)}^2 - \|\sigma^{1/2} \delta_h^{k-1}\|_{L_r^2(\Omega_0)}^2 \right] + \frac{\alpha}{2} \|\delta_h^k\|_{\tilde{H}_r^1(\Omega)}^2 - \lambda^* \|\sigma^{1/2} \delta_h^k\|_{L_r^2(\Omega_0)}^2 \\ & \leq C \left[\|\bar{\partial} \rho_h^k\|_{L_r^2(\Omega_0)}^2 + \|\rho_h^k\|_{\tilde{H}_r^1(\Omega_0)}^2 + \|\tau^k\|_{L_r^2(\Omega_0)}^2 \right] + \frac{\alpha}{4} \|\delta_h^k\|_{L_r^2(\Omega_0)}^2. \end{aligned}$$

Summing from $k = 1$ to n ($1 \leq n \leq N$) and a little algebra yields

$$\begin{aligned} & \|\sigma^{1/2} \delta_h^n\|_{L_r^2(\Omega_0)}^2 - \|\sigma^{1/2} \delta_h^0\|_{L_r^2(\Omega_0)}^2 + \frac{\alpha \Delta t}{2} \sum_{k=1}^n \|\delta_h^k\|_{\tilde{H}_r^1(\Omega)}^2 \\ & \leq 2\lambda^* \Delta t \sum_{k=1}^n \|\sigma^{1/2} \delta_h^k\|_{L_r^2(\Omega_0)}^2 + C \Delta t \sum_{k=1}^n \left[\|\bar{\partial} \rho_h^k\|_{L_r^2(\Omega_0)}^2 + \|\rho_h^k\|_{\tilde{H}_r^1(\Omega_0)}^2 + \|\tau^k\|_{L_r^2(\Omega_0)}^2 \right] \end{aligned}$$

and using that $\lambda^* \Delta t \leq 1/4$,

$$\begin{aligned} & \frac{1}{2} \|\sigma^{1/2} \delta_h^n\|_{L_r^2(\Omega_0)}^2 + \frac{\alpha \Delta t}{2} \sum_{k=1}^n \|\delta_h^k\|_{\tilde{H}_r^1(\Omega)}^2 \\ & \leq \|\sigma^{1/2} \delta_h^0\|_{L_r^2(\Omega_0)}^2 + 2\lambda^* \Delta t \sum_{k=1}^{n-1} \|\sigma^{1/2} \delta_h^k\|_{L_r^2(\Omega_0)}^2 \\ & \quad + C \Delta t \sum_{k=1}^n \left[\|\bar{\partial} \rho_h^k\|_{L_r^2(\Omega_0)}^2 + \|\rho_h^k\|_{\tilde{H}_r^1(\Omega_0)}^2 + \|\tau^k\|_{L_r^2(\Omega_0)}^2 \right]. \end{aligned}$$

Hence, by using the discrete Gronwall Lemma, we obtain for $n = 1, \dots, N$

$$\begin{aligned} & \|\sigma^{1/2} \delta_h^n\|_{L_r^2(\Omega_0)}^2 \\ & \leq C \|\sigma^{1/2} \delta_h^0\|_{L_r^2(\Omega_0)}^2 + C \Delta t \sum_{k=1}^n \left[\|\bar{\partial} \rho_h^k\|_{L_r^2(\Omega_0)}^2 + \|\rho_h^k\|_{\tilde{H}_r^1(\Omega_0)}^2 + \|\tau^k\|_{L_r^2(\Omega_0)}^2 \right], \end{aligned}$$

from which we conclude (3.36).

The second estimate follows by using the above inequality to estimate the terms $\|\sigma^{1/2} \delta_h^k\|_{L_r^2(\Omega_0)}^2$ in the right hand side of the previous one and straightforward computations.

For the third estimate, first we test (3.39) with $Z_h = \bar{\partial}\delta_h^k$ to obtain

$$\begin{aligned} & (\sigma\bar{\partial}\delta_h^k, \bar{\partial}\delta_h^k)_{L_r^2(\Omega_0)} + \tilde{a}(\delta_h^k, \bar{\partial}\delta_h^k) \\ &= -c(t_k, \delta_h^k, \bar{\partial}\delta_h^k) - (\sigma\bar{\partial}\rho_h^k, \bar{\partial}\delta_h^k)_{L_r^2(\Omega_0)} - c(t_k, \rho_h^k, \bar{\partial}\delta_h^k) + (\sigma\tau^k, \bar{\partial}\delta_h^k)_{L_r^2(\Omega_0)}. \end{aligned}$$

On the other hand, from the ellipticity of \tilde{a} , it is immediate to show that

$$\tilde{a}(\delta_h^k, \bar{\partial}\delta_h^k) \geq \frac{1}{2\Delta t} [\tilde{a}(\delta_h^k, \delta_h^k) - \tilde{a}(\delta_h^{k-1}, \delta_h^{k-1})].$$

By substituting this inequality in the previous identity and using a weighted Cauchy-Schwartz inequality, we arrive at

$$\begin{aligned} & \Delta t \|\sigma^{1/2} \bar{\partial}\delta_h^k\|_{L_r^2(\Omega_0)}^2 + \frac{1}{2} [\tilde{a}(\delta_h^k, \delta_h^k) - \tilde{a}(\delta_h^{k-1}, \delta_h^{k-1})] \\ & \leq C\Delta t \left[\|\delta_h^k\|_{\tilde{H}_r^1(\Omega_0)}^2 + \|\bar{\partial}\rho_h^k\|_{L_r^2(\Omega_0)}^2 + \|\rho_h^k\|_{\tilde{H}_r^1(\Omega_0)}^2 + \|\tau^k\|_{L_r^2(\Omega_0)}^2 \right] \\ & \quad + \frac{\Delta t}{2} \|\sigma^{1/2} \bar{\partial}\delta_h^k\|_{L_r^2(\Omega)}^2. \end{aligned}$$

Now, we sum from $k = 1$ to N to write

$$\begin{aligned} & \Delta t \sum_{k=1}^N \|\sigma^{1/2} \bar{\partial}\delta_h^k\|_{L_r^2(\Omega_0)}^2 + \tilde{a}(\delta_h^N, \delta_h^N) \\ & \leq \tilde{a}(\delta_h^0, \delta_h^0) + C\Delta t \sum_{k=1}^N \left[\|\delta_h^k\|_{\tilde{H}_r^1(\Omega_0)}^2 + \|\bar{\partial}\rho_h^k\|_{L_r^2(\Omega_0)}^2 + \|\rho_h^k\|_{\tilde{H}_r^1(\Omega_0)}^2 + \|\tau^k\|_{L_r^2(\Omega_0)}^2 \right]. \end{aligned}$$

Thus (3.38) follows from the ellipticity and the continuity of \tilde{a} and (3.37). \square

Notice that in the previous lemma the estimate (3.38) differs from (3.36) and (3.37) in that it depends on $\|\delta_h^0\|_{\tilde{H}_r^1(\Omega)}$, which in its turn depends on the chosen extension of A_h^0 to the whole Ω , namely, $A_h(0)$.

The following step is to obtain appropriate estimates for ρ_h^k and τ^k .

Lemma 3.5.2 *If $A \in H^1(0, T; H_r^2(\Omega) \cap \mathcal{V})$, then*

$$\Delta t \sum_{k=1}^N \|\bar{\partial}\rho_h^k\|_{L_r^2(\Omega_0)}^2 + h^2 \Delta t \sum_{k=0}^N \|\rho_h^k\|_{\tilde{H}_r^1(\Omega)}^2 \leq Ch^4 \|A\|_{H^1(0, T; H_r^2(\Omega))}^2,$$

and if $A \in H^2(0, T; L_r^2(\Omega_0))$, then

$$\sum_{k=1}^N \|\tau^k\|_{L_r^2(\Omega_0)}^2 \leq C\Delta t \|A\|_{H^2(0, T; L_r^2(\Omega_0))}^2.$$

Proof. For the first estimate we use Barrow's rule, to write

$$\bar{\partial} \rho_h^k = \frac{1}{\Delta t} \int_{t^{k-1}}^{t^k} \partial_t \rho_h(t) dt.$$

Hence, using a Cauchy-Schwartz inequality and (3.25) we have

$$\Delta t \sum_{k=1}^N \|\bar{\partial} \rho_h^k\|_{L_r^2(\Omega_0)}^2 \leq \int_0^T \|\partial_t \rho_h(t)\|_{L_r^2(\Omega_0)}^2 dt \leq Ch^4 \|A\|_{H^1(0,T;H_r^2(\Omega))}^2.$$

Moreover, since $\rho_h^k = A(t^k) - P_h A(t^k)$, from (3.23) we have

$$\Delta t \sum_{k=0}^N \|\rho_h^k\|_{\tilde{H}_r^1(\Omega)}^2 \leq Ch^2 \|A\|_{C^0(0,T;H_r^2(\Omega))}^2.$$

Thus, we conclude the first estimate of the lemma from the last two inequalities.

For the second estimate we use a Taylor's formula in the definition of τ^k to write

$$\tau^k = \frac{1}{\Delta t} \int_{t^{k-1}}^{t^k} (t - t^{k-1}) \partial_{tt} A(t) dt.$$

Hence, straightforward computations allow us to conclude the lemma. \square

Now we are in a position to prove the main result of this paper. Analogously to what was done for the semi-discrete problem, we define the computed magnetic field (cf. (3.13) and (3.14))

$$\mathbf{B}_h^k := \mathbf{curl}(A_h^k \mathbf{e}_\theta)$$

and the computed current density in the workpiece (cf. (3.9) and (3.15))

$$\mathbf{J}_h^k := -\sigma \bar{\partial} A_h^k \mathbf{e}_\theta + \sigma \mathbf{v} \times \mathbf{B}_h^k \quad \text{in } \Omega_0. \quad (3.40)$$

The following error estimates hold for this numerical method.

Theorem 3.5.2 *Let A be the solution to Problem 3.3.1 and assume it satisfies $A \in H^1(0, T; H_r^2(\Omega) \cap \mathcal{V}) \cap H^2(0, T; L_r^2(\Omega_0))$. Let $\Delta t > 0$ be such that $\lambda^* \Delta t < 1/4$, with λ^* as in Lemma 3.3.1. Let A_h^k , $k = 1, \dots, N$, be the solution to Problem 3.5.1, with initial data $A_h^0 = \mathcal{I}_h A^0$. Let \mathbf{B} be defined by (3.13) and (3.14) and \mathbf{J} by (3.9) and (3.15). Let \mathbf{B}_h^k and \mathbf{J}_h^k , $k = 1, \dots, N$, be defined as above. Then, there exists a positive constant C*

independent of h , Δt , and A such that

$$\begin{aligned} \max_{1 \leq k \leq N} \|A(t^k) - A_h^k\|_{L_r^2(\Omega_0)} &\leq C \left[h \|A\|_{H^1(0,T;H_r^2(\Omega))} + \Delta t \|A\|_{H^2(0,T;L_r^2(\Omega_0))} \right], \\ \left[\Delta t \sum_{k=1}^N \|\mathbf{B}(t^k) - \mathbf{B}_h^k\|_{L_r^2(\Omega)}^2 \right]^{1/2} &\leq C \left[h \|A\|_{H^1(0,T;H_r^2(\Omega))} + \Delta t \|A\|_{H^2(0,T;L_r^2(\Omega_0))} \right], \\ \left[\Delta t \sum_{k=1}^N \|\mathbf{J}(t^k) - \mathbf{J}_h^k\|_{L_r^2(\Omega_0)}^2 \right]^{1/2} &\leq C \left[h \|A\|_{H^1(0,T;H_r^2(\Omega))} + \Delta t \|A\|_{H^2(0,T;L_r^2(\Omega_0))} \right]. \end{aligned}$$

Proof. By writing $A(t^k) - A_h^k = \delta_h^k + \rho_h^k$, from Lemmas 3.5.1 and 3.5.2, we obtain for all $k = 1, \dots, N$

$$\|A(t^k) - A_h^k\|_{L_r^2(\Omega_0)} \leq \|\delta_h^0\|_{L_r^2(\Omega_0)} + C \left[h \|A\|_{H^1(0,T;H_r^2(\Omega))} + \Delta t \|A\|_{H^1(0,T;H_r^2(\Omega))} \right].$$

On the other hand, the first term in the right hand side above is bounded as follows:

$$\|\delta_h^0\|_{L_r^2(\Omega_0)} \leq \|A^0 - A_h^0\|_{L_r^2(\Omega_0)} + \|\rho_h^0\|_{L_r^2(\Omega_0)} \leq Ch \|A\|_{H^1(0,T;H_r^2(\Omega))}$$

where for the last inequality we have used that $A_h^0 = \mathcal{I}_h A^0$, Theorem 3.4.1, and (3.23). Thus the first estimate of this theorem follows from the two inequalities above.

The proof of the second estimate is essentially identical.

The proof of the third one only differs in that $\|\delta_h^0\|_{\tilde{H}_r^1(\Omega)}$ appears instead of $\|\delta_h^0\|_{L_r^2(\Omega_0)}$ when using Lemma 3.5.1. Then, from the definition of δ_h^0 , we have

$$\|\delta_h^0\|_{\tilde{H}_r^1(\Omega)} \leq \|P_h A(0) - A(0)\|_{\tilde{H}_r^1(\Omega)} + \|A(0) - A_h(0)\|_{\tilde{H}_r^1(\Omega)} \leq Ch \|A\|_{H^1(0,T;H_r^2(\Omega))},$$

where for the last inequality we have used (3.23) and Lemma 3.4.2. Using this inequality, the rest of the proof runs as those of the other estimates. \square

3.6 Numerical experiments

The numerical method analyzed above has been implemented in a FORTRAN code. Notice that the terms including the velocity lead to a non-symmetric linear system at each time step. The corresponding systems have been solved by means of the SUPERLU algorithm [23]. In this section, we will report the results obtained by applying this code to different problems. First, we will present two tests which will confirm theoretically the order of convergence of the numerical method. Finally, we will apply the code to an electromagnetic problem arising from an industrial process: the metal sheet forming.

3.6.1 Test with analytical solution

First we consider a problem with known analytical solution, although it does not fit exactly in the theoretical framework considered in the previous sections, because the source current is supported in an extremely thin coil. This test will allow us to check the convergence results proved above. This example has been taken from [13] and [10] where it was used to analyze a similar problem in harmonic regime. In what follows we describe briefly the test; we refer the reader to [10, 13] for further details.

Let us consider an infinite cylinder consisting of a core metal surrounded by a crucible and an extremely thin coil. The multi-turn coil is modeled as a continuous single one with a uniform surface current density (see Figure 3.3). The current density is taken periodic in time. If we do not consider velocity terms, then the solution of the electromagnetic problem can be obtained in the whole space, even for an axisymmetric crucible composed by different materials, provided that the physical properties are constants in each material.

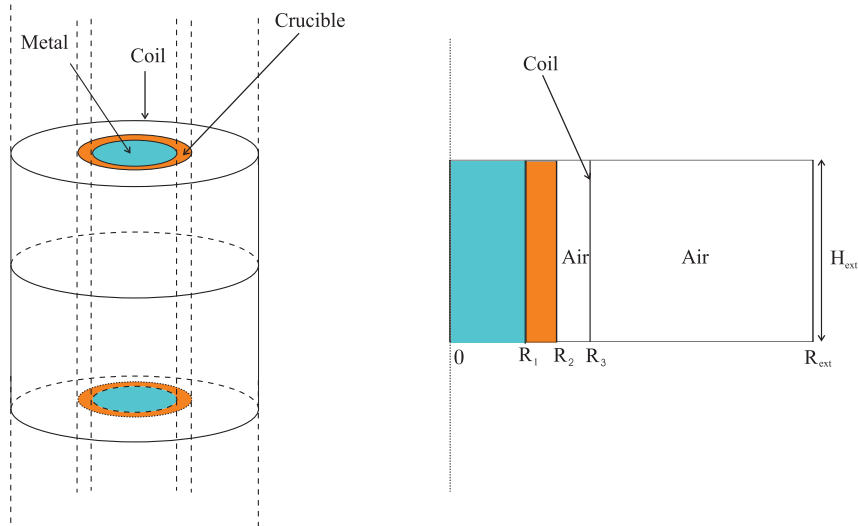


Figure 3.3: Analytical test. 3D and 2D sketches of the domain.

Since the current density is periodic in time, we assume that all the variables can be written as follows: $F(t, r, z) = \text{Re}[e^{i\omega t} \tilde{F}(r, z)]$, where $\omega > 0$ is the angular frequency of the source current. In such a case, for the problem described in Figure 3.3, the azimuthal

component of the magnetic vector potential is given by $A(t, r, z) = \operatorname{Re}[e^{i\omega t} \tilde{A}(r, z)]$, where

$$\tilde{A}(r, z) = \begin{cases} \alpha_1 I_1(r\sqrt{i\omega\mu\sigma}), & 0 < r < R_1, \\ \alpha_2 I_1(r\sqrt{i\omega\mu\sigma}) + \beta_1 K_1(r\sqrt{i\omega\mu\sigma}), & R_1 < r < R_2, \\ \alpha_3 \mu_0 \frac{r}{2} + \frac{\beta_2}{r}, & R_2 < r < R_3, \\ \frac{\beta_{\text{ext}}}{r}, & r > R_3, \end{cases}$$

with I_1 and K_1 being the first-order modified Bessel functions of the first and second kind, respectively. The coefficients μ and σ are taken constant in each material and the constants $\alpha_1, \alpha_2, \alpha_3, \beta_1, \beta_2$ and β_{ext} are chosen so that \tilde{A} and $\frac{1}{\mu r} \frac{\partial(r\tilde{A})}{\partial r}$ are continuous at $r = R_1$, $r = R_2$, and $r = R_3$.

We denote by R_{ext} and H_{ext} the width and height of the rectangular box enclosing the domain for the finite element computations (see Figure 3.3, again). For validation purposes, we have used exact Dirichlet boundary conditions, $\tilde{A} = \beta_{\text{ext}}/r$ at $r = R_{\text{ext}}$, and homogeneous Neumann conditions on the horizontal edges (recall that, for $\tilde{A} \in \tilde{H}_r^1$, there also holds $\tilde{A} = 0$ at $r = 0$).

The method has been used on several successively refined meshes by reducing the time step in a convenient way to analyze the convergence with respect to both, the mesh-size and the time step. With this aim, the numerical approximations have been compared with the analytical solution. As a first step, for each quantity A_h^k, \mathbf{B}_h^k , and \mathbf{J}_h^k , the dependence of the error on h and Δt was studied separately. To do this, first we fixed the time step to a sufficiently small value, so that the error practically depends only on the mesh-size. In this case we observed that the error of \mathbf{B}_h^k reduces linearly with respect to h , while those of A_h^k and \mathbf{J}_h^k reduces quadratically. Then, we fixed the mesh-size to a sufficiently small value for the time discretization error to prevail. In such a case we observed a linear dependence on Δt for all quantities.

We illustrate in Figures 3.4 and 3.5 the convergence behavior of the method for each of these quantities. These figures show log-log plots of the errors of A_h^k, \mathbf{J}_h^k , and \mathbf{B}_h^k in the discrete norms considered in Theorem 3.5.2 versus the number of degrees of freedom (d.o.f.). To report in one only figure the simultaneous dependence on h and Δt , we proceeded in the following way: first, we chose initial values of h and Δt , so that the time and the space discretization errors were both of approximately the same size; secondly, for each of the successively refined meshes, we have taken values of Δt proportional either to h or to h^2 , according to the previously observed dependence of the errors on the mesh-size.

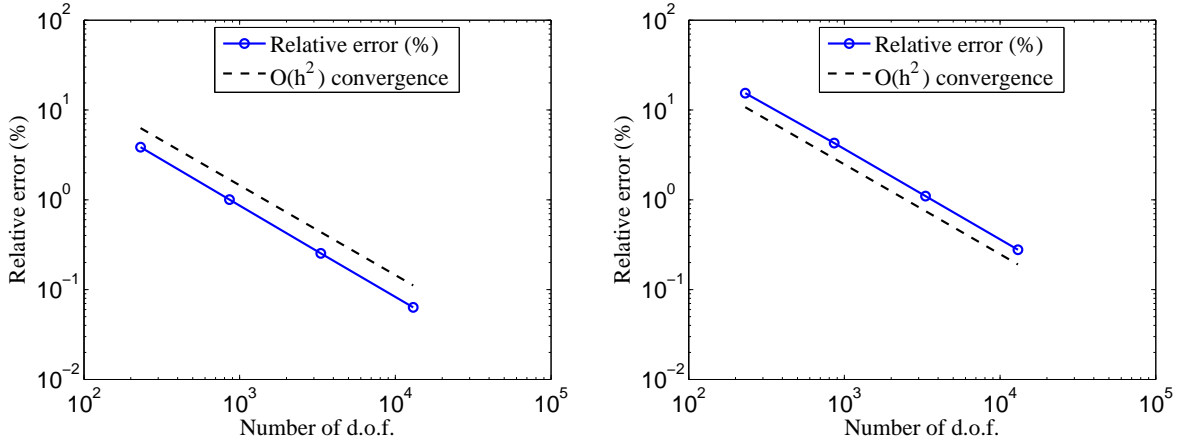


Figure 3.4: Analytical test. Relative errors for the magnetic vector potential $\max_{1 \leq k \leq N} \|A(t^k) - A_h^k\|_{L_r^2(\Omega_0)}$ (left) and the current density $[\Delta t \sum_{k=1}^N \|\mathbf{J}(t^k) - \mathbf{J}_h^k\|_{L_r^2(\Omega_0)}^2]^{1/2}$ (right) versus number of d.o.f. (log-log scale), with $\Delta t = Ch^2$ in both cases

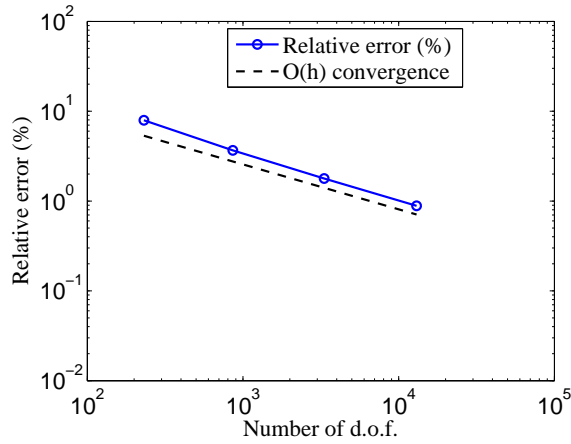


Figure 3.5: Analytical test. Relative errors for the magnetic induction $[\Delta t \sum_{k=1}^N \|\mathbf{B}(t^k) - \mathbf{B}_h^k\|_{L_r^2(\Omega)}^2]^{1/2}$ versus number of d.o.f. (log-log scale), with $\Delta t = Ch$.

A quadratic dependence on the mesh-size in the first two cases and a linear dependence in the third one can be clearly seen from these figures. Notice that the convergence behavior for all these quantities agrees with or improves the theoretically predicted order of convergence.

3.6.2 Simulation of an induction heating furnace including a moving fluid

The goal of this section is to analyze the convergence of the numerical method applied to a problem lying in the framework of the theoretical results and including the velocity term in the Ohm's law. We recall that in our analysis the domain of the conducting medium remains fixed throughout the process. This is what happens, for instance in magnetohydrodynamic problems which involve a fluid in motion occupying a fixed domain [12]. In particular, we consider the simulation of a small induction furnace composed by a graphite crucible and containing silicon in motion inside. This example has been taken from [13] where it was solved in harmonic regimen. A sketch of the domain is presented in Figure 3.6, the geometrical data are described in more detail in [13]. In the present case, we assume that each turn of the coil has a periodic in time uniform current distribution with amplitude J_0 , i.e., $J_S := J_0 \cos(\omega t)$; these source data and the physical parameters are described in Table 3.1.

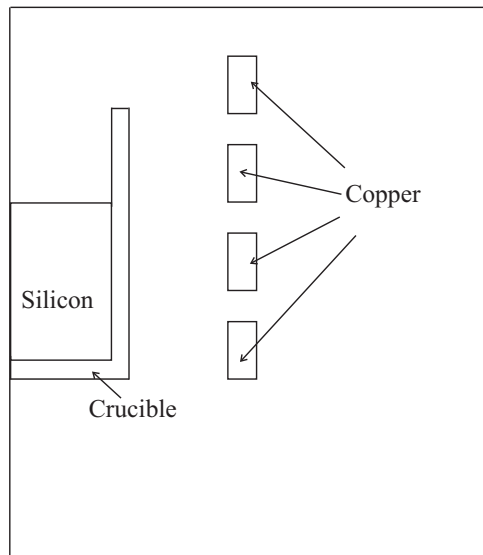


Figure 3.6: Induction Furnace. Sketch of the domain.

The radial section of the domain containing melted silicon is a rectangle $[0, r_0] \times [z_0, z_1]$ with $r_0 = 0.021$, $z_0 = 0.004$, and $z_1 = 0.05$ all the lengths measured in meters. The velocity field in this domain has been taken as $\mathbf{v} = \text{curl}(\varphi \mathbf{e}_\theta)$ with φ given by

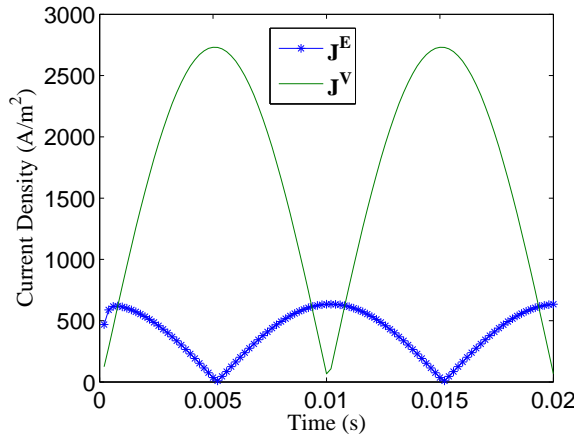
$$\varphi = cr^2 (r - r_0)^2 (z - z_0)^2 (z - z_1)^2.$$

Table 3.1: Induction Furnace. Physical data.

Number of coil turns:	4
Amplitude of current density (in each turn) (J_0):	$3 \times 10^7 \text{ A/m}^2$
Frequency (ω):	50 Hz
Electrical conductivity of silicon (σ):	$1234568 (\text{Ohm m})^{-1}$
Electrical conductivity of crucible (σ):	$240000 (\text{Ohm m})^{-1}$
Magnetic permeability of all materials (μ):	$4\pi 10^{-7} \text{ Hm}^{-1}$

The constant c has been taken large enough so that the electric current density due to this velocity be significant. In particular we have taken $c = 10^{14}$. Notice that \mathbf{v} is divergence free and vanishes on the whole boundary of the rectangle.

The current arising from the velocity term is actually significant in this problem. In fact, this can be seen from Figure 3.7, where we plot the two components $\mathbf{J}^E := \sigma \bar{\partial} A_h^k$ and $\mathbf{J}^V := \sigma \mathbf{v} \times \mathbf{B}_h^k$ of the current density (cf. (3.40)).

Figure 3.7: Induction Furnace. $\|\mathbf{J}_h^E\|_{L_r^2(\Omega_0)}$ and $\|\mathbf{J}_h^V\|_{L_r^2(\Omega_0)}$ versus time.

Since in this case there is no analytical solution to compare with, we have used as a reference solution the one obtained with the same finite element method for an extremely fine mesh. Numerical approximations \mathbf{A}_h^k , \mathbf{B}_h^k , and \mathbf{J}_h^k obtained with several successively refined meshes have been compared with the reference one. In all cases we have used a time-step sufficiently small so that the errors arising from the time discretization be

negligible with respect to the space discretization errors. Figure 3.8 and 3.9 show log-log plots of the corresponding relative errors.

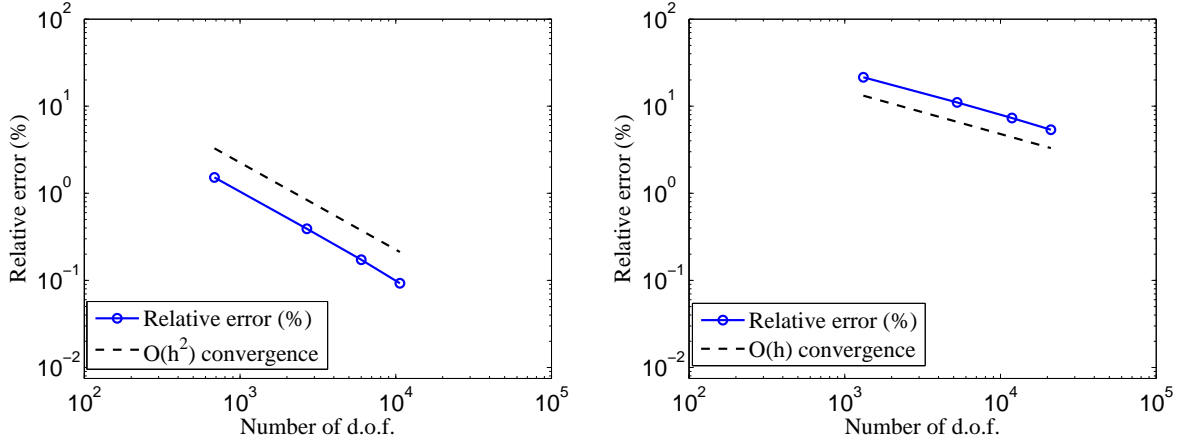


Figure 3.8: Induction furnace. Relative errors for the magnetic vector potential $\max_{1 \leq k \leq N} \|A(t^k) - A_h^k\|_{L_r^2(\Omega_0)}$ (left) and the magnetic induction $[\Delta t \sum_{k=1}^N \|\mathbf{B}(t^k) - \mathbf{B}_h^k\|_{L_r^2(\Omega)}^2]^{1/2}$ (right) versus number of d.o.f. (log-log scale), with Δt sufficiently small.

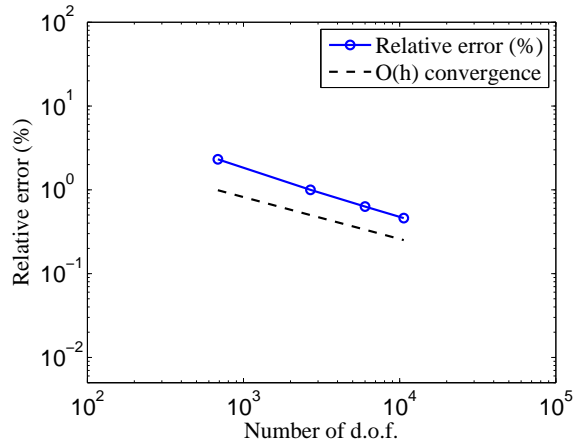


Figure 3.9: Induction furnace. Relative errors for the current density $[\Delta t \sum_{k=1}^N \|\mathbf{J}(t^k) - \mathbf{J}_h^k\|_{L_r^2(\Omega_0)}^2]^{1/2}$ versus number of d.o.f. (log-log scale), with Δt sufficiently small.

A linear order of convergence can be clearly observed for \mathbf{B}_h^k and \mathbf{J}_h^k , as predicted by the theory. This is not the case for the magnetic potential A_h^k which converges quadratically, although in Theorem 3.5.2 only a linear order of convergence has been proved. Even

though this is just an auxiliary quantity, from the theoretical point of view it would be interesting to know whether such a quadratic convergence always holds.

3.6.3 Simulation of an industrial application: An electromagnetic forming process

Finally, we have used the numerical method to compute the current density and the Lorentz force in an example taken from an electromagnetic forming process. Electromagnetic forming (EMF) is a dynamic, high strain-rate forming method. In this process, deformation of the workpiece is driven by the interaction of a transient current induced in the same workpiece by a magnetic field generated by an adjacent coil ([24]).

In this section, we consider the geometry and physical data of the axisymmetric electromagnetic forming example described in [32] (see Figure 3.10 and Table 3.2), which corresponds to a classical benchmark problem (see [32, 46] for more details).

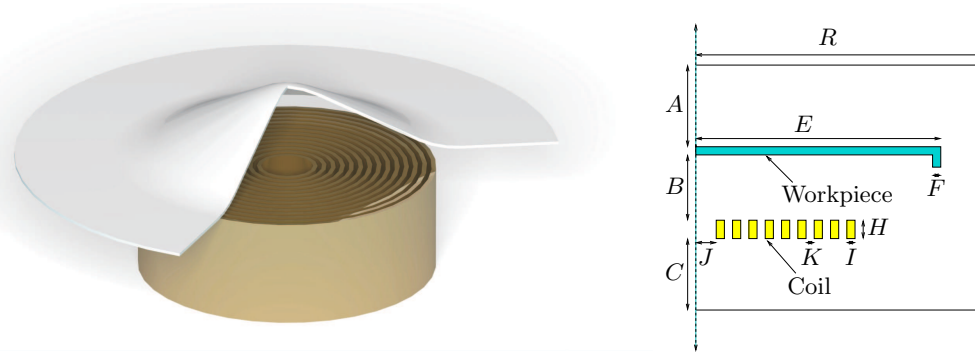


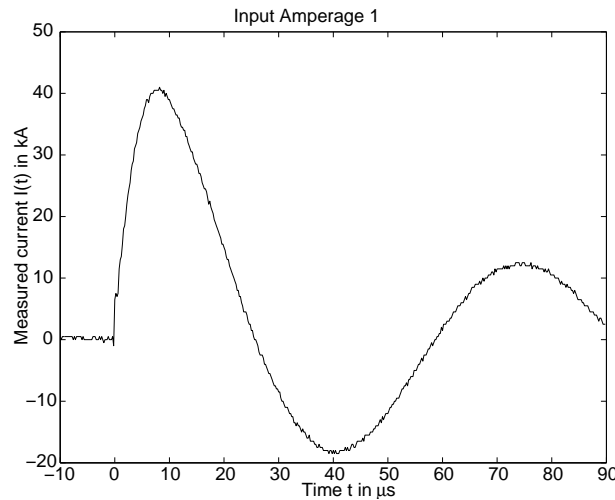
Figure 3.10: EMF. Geometry of the benchmark problem.

We are not able to compare in detail our results with those presented for the same benchmark problem in [46], because we have not included the deformation of the plate in the electromagnetic model. This deformation, which leads to an electromagnetic domain changing with time is the object of a forthcoming research. In the present case, we give some qualitative results by using the geometrical data and the current source given in [32], which is shown in Figure 3.11. Notice that it corresponds to a source attaining very large values in a very short time: $10 \mu\text{s}$.

We present in Figure 3.12 the axial component of the Lorentz force versus radius (left) and height (right) for a fixed time ($10 \mu\text{s}$). The results are qualitatively very similar to

Table 3.2: EMF. Geometrical data and physical parameters:

Thickness of the workpiece (F):	0.0012 m
Height of the tool coil (H):	0.0115 m
Width of each turn coil (I):	0.0025 m
Distance between coil turns (K):	0.0003 m
Distance coil-workpiece (B):	0.002 m
Vertical distance from coil to bottom (C):	0.05 m
Vertical distance from workpiece to the top (A):	0.05 m
Width of the workpiece (E):	0.115 m
Width of the rectangular box (R):	0.2 m
Number of coil turns:	9
Electrical conductivity of metal (σ):	$25900 \text{ (Ohm m)}^{-1}$
Magnetic permeability of all materials (μ):	$4\pi 10^{-7} \text{ Hm}^{-1}$

Figure 3.11: EMF. Current intensity (A) vs. time (μs).

those presented in Section 6 from [46].

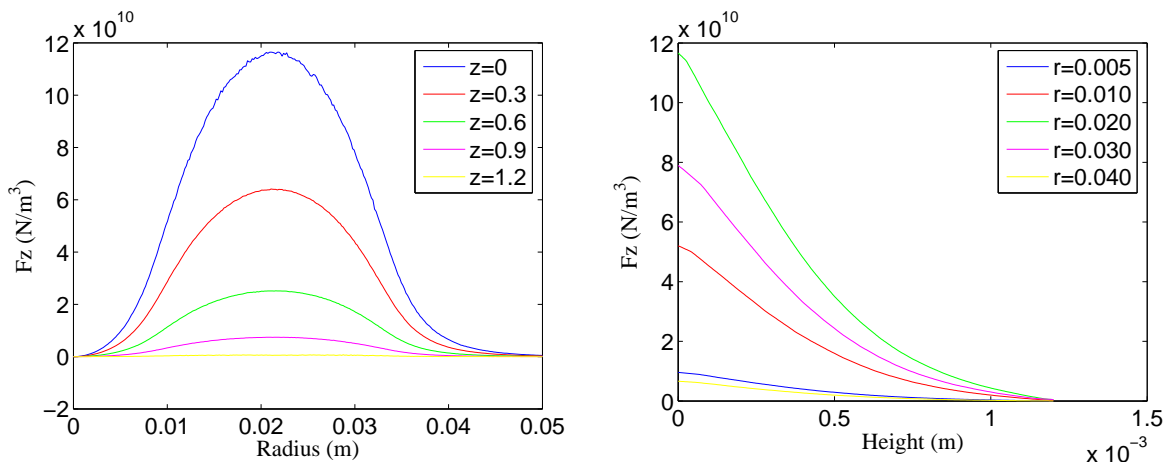


Figure 3.12: FEM. Axial component of the Lorentz force versus radius (left) and versus height (right) after $10 \mu\text{s}$.

Chapter 4

Numerical analysis of a transient eddy current problem arising from electromagnetic forming

4.1 Introduction

The Electromagnetic Forming (EMF) is a metal working process that relies on the use of electromagnetic forces to deform metallic workpieces at high speeds. A transient electric current is induced in a coil using a capacitor bank and high-speed switches. This current induces a magnetic field that penetrates the nearby conductive workpiece where an eddy current is generated. The magnetic field, together with the eddy current, induces Lorentz forces that drive the deformation of the workpiece [24, 32, 46]. The workpiece can be reshaped without any contact from a tool, although in some instances the piece may be pressed against a die or former. The technique is sometimes called high velocity forming. Since the forming operation involves high acceleration and deceleration, mass of the workpiece plays a critical role during the forming process. Moreover, the process works best with good electrical conductors such as copper or aluminum, but it can be adapted to work with poorer conductors such as steel.

The motion of the workpiece introduces two difficulties to the problem. First, the domain changes along the time, because the motion of the workpiece changes its position. Also, the velocity in the workpiece produces currents that in principle should be added

in the Ohm's law. The difficulties arising from this additional term have been studied in [14] with a fixed domain. However, in EMF typically the current density induced for the velocity terms is not significant, so we will neglect it.

The axisymmetry allows stating the eddy current problem in terms of the azimuthal component of a magnetic vector potential defined in a meridional section of the domain (see, for instance, [13]). This leads to consider a transient problem where the term involving the time derivative only appears in a part of the domain, which changes with time. In this paper we study the electromagnetic model and we take the motion of the workpiece as data. In the thorough problem, the eddy current model must be coupled with an adequate mechanical model for the deformation of the workpiece.

The classical theory for abstract parabolic problems (see, for instance, [25]) cannot be used for the mathematical analysis because the formulation is degenerate. We use a regularization argument to prove the well-posedness of the continuous problem.

For the numerical solution, first we discretize in space by standard finite elements. This leads to a singular differential algebraic system ([18]) which is proved to be well posed using the same arguments as for the continuous problem. We prove error estimates for this semidiscrete approximation by adapting the classical theory ([25]) to the degenerate character of the parabolic problem.

Next, we combine finite elements in space with a backward Euler time-discretization. The resulting scheme avoids dealing with the additional terms arising from the Reynolds Transport theorem. On the other hand, the spatial mesh does not need to be fitted to the workpiece, which allows using a fixed mesh for the whole process. All these features lead to a numerical scheme easy to implement computationally. We prove error estimates for this fully discretized scheme by adapting once more the classical theory to the degenerate character of the problem. These error estimates are valid provided some additional regularity holds for the source current density and the initial data, as well as for the solution.

The outline of this paper is as follows: in Section 4.2, we describe the transient eddy current model and introduce a magnetic vector potential formulation under axisymmetric assumptions. In Section 4.3, we state the weak formulation and prove its well-posedness. In Section 4.4, we introduce the finite element space discretization and prove error estimates. In Section 4.5, we propose a backward Euler scheme for time discretization and prove error estimates for the fully discretized problem. Finally, in Section 4.6, we report some

numerical tests which allow us to asses the performance of the proposed method.

4.2 Statement of the problem

We are interested in computing the electromagnetic field produced by a coil in a cylindrical workpiece (see Figure 4.1 for an example). In order to have a domain with cylindrical symmetry, we replace the coil by several superimposed rings having toroidal geometry and carrying the same current intensity. On the other hand, in order to solve the electromagnetic model in a bounded domain, we introduce a three dimensional cylinder $\tilde{\Omega}$ of radius R and height L containing the coil and the workpiece. Then, by the cylindrical symmetry, we can work in a meridional section of $\tilde{\Omega}$ denoted by Ω . Let $\Omega_S := \Omega_1 \cup \dots \cup \Omega_m$ where Ω_k $k = 1, \dots, m$ are the meridional sections of the coil. Let Ω_t be the meridional section on the workpiece at time t . We assume that $\Omega_t \cap \Omega_S = \emptyset$ for all t . Let $\Omega_t^A := \Omega \setminus (\Omega_S \cup \Omega_t)$ be the section of the domain occupied by the air. Finally, let Γ_0 be the intersection between $\partial\Omega$ and the symmetry axis ($r = 0$), and $\Gamma_D := \partial\Omega \setminus \Gamma_0$ (see Figure 4.2).

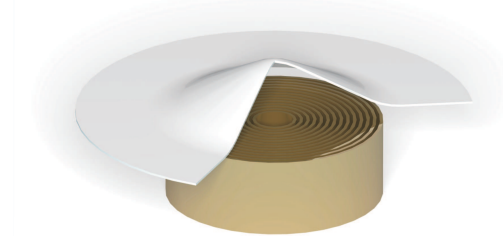


Figure 4.1: Sketch of the 3D-domain of the EMF System.

We will use standard notation in electromagnetism:

- \mathbf{E} is the electric field,
- \mathbf{B} is the magnetic induction,
- \mathbf{H} is the magnetic field,
- \mathbf{J} is the current density,
- μ is the magnetic permeability,

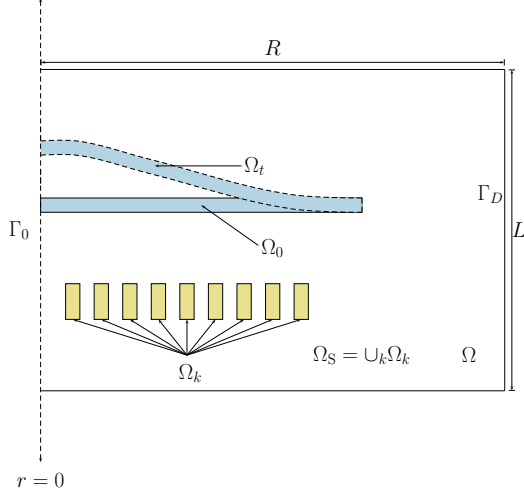


Figure 4.2: Sketch of the meridional section of the EMF system.

- σ is the electric conductivity.

The magnetic permeability μ is taken as a positive constant in the whole domain. The conductivity σ vanishes outside the workpiece. This piece can be made of different materials, each with a different conductivity. We will make this assumption more precise below; by the moment we just assume

$$\begin{aligned} 0 < \underline{\sigma} \leq \sigma \leq \bar{\sigma}, & \quad \text{in the workpiece,} \\ \sigma = 0, & \quad \text{outside of the workpiece.} \end{aligned}$$

In this kind of problem, the electric displacement can be neglected in Ampère's law, leading to the so called eddy current model:

$$\operatorname{curl} \mathbf{H} = \mathbf{J}, \tag{4.1}$$

$$\frac{\partial \mathbf{B}}{\partial t} + \operatorname{curl} \mathbf{E} = \mathbf{0}, \tag{4.2}$$

$$\operatorname{div} \mathbf{B} = 0, \tag{4.3}$$

This system must be completed with the following relations:

$$\mathbf{B} = \mu \mathbf{H},$$

and

$$\mathbf{J} = \begin{cases} \sigma \mathbf{E}, & \text{in the workpiece,} \\ \mathbf{J}_S, & \text{in the coil, (data),} \\ \mathbf{0}, & \text{in the air.} \end{cases} \quad (4.4)$$

Thus, the current density \mathbf{J} is taken as data in the coil and unknown in the workpiece Ω_t . Since σ vanishes outside Ω_t , the relation above can be written in a single equation as follows:

$$\mathbf{J} = \sigma \mathbf{E} + \mathbf{J}_S.$$

We assume that all the physical quantities are independent of the angular coordinate θ and that the source current density field has only azimuthal non-zero component, i.e.,

$$\mathbf{J}(t, r, \theta, z) = J(t, r, z) \mathbf{e}_\theta.$$

Proceeding as in [13] and [14] it can be proved that

$$\begin{aligned} \mathbf{H}(t, r, \theta, z) &= H_r(t, r, z) \mathbf{e}_r + H_z(t, r, z) \mathbf{e}_z, \\ \mathbf{B}(t, r, \theta, z) &= B_r(t, r, z) \mathbf{e}_r + B_z(t, r, z) \mathbf{e}_z, \\ \mathbf{E}(t, r, \theta, z) &= E(t, r, z) \mathbf{e}_\theta, \end{aligned}$$

Moreover, because of (4.3), we can introduce a magnetic vector potential \mathbf{A} for \mathbf{B} ,

$$\mathbf{B} = \operatorname{curl} \mathbf{A}, \quad (4.5)$$

of the form

$$\mathbf{A}(t, r, \theta, z) = A(t, r, z) \mathbf{e}_\theta \quad (4.6)$$

and such that (4.2) leads to

$$-\mathbf{E} = \frac{\partial \mathbf{A}}{\partial t}.$$

Therefore, the Maxwell system equations (4.1)-(4.3) can be rewritten in terms of the vector potential \mathbf{A} as follows:

$$\operatorname{curl} \left(\frac{1}{\mu} \operatorname{curl} \mathbf{A} \right) = \mathbf{J} = J \mathbf{e}_\theta,$$

where

$$J = \begin{cases} 0 & \text{in } \Omega_t^\Delta, \\ -\sigma(t) \frac{\partial A}{\partial t} & \text{in } \Omega_t, \\ J_S & \text{in } \Omega_S \text{ (data).} \end{cases} \quad (4.7)$$

Thus, we are lead to the following parabolic-elliptic problem:

$$\left\{ \begin{array}{ll} \sigma(t) \frac{\partial A}{\partial t} e_\theta + \operatorname{curl} \left(\frac{1}{\mu} \operatorname{curl} (A e_\theta) \right) = 0 & \text{in } \Omega_t, \\ \operatorname{curl} \left(\frac{1}{\mu} \operatorname{curl} (A e_\theta) \right) = J_S e_\theta & \text{in } \Omega_S, \\ \operatorname{curl} \left(\frac{1}{\mu} \operatorname{curl} (A e_\theta) \right) = 0 & \text{in } \Omega_t^A. \end{array} \right. \quad (4.8)$$

4.3 Weak formulation

Let $L_r^2(\Omega)$ be the weighted Lebesgue space of all measurable functions A defined in Ω such that

$$\|A\|_{L_r^2(\Omega)}^2 := \int_{\Omega} |A|^2 r \, dr \, dz < \infty.$$

The weighted Sobolev space $H_r^k(\Omega)$ consists of all functions in $L_r^2(\Omega)$ whose derivatives up to the order k are also in $L_r^2(\Omega)$. We define the norms and semi-norms in the standard way; in particular

$$\|A\|_{H_r^1(\Omega)}^2 := \int_{\Omega} (|\partial_r A|^2 + |\partial_z A|^2) r \, dr \, dz.$$

Let $L_{1/r}^2(\Omega)$ be the weighted Lebesgue space of all measurable functions A defined in Ω such that

$$\|A\|_{L_{1/r}^2(\Omega)}^2 := \int_{\Omega} \frac{|A|^2}{r} \, dr \, dz < \infty.$$

Let us define the Hilbert space $\tilde{H}_r^1(\Omega)$ by

$$\tilde{H}_r^1(\Omega) := \{A \in H_r^1(\Omega) : A \in L_{1/r}^2(\Omega)\}$$

with the norm

$$\|A\|_{\tilde{H}_r^1(\Omega)} := \left(\|A\|_{H_r^1(\Omega)}^2 + \|A\|_{L_{1/r}^2(\Omega)}^2 \right)^{1/2}.$$

Finally, let

$$\mathcal{V} := \{A \in \tilde{H}_r^1(\Omega) : A = 0 \text{ on } \Gamma_D\}.$$

Since part of our domain Ω changes with time, we need to define a reference domain $\hat{\Omega}$ and an application

$$\begin{aligned} X_t : \hat{\Omega} &\longrightarrow \Omega_t, \\ \hat{x} &\longmapsto X_t(\hat{x}), \end{aligned}$$

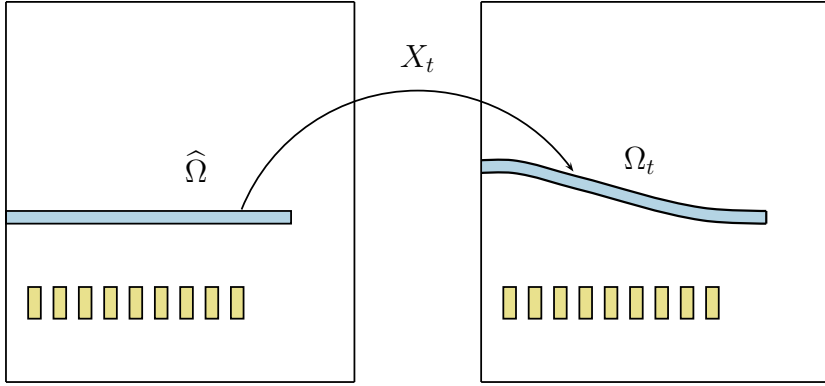


Figure 4.3: Reference Domain.

transforming $\hat{\Omega}$ into Ω_t (see Figure 4.3). We assume X_t is a sufficiently smooth diffeomorphism with respect to space and differentiable with respect to time. A usual way to define X_t is through the vector field \mathbf{v} which represents the velocity of the workpiece and which is taken as a data in our analysis. More precisely, from now on we assume \mathbf{v} is continuous with respect to time and twice continuously differentiable and globally Lipschitz with respect to space. We take $\hat{\Omega} := \Omega_{t=0}$, and define $t \mapsto X_t$ as the solution of the following problem:

$$\begin{aligned}\frac{\partial X_t}{\partial t}(\hat{x}) &= \mathbf{v}(t, X_t(\hat{x})), \\ X_0(\hat{x}) &= \hat{x}.\end{aligned}$$

On the other hand, the conductivity σ is taken such that

$$\sigma(t, x) = \hat{\sigma}(\hat{x}),$$

where $x = X_t(\hat{x})$ and $\hat{\sigma}$ is the conductivity in the reference domain $\hat{\Omega}$, which satisfies

$$\underline{\sigma} \leq \hat{\sigma}(\hat{x}) \leq \bar{\sigma}, \quad \hat{x} \in \hat{\Omega}.$$

This means that σ only depends on t through x and, from a physical point of view, that the conductivity of each material point remains constant along the process.

Let us introduce the following non-cylindrical open subset of $\Omega \times (0, T)$,

$$Q := \{(x, t) : x \in \Omega_t, t \in (0, T)\}.$$

Let us consider the following Banach spaces of functions defined in Q :

$$L_r^p(Q) := \{\varphi : Q \rightarrow \mathbb{R} \text{ measurable with } \int_0^T \int_{\Omega_t} |\varphi|^p r dr dz dt < \infty\},$$

endowed with the norm

$$\|\varphi\|_{L_r^p(Q)} := \left(\int_0^T \int_{\Omega_t} |\varphi|^p r dr dz dt \right)^{1/p},$$

and

$$W_r^{1,p}(Q) := \{\varphi \in L_r^p(Q) : \frac{\partial \varphi}{\partial t} \in L_r^p(Q), \frac{\partial \varphi}{\partial x_i} \in L_r^p(Q), i = 1, 2, 3\},$$

endowed with the norm

$$\|\varphi\|_{W_r^{1,p}(Q)} := \left(\|\varphi\|_{L_r^p(Q)}^p + \left\| \frac{\partial \varphi}{\partial t} \right\|_{L_r^p(Q)}^p + \sum_{i=1}^3 \left\| \frac{\partial \varphi}{\partial x_i} \right\|_{L_r^p(Q)}^p \right)^{1/p}.$$

Moreover we denote $H_r^1(Q) := W_r^{1,2}(Q)$. Let us recall the transport Reynolds' theorem:

Theorem 4.3.1 *Let $\varphi \in W_r^{1,1}(Q)$. Then*

$$\frac{d}{dt} \int_{\Omega_t} \varphi r dr dz = \int_{\Omega_t} \frac{\partial \varphi}{\partial t} r dr dz + \int_{\Omega_t} \varphi \operatorname{div} \mathbf{v} r dr dz + \int_{\Omega_t} \mathbf{grad} \varphi \cdot \mathbf{v} r dr dz.$$

Proof. It is an immediate consequence of the classical Reynolds' transport theorem for smooth functions and the density of the space $C^\infty(\bar{Q})$ in $W_r^{1,1}(Q)$. \square

The following result will be used in the sequel:

Corollary 4.3.1 *Let $A, Z \in W_r^{1,2}(Q)$. Then,*

$$\begin{aligned} \frac{d}{dt} \int_{\Omega_t} \sigma A Z r dr dz &= \int_{\Omega_t} \sigma \frac{\partial A}{\partial t} Z r dr dz + \int_{\Omega_t} \sigma A \frac{\partial Z}{\partial t} r dr dz \\ &\quad + \int_{\Omega_t} \sigma \operatorname{div} \mathbf{v} A Z r dr dz + \int_{\Omega_t} \sigma \mathbf{v} \cdot \mathbf{grad}(AZ) r dr dz. \end{aligned}$$

Next we deduce a variational formulation of (4.8) and prove it is well-posed. For this purpose, let us multiply (4.8) by a test vector field $Z \mathbf{e}_\theta$ with $Z \in \mathcal{V}$, integrate over Ω and use a Green's formula to obtain

$$\int_{\Omega_t} \sigma \frac{\partial A}{\partial t} Z r dr dz + a(A, Z) = \int_{\Omega_S} J_S Z r dr dz, \tag{4.9}$$

where

$$a(A, Z) := \int_{\Omega} \frac{1}{\mu} \operatorname{curl} A \mathbf{e}_\theta \cdot \operatorname{curl} Z \mathbf{e}_\theta r dr dz.$$

It is shown in [29, Propositions 2.1 and 3.1] that a is \mathcal{V} -elliptic; namely, there exists $\alpha > 0$ such that

$$a(Z, Z) \geq \alpha \|Z\|_{\tilde{H}_r^1(\Omega)}^2 \quad \forall Z \in \mathcal{V}.$$

Let the bilinear form c be defined by,

$$c(t, A, Z) := - \int_{\Omega_t} \sigma \operatorname{div} \mathbf{v} AZr dr dz - \int_{\Omega_t} \sigma \mathbf{v} \cdot \mathbf{grad}(AZ)r dr dz.$$

We have the following result:

Lemma 4.3.1 *For any $\delta > 0$ and for all $A \in \tilde{H}_r^1(\Omega)$, the following inequality holds:*

$$|c(t, A, A)| \leq \left(\bar{\sigma} \|\operatorname{div} \mathbf{v}\|_\infty + \frac{\|\mathbf{v}\|_\infty^2 \bar{\sigma}^2}{2\delta} \right) \|A\|_{L_r^2(\Omega_t)}^2 + \delta \|A\|_{H_r^1(\Omega_t)}^2.$$

Proof. By using Young's inequality, we can write for any $\delta > 0$

$$\begin{aligned} |c(t, A, A)| &= \left| \int_{\Omega_t} \sigma \operatorname{div} \mathbf{v} A^2 r dr dz + \int_{\Omega_t} \sigma \mathbf{v} \cdot \mathbf{grad}(A^2) r dr dz \right| \\ &= \left| \int_{\Omega_t} \sigma \operatorname{div} \mathbf{v} A^2 r dr dz + 2 \int_{\Omega_t} \sigma \mathbf{v} \cdot A \mathbf{grad} Ar dr dz \right| \\ &\leq \left(\bar{\sigma} \|\operatorname{div} \mathbf{v}\|_\infty + \frac{\|\mathbf{v}\|_\infty^2 \bar{\sigma}^2}{2\delta} \right) \|A\|_{L_r^2(\Omega_t)}^2 + \delta \|A\|_{H_r^1(\Omega_t)}^2. \end{aligned}$$

□

Corollary 4.3.2 *There exist strictly positive constants β and λ such that the following Gårding-like inequality holds:*

$$a(Z, Z) + c(t, Z, Z) + \lambda \int_{\Omega_t} \sigma |Z|^2 r dr dz \geq \beta \|Z\|_{\tilde{H}_r^1(\Omega)}^2 \quad \forall Z \in \tilde{H}_r^1(\Omega) \quad \forall t \in (0, T).$$

Notice that (4.9) corresponds to a degenerate parabolic problem because the term including the partial derivative of A with respect to time is only defined in Ω_t . Our next goal is to show that this problem has a unique solution.

Theorem 4.3.2 *Let $J_S \in H^1(0, T; L_r^2(\Omega_S))$ and $A^0 \in \tilde{H}_r^1(\Omega_0)$. Then, there exists a unique solution $A \in L^2(0, T; \mathcal{V})$, with $\frac{\partial A}{\partial t} \in L_r^2(Q)$, to the weak problem,*

$$\begin{aligned} \int_{\Omega_t} \sigma \partial_t AZr dr dz dt + a(A, Z) dt &= \int_{\Omega_S} J_S Zr dr dz dt \quad \forall Z \in \mathcal{V}, \text{ a.e. } t \in [0, T] \\ A(0) &= A^0 \text{ in } \Omega_0. \end{aligned} \tag{4.10}$$

Furthermore,

$$\begin{aligned} & \|\partial_t A\|_{L_r^2(Q)} + \|A\|_{L^\infty(0,T;\mathcal{V})} \\ & \leq C \left\{ \|A^0\|_{\tilde{H}_r^1(\Omega_0)}^2 + \int_0^T \|J_S(t)\|_{L_r^2(\Omega_S)}^2 dt + \int_0^T \|\partial_t J_S(t)\|_{L_r^2(\Omega_S)}^2 dt \right\}. \end{aligned} \quad (4.11)$$

Remark 4.3.1 Since $A \in L^2(0, T; \mathcal{V})$ and $\frac{\partial A}{\partial t} \in L_r^2(Q)$ then $A \in H_r^1(Q)$. From the trace theorem this implies that $A|_{\Omega_0 \times \{0\}} \in L_r^2(\Omega_0 \times \{0\}) \simeq L_r^2(\Omega_0)$. Thus the initial condition in (4.10) makes sense.

Proof. We proceed by space discretization and passing to the limit. Let $\{\phi_1, \dots, \phi_n, \dots\}$ be a basis of the Hilbert space \mathcal{V} . Let us introduce the family of finite-dimensional subspaces,

$$\mathcal{V}_N = \langle \phi_1, \dots, \phi_N \rangle.$$

We look for a function of the form

$$A_N(r, z, t) = \sum_{j=1}^N A_{jN}(t) \phi_j(r, z).$$

satisfying

$$\begin{aligned} & \int_{\Omega_t} \sigma \partial_t A_N \phi_i r dr dz + a(A_N, \phi_i) = \int_{\Omega_S} J_S \phi_i r dr dz \quad \forall i = 1, \dots, N, \text{ a.e. } t \in [0, T] \\ & A_N(0)|_{\Omega_0} = A_N^0|_{\Omega_0}, \end{aligned} \quad (4.12)$$

where $A_N^0 = \sum_{j=1}^N b_{jN} \phi_j \rightarrow A^0$ in $L_r^2(\Omega_0)$ and

$$\|A_N^0\|_{L_r^2(\Omega)} \leq C \|A^0\|_{L_r^2(\Omega_0)}, \quad (4.13)$$

$$\|A_N^0\|_{\tilde{H}_r^1(\Omega)} \leq C \|A^0\|_{\tilde{H}_r^1(\Omega_0)}, \quad (4.14)$$

for some constant C .

To obtain A_N^0 we can proceed as follows: Let $\widehat{A}^0 \in \mathcal{V}$ be an extension of A^0 to Ω such that

$$\|\widehat{A}^0\|_{\tilde{H}_r^1(\Omega)} \leq C \|A^0\|_{\tilde{H}_r^1(\Omega_0)}. \quad (4.15)$$

Such \widehat{A}^0 can be obtained by means of Nikolskii extension operator as in [36, Lemma 4.1]. Moreover, it is easy to show that this operator is also stable in $L_r^2(\Omega)$, namely

$$\|\widehat{A}^0\|_{L_r^2(\Omega)} \leq C \|A^0\|_{L_r^2(\Omega_0)}. \quad (4.16)$$

We write \widehat{A}^0 in the Hilbert basis $\widehat{A}^0 = \sum_{j=1}^{\infty} b_j \phi_i$ and define

$$A_N^0 := \sum_{j=1}^N b_j \phi_i.$$

Hence, clearly $\|A_N^0 - \widehat{A}^0\|_{\tilde{H}_r^1(\Omega)} \xrightarrow{N} 0$ which together with (4.15) implies (4.14). Moreover $\|A_N^0 - \widehat{A}^0\|_{L_r^2(\Omega)} \leq \|A_N^0 - \widehat{A}^0\|_{\tilde{H}_r^1(\Omega)} \xrightarrow{N} 0$ and hence (4.16) yields (4.13).

Since problem (4.12) is degenerated, to prove the existence of a solution we introduce a parabolic regularization as follows: for a non-negative small number ε let us replace (4.12) with the “approximate” parabolic problem,

$$\begin{aligned} \int_{\Omega_t} \sigma \partial_t A_N^\varepsilon \phi_i r \, dr \, dz + \varepsilon \int_{\Omega} \partial_t A_N^\varepsilon \phi_i r \, dr \, dz + a(A_N^\varepsilon, \phi_i) &= \int_{\Omega_S} J_S \phi_i r \, dr \, dz \quad \forall i = 1, \dots, N, \\ A_N^\varepsilon(0) &= A_N^0 \text{ in } \Omega. \end{aligned} \tag{4.17}$$

If we write $A_N^\varepsilon(t) = \sum_{j=1}^N A_{jN}^\varepsilon(t) \phi_j$, then the first equation from (4.17) reads

$$\begin{aligned} \sum_{j=1}^N \left(\int_{\Omega_t} \sigma \phi_j \phi_i r \, dr \, dz \right) \frac{d}{dt} A_{jN}^\varepsilon(t) + \varepsilon \sum_{j=1}^N \left(\int_{\Omega} \phi_j \phi_i r \, dr \, dz \right) \frac{d}{dt} A_{jN}^\varepsilon(t) + \sum_{j=1}^N a(\phi_j, \phi_i) A_{jN}^\varepsilon(t) \\ = \left(\int_{\Omega_S} J_S \phi_i r \, dr \, dz \right), \quad i = 1, \dots, N. \end{aligned}$$

Let $\mathbf{A}_N^\varepsilon(t) := (A_{jN}^\varepsilon(t))_{1 \leq j \leq N}$ and $\mathbf{F}_N(t) = ((J_S(t), \phi_i)_{L_r^2(\Omega_S)})_{1 \leq i \leq N}$. Let $\mathcal{K} \in \mathbb{R}^{N \times N}$, $\mathcal{M} \in \mathbb{R}^{N \times N}$ and $\mathcal{N} \in \mathbb{R}^{N \times N}$ be the matrices given by

$$\mathcal{K}_{i,j} := a(\phi_i, \phi_j), \quad \mathcal{M}_{i,j}(t) := (\sigma \phi_i, \phi_j)_{L_r^2(\Omega_t)}, \quad \mathcal{N}_{i,j} := (\phi_i, \phi_j)_{L_r^2(\Omega)}, \quad 1 \leq i, j \leq N.$$

Finally, let $(\mathbf{b}_N)_i := b_i^N$. Then, problem (4.12) reads as follows:

Find $\mathbf{A}^\varepsilon(t) \in \mathbb{R}^N$ such that

$$\begin{cases} (\mathcal{M}(t) + \varepsilon \mathcal{N}) \frac{d}{dt} \mathbf{A}_N^\varepsilon(t) + \mathcal{K} \mathbf{A}_N^\varepsilon(t) = \mathbf{F}_N(t), \\ \mathbf{A}_N^\varepsilon(0) = \mathbf{b}_N. \end{cases}$$

Since \mathcal{M} is positive semidefinite and \mathcal{N} is positive definite, then $\mathcal{M}(t) + \varepsilon \mathcal{N}$ is invertible and this problem has a unique solution, \mathbf{A}^ε , in the interval $[0, T]$. Furthermore, $\mathbf{A}^\varepsilon \in$

$H^1(0, T; \mathbb{R}^N)$, because

$$\begin{aligned}\|\partial_t \mathbf{A}^\varepsilon\|_{L^2(0,T;\mathbb{R}^N)} &\leq \sup_{0 \leq t \leq T} |(\mathcal{M} + \varepsilon \mathcal{N})^{-1}| (\|\mathbf{F}_N\|_{L^2(0,T;\mathbb{R}^N)} + \|\mathcal{K} A_N^\varepsilon\|_{L^2(0,T;\mathbb{R}^N)}) \\ &\leq \frac{1}{\varepsilon} |\mathcal{N}^{-1}| (\|\mathbf{F}_N\|_{L^2(0,T;\mathbb{R}^N)} + |\mathcal{K}| \|A_N^\varepsilon\|_{L^2(0,T;\mathbb{R}^N)}) \\ &< \infty,\end{aligned}$$

where $|\cdot|$ denotes the matrix norm induced by the Euclidean norm in \mathbb{R}^N . In order to pass to the limit as ε goes to 0 we need a priori estimates. Let us multiply the first equation in (4.17) by $A_{iN}^\varepsilon(t)$ and then sum from $i = 1$ to N . We obtain

$$\int_{\Omega_t} \sigma \partial_t A_N^\varepsilon A_N^\varepsilon r \, dr \, dz + \varepsilon \int_{\Omega} \partial_t A_N^\varepsilon A_N^\varepsilon r \, dr \, dz + a(A_N^\varepsilon, A_N^\varepsilon) = \int_{\Omega_S} J_S A_N^\varepsilon r \, dr \, dz. \quad (4.18)$$

From Corollary 4.3.1 we have,

$$\begin{aligned}\int_{\Omega_t} \sigma \partial_t (A_N^\varepsilon)^2 r \, dr \, dz &= \frac{d}{dt} \int_{\Omega_t} \sigma (A_N^\varepsilon)^2 r \, dr \, dz - \int_{\Omega_t} \sigma \operatorname{div} \mathbf{v} (A_N^\varepsilon)^2 r \, dr \, dz \\ &\quad - \int_{\Omega_t} \sigma \mathbf{v} \cdot \mathbf{grad} (A_N^\varepsilon)^2 r \, dr \, dz = \frac{d}{dt} \int_{\Omega_t} \sigma (A_N^\varepsilon)^2 r \, dr \, dz + c(t, A_N^\varepsilon, A_N^\varepsilon).\end{aligned} \quad (4.19)$$

Using (4.19) in (4.18), we write

$$\frac{1}{2} \frac{d}{dt} \int_{\Omega_t} \sigma (A_N^\varepsilon)^2 r \, dr \, dz + \frac{\varepsilon}{2} \frac{d}{dt} \int_{\Omega} (A_N^\varepsilon)^2 r \, dr \, dz + a(A_N^\varepsilon, A_N^\varepsilon) = \int_{\Omega_S} J_S A_N^\varepsilon r \, dr \, dz - \frac{1}{2} c(t, A_N^\varepsilon, A_N^\varepsilon). \quad (4.20)$$

We estimate the right hand side of (4.20) by using Corollary 4.3.2, and a weighted Cauchy-Schwartz inequality. Thus, we have for all $\delta_1 > 0$,

$$\begin{aligned}\frac{1}{2} \frac{d}{dt} \int_{\Omega_t} \sigma (A_N^\varepsilon)^2 r \, dr \, dz + \frac{\varepsilon}{2} \frac{d}{dt} \int_{\Omega} (A_N^\varepsilon)^2 r \, dr \, dz + \frac{\beta}{2} \|A_N^\varepsilon\|_{\tilde{H}_r^1(\Omega)}^2 \\ \leq \frac{1}{4\delta_1} \|J_S\|_{L_r^2(\Omega_S)}^2 + \delta_1 \|A_N^\varepsilon\|_{L_r^2(\Omega)}^2 + \frac{\lambda}{2} \int_{\Omega_t} \sigma (A_N^\varepsilon)^2 r \, dr \, dz.\end{aligned}$$

If $\delta_1 \leq \beta/4$, then

$$\begin{aligned}\frac{1}{2} \frac{d}{dt} \int_{\Omega_t} \sigma (A_N^\varepsilon)^2 r \, dr \, dz + \frac{\varepsilon}{2} \frac{d}{dt} \int_{\Omega} (A_N^\varepsilon)^2 r \, dr \, dz + \frac{\beta}{4} \|A_N^\varepsilon\|_{\tilde{H}_r^1(\Omega)}^2 \\ \leq \frac{1}{4\delta_1} \|J_S\|_{L_r^2(\Omega_S)}^2 + \frac{\lambda}{2} \int_{\Omega_t} \sigma (A_N^\varepsilon)^2 r \, dr \, dz.\end{aligned} \quad (4.21)$$

Therefore

$$\frac{1}{2} \frac{d}{dt} \int_{\Omega_t} \sigma(A_N^\varepsilon)^2 r dr dz + \frac{\varepsilon}{2} \frac{d}{dt} \int_{\Omega} (A_N^\varepsilon)^2 r dr dz \leq C \left\{ \|J_S\|_{L_r^2(\Omega_S)}^2 + \int_{\Omega_t} \sigma(A_N^\varepsilon)^2 r dr dz \right\}.$$

Now, we use the Gronwall's lemma to conclude that

$$\begin{aligned} \int_{\Omega_t} \sigma(A_N^\varepsilon)^2 r dr dz + \frac{\varepsilon}{2} \int_{\Omega} (A_N^\varepsilon)^2 r dr dz &\leq C \left\{ \int_{\Omega_0} \sigma(A_N^0)^2 r dr dz + \int_{\Omega} \sigma(A_N^0)^2 r dr dz \right. \\ &\quad \left. + \int_0^T \|J_S(s)\|_{L_r^2(\Omega_S)}^2 ds \right\} \\ &= C \left\{ \int_{\Omega_0} \sigma(A^0)^2 r dr dz + \int_0^T \|J_S(s)\|_{L_r^2(\Omega_S)}^2 ds \right\}, \end{aligned} \quad (4.22)$$

where we have used the second equation of (4.17) and (4.13).

Finally, we integrate (4.21) with respect to time and use (4.22) and (4.14) to obtain

$$\begin{aligned} \frac{\varepsilon}{2} \int_{\Omega} (A_N^\varepsilon(t))^2 r dr dz + \int_0^t \|A_N^\varepsilon(s)\|_{\tilde{H}_r^1(\Omega)}^2 ds &\leq C \left\{ \int_{\Omega_0} \sigma(A^0)^2 r dr dz \right. \\ &\quad \left. + \int_0^T \|J_S(s)\|_{L_r^2(\Omega_S)}^2 ds \right\}. \end{aligned} \quad (4.23)$$

Therefore, we obtain the following a priori estimates, which are independent of both ε and N :

- A_N^ε is bounded in $L^2(0, T; \mathcal{V})$,
- $\sqrt{\varepsilon} A_N^\varepsilon$ is bounded in $L^\infty(0, T; L_r^2(\Omega))$.

Next, let us multiply the first equation in (4.17) by $\partial_t A_{iN}^\varepsilon(t)$ and then sum from $i = 1$ to N . We obtain,

$$\int_{\Omega_t} \sigma(\partial_t A_N^\varepsilon)^2 r dr dz + \varepsilon \int_{\Omega} (\partial_t A_N^\varepsilon)^2 r dr dz + \frac{1}{2} \frac{d}{dt} a(A_N^\varepsilon, A_N^\varepsilon) = \int_{\Omega_S} J_S \partial_t A_N^\varepsilon r dr dz.$$

Integrating in time from 0 to T and using an integration by parts formula on the right-hand side we deduce,

$$\begin{aligned} \int_0^T \left[\int_{\Omega_t} \sigma(\partial_t A_N^\varepsilon)^2 r dr dz \right] dt + \varepsilon \int_0^T \left[\int_{\Omega} (\partial_t A_N^\varepsilon)^2 r dr dz \right] dt + \frac{1}{2} a(A_N^\varepsilon(T), A_N^\varepsilon(T)) \\ = \frac{1}{2} a(A_N^0, A_N^0) + \int_{\Omega_S} J_S(T) A_N^\varepsilon(T) r dr dz - \int_{\Omega_S} J_S(0) A_N^0 r dr dz \\ - \int_0^T \left[\int_{\Omega_S} \partial_t J_S A_N^\varepsilon r dr dz \right] dt, \end{aligned}$$

from which it follows that

$$\begin{aligned} & \int_0^T \left[\int_{\Omega_t} \sigma(\partial_t A_N^\varepsilon)^2 r dr dz \right] dt + \varepsilon \int_0^T \left[\int_\Omega (\partial_t A_N^\varepsilon)^2 r dr dz \right] dt + \frac{\alpha}{4} \|A_N^\varepsilon(T)\|_{\tilde{H}_r^1(\Omega)}^2 \\ & \leq C \left\{ \|A^0\|_{\tilde{H}_r^1(\Omega)}^2 + \int_0^T \|J_S(t)\|_{L_r^2(\Omega_S)}^2 dt + \int_0^T \|\partial_t J_S(t)\|_{L_r^2(\Omega_S)}^2 dt \right\}, \end{aligned} \quad (4.24)$$

by using (4.14) and (4.23).

Thus, we have proved the following a priori estimates:

- $\partial_t A_N^\varepsilon$ is bounded in $L_r^2(Q)$,
- $\sqrt{\varepsilon} \partial_t A_N^\varepsilon$ is bounded in $L^2(0, T; L_r^2(\Omega))$,
- A_N^ε is bounded in $L^\infty(0, T; \mathcal{V})$.

Therefore, for fixed N , there exists $A_N \in L^2(0, T; \mathcal{V})$ with $\partial_t A_N \in L_r^2(Q)$ and a sequence $\{\varepsilon_n\}$ converging to 0 such that,

- $\{A_N^{\varepsilon_n}\} \rightharpoonup A_N$ weakly in $L^2(0, T; \mathcal{V})$,
- $\{\partial_t A_N^{\varepsilon_n}\} \rightharpoonup \partial_t A_N$ weakly in $L_r^2(Q)$,
- $\{\sqrt{\varepsilon_n} \partial_t A_N^{\varepsilon_n}\} \rightharpoonup 0$ weakly in $L^2(0, T; L_r^2(\Omega))$.

In particular, this implies $A_N(0)|_{\Omega_0} = \lim_{n \rightarrow \infty} \{A_N^{\varepsilon_n}(0)|_{\Omega_0}\} = A_N^0|_{\Omega_0}$ weakly in $L_r^2(\Omega_0)$, so that the initial condition in (4.12) is satisfied by A_N .

Finally, one can pass to the limit in the first equation of (4.17) for $\varepsilon = \varepsilon_n$ as $n \rightarrow \infty$ and show that A_N is a solution of the semi-discretized problem (4.12).

It is also possible to pass to the limit in the estimates (4.22) and (4.23) to obtain,

$$\int_{\Omega_t} \sigma(A_N(t))^2 r dr dz + \int_0^t \|A_N(s)\|_{\tilde{H}_r^1(\Omega)}^2 ds \leq C \left\{ \int_{\Omega_0} \sigma(A^0)^2 r dr dz + \int_0^T \|J_S(s)\|_{L_r^2(\Omega_S)}^2 ds \right\}. \quad (4.25)$$

Indeed, the norm is a convex strongly continuous functional and then it is also weakly lower semi-continuous (recall that a function $\psi : \mathcal{B} \rightarrow \mathbb{R}$, \mathcal{B} being a Banach space, is said weakly lower semi-continuous if, for all sequence $\{y_n\} \subset \mathcal{B}$ such that $\{y_n\} \rightharpoonup y \in \mathcal{B}$, the following inequality holds: $\psi(y) \leq \liminf_{n \rightarrow \infty} \{\psi(y_n)\}$).

Since problem (4.12) is linear, the above estimate (4.25) for $t = T$ implies that A_N is its unique solution.

Similarly, passing to the limit in (4.24) we have

$$\begin{aligned} & \int_0^T \left[\int_{\Omega_t} \sigma(\partial_t A_N)^2 r dr dz \right] dt + \frac{\alpha}{4} \|A_N(T)\|_{\tilde{H}_r^1(\Omega)}^2 \\ & \leq C \left\{ \|A^0\|_{\tilde{H}_r^1(\Omega_0)}^2 + \int_0^T \|J_S(t)\|_{L_r^2(\Omega_S)}^2 dt + \int_0^T \|\partial_t J_S(t)\|_{L_r^2(\Omega_S)}^2 dt \right\}. \end{aligned} \quad (4.26)$$

Now estimates (4.25) and (4.26) allows us to affirm that there exists $A \in L^2(0, T; \mathcal{V})$ with $\partial_t A \in L_r^2(Q)$ and a subsequence of $\{A_N\}$ still denoted in the same way such that,

- $\{A_N\} \rightharpoonup A$ weakly in $L^2(0, T; \mathcal{V})$,
- $\{\partial_t A_N\} \rightharpoonup \partial_t A$ weakly in $L_r^2(Q)$.

In particular, this implies $A(0) = \lim_{N \rightarrow \infty} \{A_N(0)\} = \lim_{N \rightarrow \infty} \{A_N^0\} = A^0$, where the limits are weak in $L_r^2(\Omega_0)$, so that A satisfies the initial condition in (4.10).

In order to pass to the limit as $N \rightarrow \infty$ we take any $i \in \mathbb{N}$. Then, for $N \geq i$, $\phi_i \in \mathcal{V}_N$ and so (4.12) holds. Thus we can pass to the limit as $N \rightarrow \infty$ to get

$$\int_{\Omega_t} \sigma \partial_t A \phi_i r dr dz + a(A, \phi_i) = \int_{\Omega_S} J_S \phi_i r dr dz \quad \forall i \in \mathbb{N}. \quad (4.27)$$

Since the finite linear combinations of functions ϕ_i are dense in \mathcal{V} we deduce from (4.27),

$$\int_{\Omega_t} \sigma \partial_t A Z r dr dz + a(A, Z) = \int_{\Omega_S} J_S Z r dr dz \quad \forall Z \in \mathcal{V}.$$

Finally, passing to the limit as $N \rightarrow \infty$ in estimate (4.26) we obtain (4.11). \square

Remark 4.3.2 We notice that, from (4.25), we easily deduce

$$\int_0^T \|A(s)\|_{\tilde{H}_r^1(\Omega)}^2 ds \leq C \left\{ \int_{\Omega_0} \sigma (A^0)^2 r dr dz + \int_0^T \|J_S(s)\|_{L_r^2(\Omega_S)}^2 ds \right\},$$

which shows that the linear mapping giving the solution of (4.10) from the data $A^0 \in \tilde{H}_r^1(\Omega_0)$ and $J_S \in H^1(0, T; L^2(\Omega_S))$ is continuous from $L_r^2(\Omega_0) \times L^2(0, T; L_r^2(\Omega_S))$ to $L^2(0, T; \mathcal{V})$. Hence it can be uniquely extended by continuity and density for data $A^0 \in L^2(\Omega_0)$ and $J_S \in L^2(0, T; L_r^2(\Omega_S))$. The extended solutions belong to the space $L^2(0, T; \mathcal{V})$.

4.4 Semi-discrete problem. Finite element approximation

Let $\{\mathcal{T}_h\}_{h>0}$ be a regular family of triangulations of Ω where h is the mesh-size. Let

$$\mathcal{V}_h := \{A_h \in \mathcal{V} : A_h|_T \in \mathbb{P}_1 \quad \forall T \in \mathcal{T}_h\}.$$

Let us emphasize that in principle we do not assume that the meshes are fitted to Ω_0 .

We introduce the following semi-discrete problem: find $A_h \in L^2(0, T; \mathcal{V}_h)$ with $\partial_t A_h \in L^2(Q)$ such that

$$\begin{aligned} \int_{\Omega_t} \sigma \partial_t A_h Z_h r \, dr \, dz + a(A, Z_h) &= \int_{\Omega_S} J_S Z_h r \, dr \, dz \quad \forall Z_h \in \mathcal{V}_h, \\ A_h(0)|_{\Omega_0} &= A_h^0|_{\Omega_0} \end{aligned} \tag{4.28}$$

where A_h^0 has to satisfy the following conditions (see the proof of Theorem 4.3.2):

$$A_h^0|_{\Omega_0} \rightarrow A^0 \quad \text{in } L_r^2(\Omega_0), \tag{4.29}$$

$$\|A_h^0\|_{\tilde{H}_r^1(\Omega)} \leq C \|A^0\|_{\tilde{H}_r^1(\Omega_0)}. \tag{4.30}$$

To obtain A_h^0 we proceed as in the proof of Theorem 4.3.2. Let $\hat{A}^0 \in \mathcal{V}$ as in that proof and A_h^0 the Clément interpolant in \mathcal{V}_h of \hat{A}^0 as defined in [36, Section 7]. From the properties proved in this reference we have that

$$\|A_h^0\|_{\tilde{H}_r^1(\Omega)} \leq C \|\hat{A}^0\|_{\tilde{H}_r^1(\Omega)}$$

and

$$\|A_h^0 - \hat{A}^0\|_{L_r^2(\Omega)} \xrightarrow{h} 0.$$

Therefore, straightforward computations allow us to conclude (4.29) and (4.30).

Similar to the proof of Theorem 4.3.2 one can show that problem (4.28) has a unique solution for $A^0 \in \tilde{H}_r^1(\Omega_0)$ and $J_S \in H^1(0, T; L_r^2(\Omega_S))$. Moreover, the following estimate holds:

$$\begin{aligned} \sup_{t \in [0, T]} \int_{\Omega_t} \sigma(A_h(t))^2 r \, dr \, dz + \int_0^T \|A_h(s)\|_{\tilde{H}_r^1(\Omega)}^2 \, ds &\leq C \left\{ \int_{\Omega_0} \sigma(A^0)^2 r \, dr \, dz \right. \\ &\quad \left. + \int_0^T \|J_S(s)\|_{L_r^2(\Omega_S)}^2 \, ds \right\}. \end{aligned}$$

In this section we will prove error estimates for this semi-discrete problem by using the properties of an elliptic projector (see for instance [25]).

Let us introduce the elliptic projector $\mathbf{P}_h \in \mathcal{L}(\mathcal{V}, \mathcal{V}_h)$ associated to a :

$$a(\mathbf{P}_h Y, Z_h) = a(Y, Z_h) \quad \forall Z_h \in \mathcal{V}_h.$$

The following result follows from Cea's lemma and a duality argument (see Section 4 of [14]):

Lemma 4.4.1 *For all $Z \in H_r^2(\Omega) \cap \mathcal{V}$, we have*

$$h\|Z - \mathbf{P}_h Z\|_{\tilde{H}_r^1(\Omega)} + \|Z - \mathbf{P}_h Z\|_{L_r^2(\Omega)} \leq Ch^2\|Z\|_{H_r^2(\Omega)}. \quad (4.31)$$

Let A and A_h be the solutions of problems (4.10) and (4.28), respectively. We write

$$A(t) - A_h(t) = \delta_h(t) + \rho_h(t),$$

where

$$\delta_h(t) := \mathbf{P}_h A(t) - A_h(t) \quad \text{and} \quad \rho_h(t) := A(t) - \mathbf{P}_h A(t).$$

Provided A is smooth enough, we notice that $\partial_t(\mathbf{P}_h A) = \mathbf{P}_h(\partial_t A)$ (cf [55]) and then we have from (4.31)

$$\|\partial_t \rho_h\|_{L_r^2(\Omega)} \leq Ch^2\|\partial_t A\|_{H_r^2(\Omega)}. \quad (4.32)$$

Lemma 4.4.2 *If $A \in H^1(0, T; H_r^2(\Omega) \cap \mathcal{V})$, then for all $t \in [0, T]$ we have*

$$\sup_{t \in [0, T]} \int_{\Omega_t} \sigma \delta_h(t)^2 r dr dz + \int_0^T \|\delta_h(s)\|_{\tilde{H}_r^1(\Omega)}^2 ds \leq C \left\{ \|\delta_h(0)\|_{L_r^2(\Omega_0)}^2 + \int_0^T \int_{\Omega} (\partial_s \rho_h(s))^2 r dr dz ds \right\}, \quad (4.33)$$

$$\int_0^T \int_{\Omega_t} \sigma (\partial_s \delta_h(s))^2 r dr dz ds \leq C \left\{ \|\delta_h(0)\|_{\tilde{H}_r^1(\Omega)}^2 + \int_0^T \int_{\Omega} (\partial_s \rho_h(s))^2 r dr dz ds \right\}. \quad (4.34)$$

Proof. The following equalities hold for the solution of the continuous and the semi-discrete problems:

$$\int_{\Omega_t} \sigma \partial_t A Z_h r dr dz + a(A, Z_h) = \int_{\Omega_S} J_S Z_h r dr dz \quad \forall Z_h \in \mathcal{V}_h, \quad (4.35)$$

$$\int_{\Omega_t} \sigma \partial_t A_h Z_h r dr dz + a(A_h, Z_h) = \int_{\Omega_S} J_S Z_h r dr dz \quad \forall Z_h \in \mathcal{V}_h,$$

where we have used that $\partial_t A \in L^2(Q)$ to write (4.35) (see 4.10). Now, we can write

$$\int_{\Omega_t} \sigma \partial_t (A(t) - A_h(t)) Z_h r dr dz + a(A(t) - A_h(t), Z_h) = 0.$$

Using the definitions of δ_h and ρ_h , the last equation becomes

$$\int_{\Omega_t} \sigma \partial_t \delta_h(t) Z_h r dr dz + a(\delta_h(t), Z_h) = - \int_{\Omega_t} \sigma \partial_t \rho_h(t) Z_h r dr dz. \quad (4.36)$$

Now, we test with $Z_h = \delta_h(t)$ to obtain

$$\int_{\Omega_t} \sigma \partial_t \delta_h(t) \delta_h(t) r dr dz + a(\delta_h(t), \delta_h(t)) = - \int_{\Omega_t} \sigma \partial_t \rho_h(t) \delta_h(t) r dr dz.$$

By using Corollary 4.3.1 and Lemma 4.3.1, we have for $\epsilon_1, \epsilon_2 > 0$,

$$\begin{aligned} \frac{1}{2} \frac{d}{dt} \int_{\Omega_t} \sigma \delta_h(t)^2 r dr dz + \alpha \|\delta_h(t)\|_{\tilde{H}_r^1(\Omega)}^2 &\leq \frac{1}{4\epsilon_1} \int_{\Omega_t} \sigma (\partial_t \rho_h(t))^2 r dr dz + \epsilon_1 \int_{\Omega_t} \sigma \delta_h(t)^2 r dr dz \\ &\quad + \frac{1}{4\epsilon_2} \int_{\Omega_t} \sigma \delta_h(t)^2 r dr dz + \epsilon_2 \|A_h\|_{H_r^1(\Omega_t)}^2. \end{aligned}$$

Taking ϵ_1 and ϵ_2 such that $\epsilon_1 + \epsilon_2 \leq \alpha/2$,

$$\frac{1}{2} \frac{d}{dt} \int_{\Omega_t} \sigma \delta_h(t)^2 r dr dz + \frac{\alpha}{2} \|\delta_h(t)\|_{\tilde{H}_r^1(\Omega)}^2 \leq \frac{1}{4\epsilon_1} \int_{\Omega_t} \sigma (\partial_t \rho_h(t))^2 r dr dz + \frac{1}{4\epsilon_2} \int_{\Omega_t} \sigma \delta_h(t)^2 r dr dz.$$

Moreover, for each $t \in [0, T]$

$$\int_{\Omega_t} \sigma (\partial_t \rho_h(t))^2 r dr dz \leq \bar{\sigma} \int_{\Omega} (\partial_t \rho_h(t))^2 r dr dz$$

and hence

$$\begin{aligned} \frac{d}{dt} \int_{\Omega_t} \sigma \delta_h(t)^2 r dr dz + \alpha \|\delta_h(t)\|_{\tilde{H}_r^1(\Omega)}^2 &\leq C \int_{\Omega} (\partial_t \rho_h(t))^2 r dr dz + C \int_{\Omega_t} \sigma \delta_h(t)^2 r dr dz. \end{aligned} \quad (4.37)$$

We use the Gronwall's lemma in the last equation to write, for all $t \in [0, T]$

$$\int_{\Omega_t} \sigma \delta_h(t)^2 r dr dz + \leq C \left\{ \int_{\Omega_0} \sigma \delta_h(0)^2 r dr dz + \int_0^T \int_{\Omega} (\partial_s \rho_h(s))^2 r dr dz ds \right\}. \quad (4.38)$$

We integrate (4.37) with respect to time and use (4.38), to write

$$\int_0^T \|\delta_h(s)\|_{\tilde{H}_r^1(\Omega)}^2 ds \leq C \left\{ \int_{\Omega_0} \sigma \delta_h(0)^2 r dr dz + \int_0^T \int_{\Omega} (\partial_s \rho_h(s))^2 r dr dz ds \right\}.$$

Thus, estimate (4.33) follows from the last two inequalities. On the other hand, by testing (4.36) with $Z_h = \partial_t \delta_h(t)$, we write

$$\int_{\Omega_t} \sigma(\partial_t \delta_h(t))^2 r dr dz + a(\delta_h(t), \partial_t \delta_h(t)) = - \int_{\Omega_t} \sigma \partial_t \rho_h(t) \partial_t \delta_h(t) r dr dz.$$

Therefore, for $\epsilon_1 > 0$,

$$\begin{aligned} \int_{\Omega_t} \sigma(\partial_t \delta_h(t))^2 r dr dz + \frac{1}{2} \partial_t a(\delta_h(t), \delta_h(t)) &\leq \frac{1}{4\epsilon_1} \int_{\Omega_t} \sigma(\partial_t \rho_h(t))^2 r dr dz \\ &\quad + \epsilon_1 \int_{\Omega_t} \sigma(\partial_t \delta_h(t))^2 r dr dz. \end{aligned}$$

Taking $\epsilon_1 \leq 1/2$ and integrating with respect to time, we have

$$\begin{aligned} \frac{1}{2} \int_0^T \int_{\Omega_t} \sigma(\partial_s \delta_h(s))^2 r dr dz ds + \frac{1}{2} a(\delta_h(T), \delta_h(T)) &\leq \frac{1}{2} a(\delta_h(0), \delta_h(0)) \\ &\quad + \frac{1}{4\epsilon_1} \int_0^T \int_{\Omega} \bar{\sigma}(\partial_s \rho_h(s))^2 r dr dz ds \end{aligned}$$

and (4.34) follows from the continuity and the ellipticity of a . \square

Now we are in a position to prove error estimates for the computed vector potential A_h as well as for the physical quantities of interest that can be derived from it, namely, the approximations \mathbf{B}_h and \mathbf{J}_h of the magnetic induction \mathbf{B} and the current density \mathbf{J} . According to (4.5) and (4.6), let us define

$$\mathbf{B}_h := \mathbf{curl}(A_h \mathbf{e}_\theta).$$

The current density \mathbf{J} in the workpiece is given by $\mathbf{J} = \sigma(-\frac{\partial A}{\partial t}) \mathbf{e}_\theta$. Hence we define the computed current density as follows:

$$\mathbf{J}_h := -\sigma \left(\frac{\partial A_h}{\partial t} \right) \mathbf{e}_\theta \quad \text{in } \Omega_t.$$

The following error estimates hold.

Theorem 4.4.1 *Let A and A_h be the solutions of problems (4.9) and (4.12), respectively. Let \mathbf{B} be defined by (4.5) and (4.6) and \mathbf{J} by (4.4) and (4.7). Let \mathbf{B}_h and \mathbf{J}_h be defined as above. If $A \in H^1(0, T; H_r^2(\Omega))$, then, there exists a positive constant C , independent of h , such that*

$$\|A - A_h\|_{C^0(0, T; L_r^2(\Omega_t))} \leq C \left\{ \|A(0) - A_h(0)\|_{L_r^2(\Omega_0)} + h^2 \|A\|_{H^1(0, T; H_r^2(\Omega))} \right\}, \quad (4.39)$$

$$\|\mathbf{B} - \mathbf{B}_h\|_{L^2(0, T; L_r^2(\Omega))} \leq C \left\{ \|A(0) - A_h(0)\|_{L_r^2(\Omega_0)} + h \|A\|_{H^1(0, T; H_r^2(\Omega))} \right\}, \quad (4.40)$$

$$\|\mathbf{J} - \mathbf{J}_h\|_{L^2(0, T; L_r^2(\Omega_t))} \leq C \left\{ \|A(0) - A_h(0)\|_{\tilde{H}_r^1(\Omega)} + h^2 \|A\|_{H^1(0, T; H_r^2(\Omega))} \right\}. \quad (4.41)$$

Proof. We use that $A - A_h = \delta_h + \rho_h$, (4.31), (4.32) and (4.33) to write

$$\begin{aligned} \|A - A_h\|_{C^0(0,T;L_r^2(\Omega_t))} &\leq \sup_{t \in [0,T]} \|\delta_h(t)\|_{L_r^2(\Omega_t)} + \sup_{t \in [0,T]} \|\rho_h(t)\|_{L_r^2(\Omega_t)} \\ &\leq C \left\{ \|A(0) - A_h(0)\|_{L_r^2(\Omega_0)} + \|\rho_h(0)\|_{L_r^2(\Omega_0)} + h^2 \|A\|_{H^1(0,T;H_r^2(\Omega))} \right. \\ &\quad \left. + \sup_{t \in [0,T]} \|\rho_h(t)\|_{L_r^2(\Omega_t)} \right\} \\ &\leq C \left\{ \|A(0) - A_h(0)\|_{L_r^2(\Omega_0)} + h^2 \|A\|_{H^1(0,T;H_r^2(\Omega))} \right\} \end{aligned}$$

from which we conclude (4.39).

For the second inequality we use the definitions of \mathbf{B} and \mathbf{B}_h , (4.33), and (4.31) to write

$$\begin{aligned} \|\mathbf{B} - \mathbf{B}^h\|_{L^2(0,T;L_r^2(\Omega))} &\leq \|\delta_h\|_{L^2(0,T;\tilde{H}_r^1(\Omega))} + \|\rho_h\|_{L^2(0,T;\tilde{H}_r^1(\Omega))} \\ &\leq C \left\{ \|A(0) - A_h(0)\|_{L_r^2(\Omega_0)} + h \|A\|_{H^1(0,T;H_r^2(\Omega))} \right\}. \end{aligned}$$

On the other hand, according to the definitions of \mathbf{J} and \mathbf{J}_h we need the following one, which follows from (4.34), (4.31) and (4.32):

$$\begin{aligned} \|\partial_t A - \partial_t A_h\|_{L^2(0,T;L_r^2(\Omega_t))} &\leq \|\partial_t \delta_h\|_{L^2(0,T;L_r^2(\Omega_t))} + \|\partial_t \rho_h\|_{L^2(0,T;L_r^2(\Omega_t))} \\ &\leq \|\delta_h(0)\|_{\tilde{H}_r^1(\Omega)} + \|\partial_t \rho_h\|_{L^2(0,T;L_r^2(\Omega))} \\ &\leq \|A(0) - A_h(0)\|_{\tilde{H}_r^1(\Omega)} + \|\rho_h(0)\|_{\tilde{H}_r^1(\Omega)} + \|\partial_t \rho_h\|_{L^2(0,T;L_r^2(\Omega))} \\ &\leq \|A(0) - A_h(0)\|_{\tilde{H}_r^1(\Omega)} + h \|A\|_{H^1(0,T;H_r^2(\Omega))} \end{aligned}$$

Thus, we conclude the proof. \square

Remark 4.4.1 If the meshes are fitted to Ω_0 , then, we already showed that $A_h(0)$ is defined in Ω_0 by the second equation of (4.12), i.e.,

$$\int_{\Omega_0} \sigma A_h(0) Z_h r dr dz = \int_{\Omega_0} \sigma A^0 Z_h r dr dz \quad \forall Z_h \in \mathcal{V}_h^0.$$

Hence, $A_h(0)|_{\Omega_0}$ is the $L_r^2(\Omega_0)$ -projection of $A(0)$ onto \mathcal{V}_h^0 and the following estimate is a consequence of (4.31):

$$\|A(0) - A_h(0)\|_{L_r^2(\Omega_0)} \leq Ch^2 \|A(0)\|_{H_r^2(\Omega_0)}.$$

This last inequality allows us to improve the error estimates (4.39) and (4.40). However, this is not the case with estimate (4.41).

4.5 Fully discrete problem

In this section we present the full discretization of the problem. We consider a uniform partition of the time interval $[0, T]$: $\{t^k := k\Delta t, k = 1, \dots, N\}$ with time step $\Delta t := \frac{T}{N}$. We use the backward Euler approximation for the time discretization:

$$\int_{\Omega_{t^k}} \sigma(t^k) \frac{\partial A_h}{\partial t} Z_h r dr dz \approx \frac{1}{\Delta t} \int_{\Omega_{t^k}} \sigma(t^k) (A_h^k - A_h^{k-1}) Z_h r dr dz.$$

Thus, the fully discrete approximation of problem (4.12) is defined as follows:

Given $A_h^0 \in \mathcal{V}_h$, for $k = 1, \dots, N$, find $A_h^k \in \mathcal{V}_h$ such that

$$\frac{1}{\Delta t} \int_{\Omega_{t^k}} \sigma(t^k) (A_h^k - A_h^{k-1}) Z_h r dr dz + a(A_h^k, Z_h) = \int_{\Omega_S} J_S Z_h r dr dz \quad \forall Z_h \in \mathcal{V}_h. \quad (4.42)$$

The previous scheme needs an initial data in a neighborhood of Ω_0 containing Ω_{t^1} . Let us assume that $A(0)$ is known in all Ω and take A_h^0 as an approximation of $A(0)$.

Theorem 4.5.1 *If $J_S \in H^1(0, T; L_r^2(\Omega))$, then problem (4.42) has a unique solution and there exists a positive constant C such that*

$$\max_{1 \leq k \leq N} \|A_h^k\|_{\tilde{H}_r^1(\Omega)} \leq C \left\{ \|A_h^0\|_{\tilde{H}_r^1(\Omega)} + \|J_S\|_{H^1(0, T; L_r^2(\Omega))} \right\}.$$

Proof. The well-posedness is an immediate consequence of the following inequality

$$\frac{1}{\Delta t} \int_{\Omega_{t^k}} \sigma(t^k) Z_h^2 r dr dz + a(Z_h, Z_h) \geq C \|Z_h\|_{\tilde{H}_r^1(\Omega)}^2,$$

which in its turn results from the ellipticity of a .

In order to prove the stability estimate we test (4.42) with $Z = A_h^k - A_h^{k-1}$

$$\frac{1}{\Delta t} \int_{\Omega_{t^k}} \sigma(t^k) (A_h^k - A_h^{k-1})^2 r dr dz + a(A_h^k, A_h^k - A_h^{k-1}) = \int_{\Omega_S} J_S(t^k) (A_h^k - A_h^{k-1}) r dr dz.$$

By using that $2(p-q)p = p^2 + (p-q)^2 - q^2$, we write

$$a(A_h^k, A_h^k) + a(A_h^k - A_h^{k-1}, A_h^k - A_h^{k-1}) - a(A_h^{k-1}, A_h^{k-1}) \leq 2 \int_{\Omega_S} J_S(t^k) (A_h^k - A_h^{k-1}) r dr dz.$$

Then

$$a(A_h^k, A_h^k) - a(A_h^{k-1}, A_h^{k-1}) \leq 2 \int_{\Omega_S} J_S(t^k) (A_h^k - A_h^{k-1}) r dr dz, \quad k = 1, \dots, N.$$

Given $n \in \{1, \dots, N\}$, summing the above equation from $k = 1$ to n , we have

$$\begin{aligned} a(A_h^n, A_h^n) &\leq a(A_h^0, A_h^0) + 2 \sum_{k=1}^n \int_{\Omega_S} J_S(t^k)(A_h^k - A^{k-1})r \, dr \, dz \\ &= a(A_h^0, A_h^0) + 4 \left[\int_{\Omega_S} J_S(t^n) A_h^n r \, dr \, dz - \int_{\Omega_S} J_S(t^0) A_h^0 r \, dr \, dz \right. \\ &\quad \left. - \Delta t \sum_{k=1}^n \int_{\Omega_S} \left(\frac{J_S(t^k) - J_S(t^{k-1})}{\Delta t} \right) A_h^{k-1} r \, dr \, dz \right], \end{aligned}$$

where we have used summation by parts. Next, we use the ellipticity of a and a weighted Cauchy-Schwartz inequality to write

$$\begin{aligned} \alpha \|A_h^n\|_{\tilde{H}_r^1(\Omega)}^2 &\leq a(A_h^0, A_h^0) + C \|J_S(t^0)\|_{L_r^2(\Omega)}^2 + C \|A_h^0\|_{L_r^2(\Omega)}^2 + C \|J_S(t^n)\|_{L_r^2(\Omega)}^2 + \frac{\alpha}{2} \|A_h^n\|_{L_r^2(\Omega)}^2 \\ &\quad + \Delta t \sum_{k=1}^n \int_{\Omega_S} \left(\frac{J_S(t^k) - J_S(t^{k-1})}{\Delta t} \right)^2 r \, dr \, dz + \Delta t \sum_{k=0}^{n-1} \|A_h^k\|_{\tilde{H}_r^1(\Omega)}^2. \end{aligned}$$

Using Barrow's rule

$$J_S(t^k) - J_S(t^{k-1}) = \int_{t^{k-1}}^{t^k} J'_S(t) \, dt$$

and a Cauchy-Schwartz inequality, straightforward computations lead to

$$\|A_h^n\|_{\tilde{H}_r^1(\Omega)}^2 \leq C \left\{ \|A_h^0\|_{\tilde{H}_r^1(\Omega)}^2 + \|J_S\|_{H^1(0,T;L_r^2(\Omega))}^2 \right\} + \Delta t \sum_{k=0}^{n-1} \|A_h^k\|_{\tilde{H}_r^1(\Omega)}^2.$$

Finally, by using the Gronwall's lemma we obtain

$$\|A_h^n\|_{\tilde{H}_r^1(\Omega)}^2 \leq C \left\{ \|A_h^0\|_{\tilde{H}_r^1(\Omega)}^2 + C \|J_S\|_{H^1(0,T;L_r^2(\Omega))}^2 \right\}.$$

Since this holds for all $n \in \{1, \dots, N\}$, we conclude the proof. \square

Remark 4.5.1 Since the domain where the derivative of A is approximated changes with time, terms like $\int_{\Omega_{t_k}} \sigma(t^k) A_h^{k-1}$ appear in the numerical scheme. This is the reason why we cannot follow a more standard approach as that used for the semidiscrete problem. Anyway we succeeded in proving the stability of the fully discrete scheme by assuming further regularity for J_S .

Our next goal is to prove error estimates for the solution of the discrete problem (4.42). To do this we introduce some notation. Given $(\phi^0, \dots, \phi^N) \in \mathbb{R}^{N+1}$, we define the backward difference quotient

$$\bar{\partial} \phi^k := \frac{\phi^k - \phi^{k-1}}{\Delta t}, \quad k = 1, \dots, N.$$

For A being the solution of (4.10) and A_h^k that of (4.42), we write

$$A(t^k) - A_h^k = \delta_h^k + \rho_h^k,$$

with

$$\delta_h^k := \mathbf{P}_h A(t^k) - A_h^k, \quad k = 1, \dots, N,$$

and

$$\rho_h^k := A(t^k) - \mathbf{P}_h A(t^k), \quad k = 0, \dots, N.$$

To define δ_h^0 we use the approximation A_h^0 of $A(0)$:

$$\delta_h^0 := \mathbf{P}_h A(0) - A_h^0.$$

Finally, we define the truncation errors

$$\tau^k := \bar{\partial} A(t^k) - \partial_t A(t^k), \quad k = 1, \dots, N.$$

The first step is to estimate δ_h^k in terms of ρ_h^k and τ^k .

Lemma 4.5.1 *Let $A \in \mathcal{C}^0(0, T; \mathcal{V}) \cap \mathcal{C}^1(0, T; L_r^2(\Omega))$ be the solution of problem (4.10), and let $\tau^k := \bar{\partial} A(t^k) - \partial_t A(t^k)$. Then*

$$\begin{aligned} \Delta t \sum_{k=1}^N \int_{\Omega_{t^k}} \sigma(t^k) (\bar{\partial} \delta_h^k)^2 r dr dz + \max_{1 \leq k \leq N} \|\delta_h^k\|_{\tilde{H}_r^1(\Omega)}^2 \\ \leq C \|\delta_h^0\|_{\tilde{H}_r^1(\Omega)}^2 + C \Delta t \sum_{k=1}^N \left\{ \|\bar{\partial} \rho_h^k\|_{L_r^2(\Omega_{t^k})}^2 + \|\tau^k\|_{L_r^2(\Omega_{t^k})}^2 \right\} \end{aligned}$$

Proof. We test problems (4.10) and (4.42) with $Z_h \in \mathcal{V}_h \subset \mathcal{V}$ and subtract to obtain

$$\int_{\Omega_{t^k}} \sigma(t^k) \left\{ \partial_t A(t^k) - \frac{A_h^k - A_h^{k-1}}{\Delta t} \right\} Z_h r dr dz + a(A(t^k) - A_h^k, Z_h) = 0.$$

Straightforward calculations yield

$$\partial_t A(t^k) - \frac{A_h^k - A_h^{k-1}}{\Delta t} = -\tau^k + \bar{\partial} \rho_h^k + \bar{\partial} \delta_h^k$$

and hence

$$\int_{\Omega_{t^k}} \sigma(t^k) \bar{\partial} \delta_h^k Z_h r dr dz + a(\delta_h^k, Z_h) = - \int_{\Omega_{t^k}} \sigma(t^k) \bar{\partial} \rho_h^k Z_h r dr dz + \int_{\Omega_{t^k}} \sigma(t^k) \tau^k Z_h r dr dz.$$

We set $Z_h = \Delta t \bar{\partial} \delta_h^k$ above, to write

$$\begin{aligned} \Delta t \int_{\Omega_{t^k}} \sigma(t^k) (\bar{\partial} \delta_h^k)^2 r dr dz + \Delta t a(\delta_h^k, \bar{\partial} \delta_h^k) &= -\Delta t \int_{\Omega_{t^k}} \sigma(t^k) \bar{\partial} \rho_h^k \bar{\partial} \delta_h^k r dr dz \\ &\quad + \Delta t \int_{\Omega_{t^k}} \sigma(t^k) \tau^k \bar{\partial} \delta_h^k r dr dz. \end{aligned} \quad (4.43)$$

On the other hand, it is easy to show that

$$2\Delta t a(\delta_h^k, \bar{\partial} \delta_h^k) \geq a(\delta_h^k, \delta_h^k) - a(\delta_h^{k-1}, \delta_h^{k-1}).$$

Using this inequality in (4.43) and estimating the right hand side by a Cauchy-Schwartz inequality, we obtain

$$\begin{aligned} \Delta t \int_{\Omega_{t^k}} \sigma(t^k) (\bar{\partial} \delta_h^k)^2 r dr dz + \frac{1}{2} a(\delta_h^k, \delta_h^k) - \frac{1}{2} a(\delta_h^{k-1}, \delta_h^{k-1}) \\ \leq C \Delta t \left\{ \|\bar{\partial} \rho_h^k\|_{L_r^2(\Omega_{t^k})}^2 + \|\tau^k\|_{L_r^2(\Omega_{t^k})}^2 \right\} + \frac{\Delta t}{2} \int_{\Omega_{t^k}} \sigma(t^k) (\bar{\partial} \delta_h^k)^2 r dr dz. \end{aligned}$$

Given $n \in \{1, \dots, N\}$, summing from $k = 1$ to n , we have

$$\begin{aligned} \Delta t \sum_{k=1}^n \int_{\Omega_{t^k}} \sigma(t^k) (\bar{\partial} \delta_h^k)^2 r dr dz + a(\delta_h^n, \delta_h^n) &\leq C a(\delta_h^0, \delta_h^0) \\ &\quad + C \Delta t \sum_{k=1}^n \left\{ \|\bar{\partial} \rho_h^k\|_{L_r^2(\Omega_{t^k})}^2 + \|\tau^k\|_{L_r^2(\Omega_{t^k})}^2 \right\}. \end{aligned}$$

Hence the result follows from the continuity and the ellipticity of a . \square

Next, we give appropriate estimates for $\bar{\partial} \rho_h^k$ and τ^k .

Lemma 4.5.2 *Let A be the solution of problem (4.10). There exists C independent of h and Δt such that, if $A \in H^1(0, T; H_r^2(\Omega))$, then*

$$\left(\Delta t \sum_{k=1}^N \|\bar{\partial} \rho_h^k\|_{L_r^2(\Omega_{t^k})}^2 \right)^{1/2} \leq C h^2 \|A\|_{H^1(0, T; H_r^2(\Omega))}$$

and, if $A \in H^2(0, T; L_r^2(\Omega))$, then

$$\left(\Delta t \sum_{k=1}^N \|\tau^k\|_{L_r^2(\Omega_{t^k})}^2 \right)^{1/2} \leq C \Delta t \|A\|_{H^2(0, T; L_r^2(\Omega))}.$$

Proof. Barrow's rule,

$$\bar{\partial} \rho_h^k = \frac{1}{\Delta t} \int_{t^{k-1}}^{t^k} \partial_t \rho_h(t) dt,$$

leads to

$$\begin{aligned} \Delta t \sum_{k=1}^N \|\bar{\partial} \rho_h^k\|_{L_r^2(\Omega_{t^k})}^2 &\leq \frac{1}{\Delta t} \sum_{k=1}^N \int_{\Omega_{t^k}} \left[\int_{t^{k-1}}^{t^k} dt \right] \left[\int_{t^{k-1}}^{t^k} |\partial_t \rho_h(t)|^2 dt \right] r dr dz \\ &\leq \int_0^T \|\partial_t \rho_h(t)\|_{L_r^2(\Omega_{t^k})}^2 dt \\ &\leq Ch^4 \|A\|_{H^1(0,T;H_r^2(\Omega))}^2, \end{aligned}$$

where for that last inequality we have used (4.32) and Cauchy-Schwartz inequality.

On the other hand, we recall that

$$\partial_t A(t^k) = \frac{A(t^k) - A(t^{k-1})}{\Delta t} + \frac{1}{\Delta t} \int_{t^{k-1}}^{t^k} (t - t^{k-1}) \partial_{tt} A dt.$$

Then, from the definition of τ^k

$$\tau^k = -\frac{1}{\Delta t} \int_{t^{k-1}}^{t^k} (t - t^{k-1}) \partial_{tt} A dt.$$

Therefore, using Cauchy-Schwartz inequality we have that

$$\begin{aligned} \Delta t \sum_{k=1}^N \|\tau^k\|_{L_r^2(\Omega_{t^k})}^2 &= \Delta t \sum_{k=1}^N \int_{\Omega_{t^k}} \left[\frac{1}{\Delta t} \int_{t^{k-1}}^{t^k} (t - t^{k-1}) \partial_{tt} A dt \right]^2 r dr dz \\ &\leq \frac{1}{\Delta t} \sum_{k=1}^N \int_{\Omega_{t^k}} \left[\int_{t^{k-1}}^{t^k} (t - t^{k-1})^2 dt \right] \left[\int_{t^{k-1}}^{t^k} |\partial_{tt} A|^2 dt \right] r dr dz \\ &\leq \Delta t^2 \|A\|_{H^2(0,T;L_r^2(\Omega))}^2. \end{aligned}$$

□

We end this section proving error estimates for the computed vector potential A_h^k as well as for the physical quantities of interest that can be derived from it: approximations \mathbf{B}_h^k and \mathbf{J}_h^k of the magnetic induction \mathbf{B} and the current density \mathbf{J} , which are defined as follows:

$$\mathbf{B}_h^k := \mathbf{curl}(A_h^k \mathbf{e}_\theta),$$

$$\mathbf{J}_h^k := -\sigma(t^k) \bar{\partial} A_h^k \mathbf{e}_\theta \quad \text{in } \Omega_{t^k}.$$

The error estimates for this quantities will be a consequence of Lemmas 4.5.1 and 4.5.2. The former depends on the particular approximation A_h^0 of $A(0)$ used in problem

(4.42). In fact, recall that A_h^0 appears in the definition of δ_h^0 . If the solution to problem (4.10) is sufficiently smooth at time $t = 0$, namely $A(0) \in H_r^2(\Omega) \cap \mathcal{V}$, then we can take as A_h^0 the Lagrange interpolant of $A(0)$:

$$A_h^0 := \mathcal{I}_h A(0),$$

where we denote by \mathcal{I}_h the Lagrange interpolant operator. In such a case we have the following result.

Theorem 4.5.2 *Let A and A_h^k be the solutions of problems (4.10) and (4.42), respectively. Let $\mathbf{B} = \operatorname{curl}(A\mathbf{e}_\theta)$, $\mathbf{J} = -\sigma(\partial_t A)|_{\Omega_t} \mathbf{e}_\theta$ and \mathbf{B}_h^k and \mathbf{J}_h^k be as defined above. If $A \in H^1(0, T; H_r^2(\Omega) \cap \mathcal{V}) \cap H^2(0, T; L_r^2(\Omega))$ and $A_h^0 := \mathcal{I}_h A(0)$, then there exists C independent of h , and Δt such that*

$$\begin{aligned} \max_{1 \leq k \leq N} \|\mathbf{B}(t^k) - \mathbf{B}_h^k\|_{L_r^2(\Omega)} &\leq C \{ h \|A\|_{H^1(0, T; H_r^2(\Omega))} + \Delta t \|A\|_{H^2(0, T; L_r^2(\Omega))} \}, \\ \left\{ \Delta t \sum_{k=1}^N \|\mathbf{J}(t^k) - \mathbf{J}_h^k\|_{L_r^2(\Omega_{t^k})}^2 \right\}^{1/2} &\leq C \{ h \|A\|_{H^1(0, T; H_r^2(\Omega))} + \Delta t \|A\|_{H^2(0, T; L_r^2(\Omega))} \}. \end{aligned}$$

Proof.

By writing $A(t^k) - A_h^k = \delta_h^k + \rho_h^k$, $k = 1, \dots, N$, from Lemma 4.5.1 and Lemma 4.5.2, we obtain

$$\max_{1 \leq k \leq N} \|\mathbf{B}(t^k) - \mathbf{B}_h^k\|_{L_r^2(\Omega_0)} \leq \|\delta_h^0\|_{\tilde{H}_r^1(\Omega)} + C (h \|A\|_{H^1(0, T; H_r^2(\Omega))} + \Delta t \|A\|_{H^1(0, T; H_r^2(\Omega))})$$

On the other hand, the first term in the right hand side above is bounded as follows:

$$\|\delta_h^0\|_{\tilde{H}_r^1(\Omega)} \leq \|\mathbf{P}_h A(0) - A(0)\|_{\tilde{H}_r^1(\Omega)} + \|A(0) - \mathcal{I}_h A(0)\|_{\tilde{H}_r^1(\Omega)} \leq Ch \|A(0)\|_{H^1(0, T; H_r^2(\Omega))}$$

where we have used (4.31) and error estimate for the Lagrange interpolant (see [36, Prop. 6.1]). Thus the first estimate of this theorem follows from the two inequalities above. The proof of the second estimate is essentially identical. \square

4.6 Numerical tests

We have implemented the numerical scheme (4.42) in a FORTRAN code. Let us recall that the method does not need a mesh fitted to the workpiece, which allows us to avoid

remeshing at each time step. Therefore, we have used a fixed mesh for the whole process, more refined in a subdomain containing Ω_t for all $t \in [0, T]$ (see, for instance, Figure 4.14 below). In what follows we report the results of two tests, one with a known analytical solution and the other corresponding to an EMF process.

4.6.1 Test 1: An example with analytical solution

First, the code has been validated by solving a problem with known analytical solution. We have used this test to confirm the theoretical order of convergence, too. In this case, $\Omega := [1, 2] \times [0, 3]$ and the workpiece moves as a rigid body, with velocity $\mathbf{v} = \mathbf{e}_z$. and initial position $\Omega_0 := [1, 2] \times [1, 2]$ (see Figure 4.4).

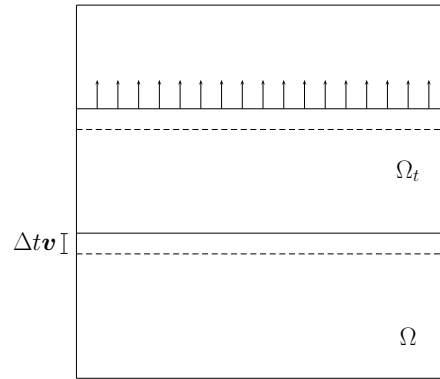


Figure 4.4: Test 1. Sketch of the domain.

We solved the following problem

$$\sigma \frac{\partial A}{\partial t} \mathbf{e}_\theta + \operatorname{curl} \left(\frac{1}{\mu} \operatorname{curl} (A \mathbf{e}_\theta) \right) = f \mathbf{e}_\theta$$

with $\mu = 1$ and

$$\sigma = \begin{cases} 1 & \text{in } \Omega_t, \\ 0 & \text{in } \Omega \setminus \Omega_t. \end{cases}$$

The term f has been chosen so that the solution be

$$A(t, r, z) = \sin(2\pi t)(r^2 + z^2).$$

We have used uniform meshes obtained by successively refining the coarse one shown in Figure 4.5

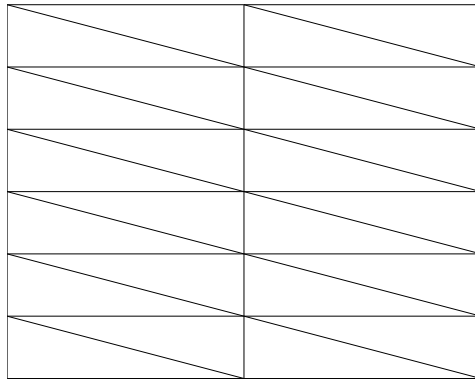
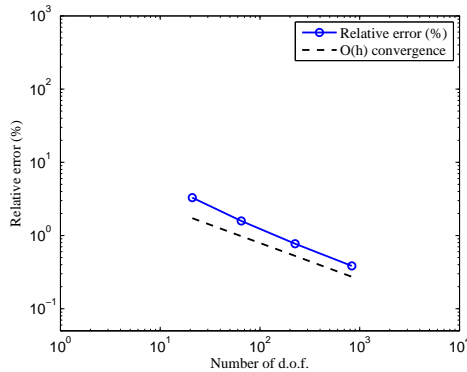


Figure 4.5: Test 1. Coarse initial mesh.

Notice that all the meshes are fitted to the initial position Ω_0 of the workpiece. However this does not happen at all the other time steps t^k . Therefore, since $\sigma(t^k)$ vanishes out of Ω_{t^k} , the computation of the terms $\int_{\Omega_{t^k}} \sigma(t^k) (A_h^k - A_h^{k-1})$ in (4.42) involve integrals on triangles of piecewise smooth (but not smooth) functions. These integrals were computed by using low order quadrature rules with a large number of integration points, which was determined in advance so that the results be essentially indifferent of this number.

Figure 4.6 shows a log-log plot of the error for the computed vector potential A_h^k . It can be seen that the method converges with order $O(h)$ as predicted.

Figure 4.6: Test 1. Relative errors for $\max_{1 \leq k \leq N} \|A(t^k) - A_h^k\|_{\tilde{H}_r^1(\Omega)}$ versus number of degrees of freedom (d.o.f.) (log-log scale).

4.6.2 Test 2: Numerical solution of an EMF process

We have used the numerical method to compute the current density and the Lorentz force in an example taken from an electromagnetic forming process. We consider the geometry and physical data of the axisymmetric electromagnetic forming test described in [32] (see Figure 4.7) which is a classical benchmark (see [32, 46] for more details). The geometrical and physical data are given in Table 4.1.

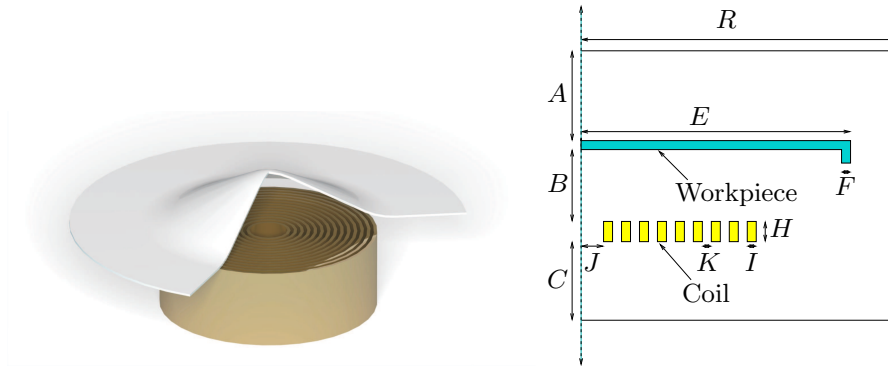


Figure 4.7: Test 2. Geometry of the EMF benchmark.

Table 4.1: Test 2. Geometrical data and physical parameters:

Thickness of the workpiece (F):	0.0012 m
Height of the tool coil (H):	0.0115 m
Width of each turn coil (I):	0.0025 m
Distance between coil turns (K):	0.0003 m
Distance coil-workpiece (B):	0.002 m
Vertical distance from coil to bottom (C):	0.05 m
Vertical distance from workpiece to the top (A):	0.05 m
Width of the workpiece (E):	0.115 m
Width of the rectangular box (R):	0.2 m
Number of coil turns:	9
Electrical conductivity of metal (σ):	$25900 \text{ (Ohm m)}^{-1}$
Magnetic permeability of all materials (μ):	$4\pi 10^{-7} \text{ Hm}^{-1}$
Final time (T):	$90\mu\text{s}$

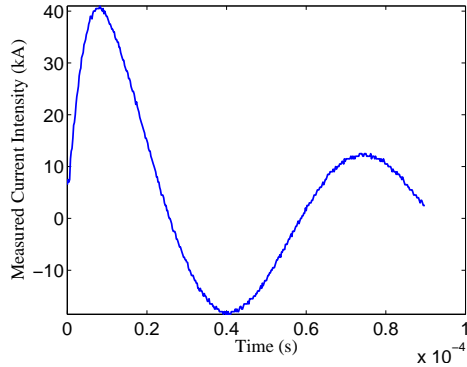


Figure 4.8: Test 2. Current intensity (kA) vs. time (s).

The current density J_S was assumed to be constant in each turn of the coil. It was obtained from [32] where the corresponding intensity was reported. Figure 4.8 shows this intensity during the whole process. To determine Ω_t , we assumed that the workpiece is a rigid body moving under the action of a Lorentz force $\mathbf{f} = \mathbf{J} \times \mathbf{B}$. To compute \mathbf{f} , we made a preliminary estimate of \mathbf{J} and \mathbf{B} by solving the electromagnetic model with the workpiece at a fixed domain Ω_0 , as described in Section 6.3 of [14].

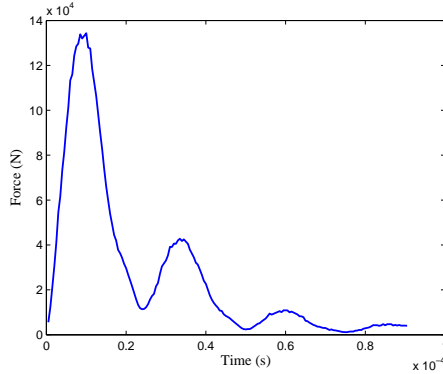


Figure 4.9: Test 2. Lorentz force in N vs. time (s).

We have used the mesh shown in Figure 4.14 which is more refined in the zone occupied by Ω_t for $t \in [0, T]$. We have used a low order integration rule as in the previous test to compute the integrals of piecewise smooth functions. Figure 4.10 shows the resulting velocity of the rigid workpiece. Figures 4.11-4.13 show the computed current densities at 10ms, 35ms, and 90ms, respectively.

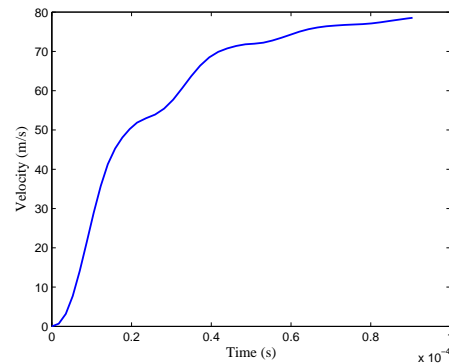
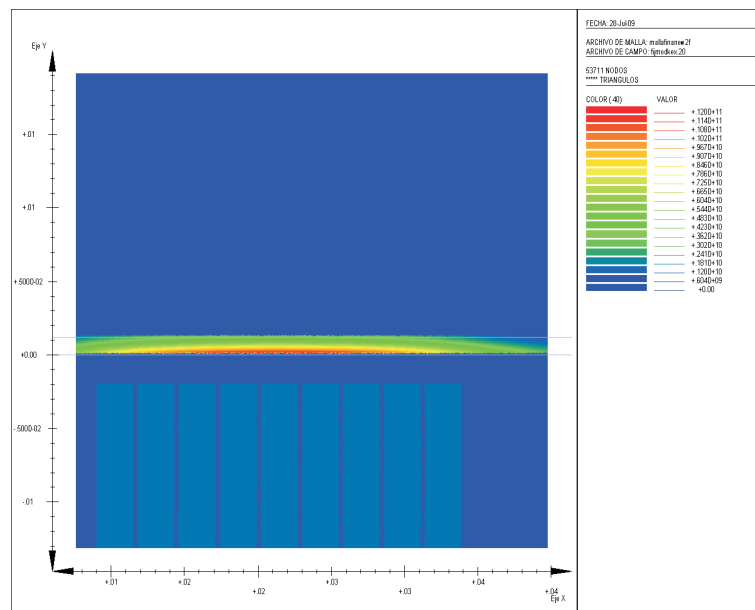


Figure 4.10: Test 2. Velocity (m/s) vs. time (s).

Figure 4.11: Test 2. Current Density in A/m^2 at $10\mu\text{s}$.

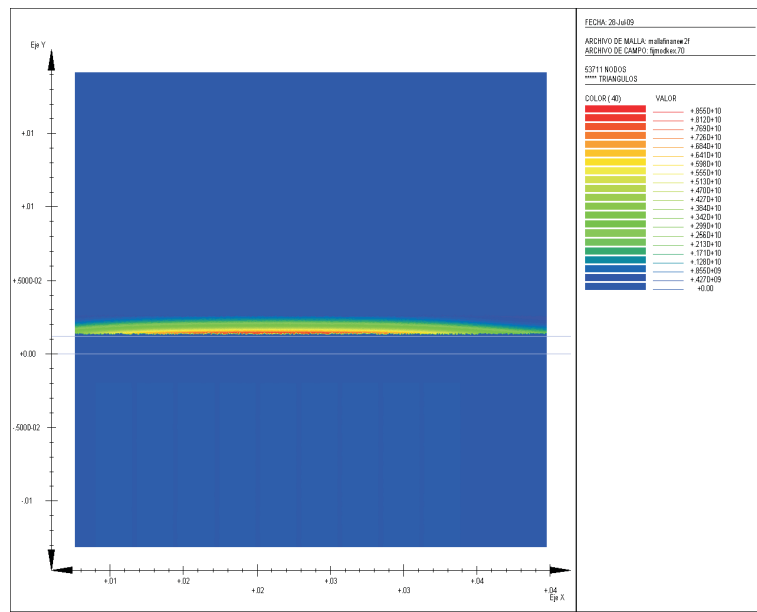


Figure 4.12: Test 2. Current Density in A/m^2
at $35\mu\text{s}$.

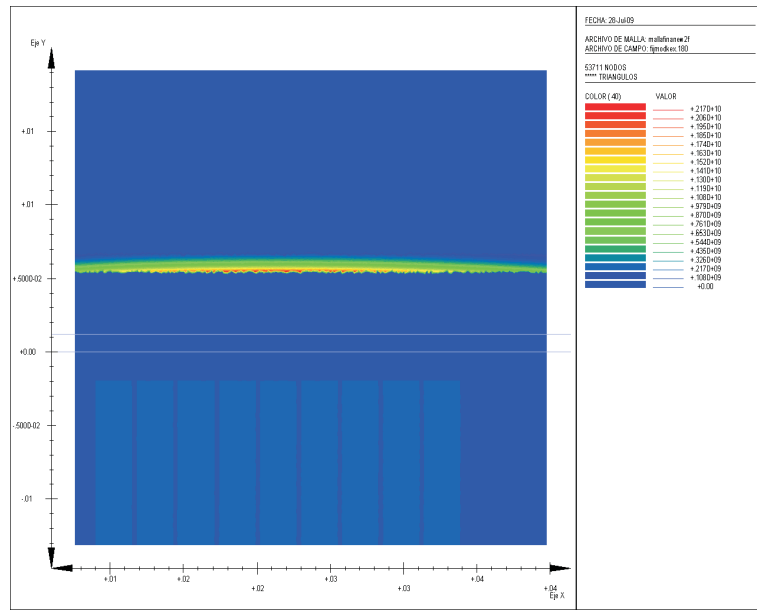


Figure 4.13: Test 2. Current Density in A/m^2
at $90\mu\text{s}$.

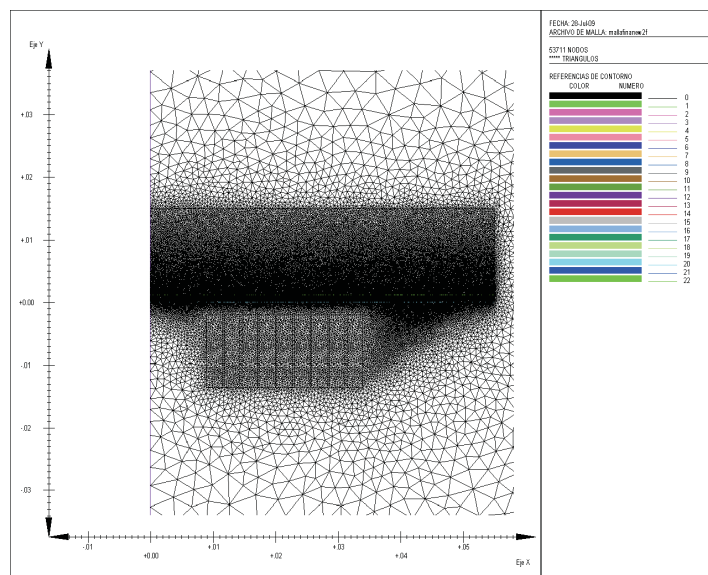


Figure 4.14: Test 2. Meshes zoom.

Chapter 5

Conclusiones y trabajo futuro

A continuación se presenta un resumen de las principales aportaciones de esta tesis y una descripción del trabajo futuro a desarrollar.

5.1 Conclusiones

1. Se analizaron métodos numéricos para resolver problemas de corrientes inducidas en dominios axisimétricos en regímenes armónico y no armónico. Todos los modelos axisimétricos estudiados se han planteado en términos de un potencial vectorial magnético, que en este caso tiene únicamente componente azimutal.
2. Se analizó un método numérico para resolver un problema de corrientes inducidas en régimen armónico derivado del modelado de un horno de inducción con intensidades de corriente como dato. Dicho análisis abarcó el estudio de la existencia, unicidad y regularidad adicional de la solución de la formulación variacional así como la convergencia del método de elementos finitos propuesto.
3. Se estudiaron problemas de corrientes inducidas en régimen no armónico en un dominio axisimétrico cuya parte correspondiente al conductor está en movimiento y con las densidades de corriente como dato. Primero, se abordó el modelo electromagnético incluyendo un término de velocidad en la ley de Ohm pero con dominio fijo a lo largo del tiempo. A continuación se abordó el análisis del modelo electromagnético considerando movimiento en parte del dominio conductor. Ambos modelos han sido analizados desde un punto de vista matemático y numérico obteniéndose

resultados de convergencia para los esquemas de discretización temporal y espacial propuestos.

4. En todos los problemas estudiados, se han obtenidos estimaciones de error para las variables físicas de interés, como la inducción magnética o la densidad de corriente.
5. Para todos los esquemas numéricos estudiados se desarrollaron códigos Fortran. Estos códigos fueron validados con ejemplos analíticos que prueban la convergencia de los métodos y usados exitosamente para calcular soluciones numéricas de los problemas metalúrgicos reales que motivaron la introducción de los métodos.

5.2 Trabajo futuro

1. Iniciaremos el estudio del proceso del conformado electromagnético completo. Para ello se debe acoplar el submodelo electromagnético ya estudiado con un submodelo mecánico para la deformación de la pieza metálica. Recordemos, que ambos modelos están acoplados, al menos, por las siguientes razones
 - La fuerza de Lorentz, calculada en el modelo electromagnético es la fuerza volumétrica que deforma la pieza por lo que debe usarse en el modelo mecánico como fuente.
 - El dominio del modelo electromagnético cambia con el tiempo, debido a la deformación mecánica de las piezas.

Estos dos fenómenos generan no linealidades del problema acoplado que enriquecen significativamente el análisis del mismo. Desde el punto de vista computacional, se acoplará el código desarrollado para el submodelo electromagnético con códigos existentes para la deformación mecánica de la pieza.

2. Para el proceso del conformado electromagnético se estudiará la posibilidad de introducir las fuentes de corrientes mediante intensidades y no densidades de corriente. Cabe mencionar que en la práctica las intensidades son datos fáciles de medir, mientras que las densidades provienen de hipótesis adicionales. El usar intensidades como datos conduce a formulaciones variacionales mixtas como las del Capítulo 2 de la tesis.

3. En el análisis del problema que incluye términos de velocidad, alguna de las cantidades físicas (como por ejemplo el potencial magnético) convergen en los experimentos numéricos con un orden mejor que el demostrado. Se intentará demostrar estimaciones del error óptimas para esas cantidades.

Bibliography

- [1] R. ACEVEDO, S. MEDDAHI, AND R. RODRÍGUEZ, *An E -based mixed formulation for a time-dependent eddy current problem*, Math. Comp., 78 (2009), pp. 1929–1949.
- [2] A. ALONSO RODRÍGUEZ AND A. VALLI, *Voltage and current excitation for time-harmonic eddy current problems*, SIAM J. Appl. Math., 68 (2008), pp. .1477–1494.
- [3] H. AMMARI, A. BUFFA AND J.-C. NÉDÉLEC, *A justification of eddy currents model for the Maxwell equations*, SIAM J. Appl. Math., 60 (2000), pp. 1805–1823.
- [4] C. AMROUCHE, C. BERNARDI, M. DAUGE, M., AND V. GIRAUT. *Vector potentials in three-dimensional non-smooth domains*, Math. Methods Appl. Sci., 21 (1998), pp. 823–864.
- [5] F. ASSOUS,P. CIARLET JR., AND S. LABRUNIE. *Theoretical tools to solve the axisymmetric Maxwell equations*, Math. Methods Appl. Sci., 25 (2002), pp. 49–78.
- [6] F. ASSOUS, P. CIARLET JR, S. LABRUNIE, AND J. SEGRÉ. *Numerical solution to the time-dependent Maxwell equations in axisymmetric singular domains: the singular complement method*, J. Comput. Phys., 191 (2003), pp. 147–176.
- [7] F. AZZOZ, B. BENDJIMA, M. FÉLIACHI, AND M. LATRÉCHE, *Application of Macro-element and finite element coupling for the behavior analysis of magnetoforming system*, IEEE Transaction on Magnetics, 35 (1999), pp. 1845–1848.
- [8] M.A. BAHMANI, K. NIAYESH., AND A. KARIMI. *3D Simulation of magnetic field distribution in electromagnetic forming systems with field-shaper*, Journal of Materials Processing Technology, 209 (2009), pp. 2295-2301.

- [9] Z. BELHACHMI, C. BERNARDI, AND S. DEPARIS. *Weighted Clément operator and application to the finite element discretization of the axisymmetric Stokes problem*, Numer. Math., 105 (2002), pp. 217–247.
- [10] A. BERMÚDEZ, D. GÓMEZ, M.C. MUÑIZ, AND P. SALGADO. *Transient numerical simulation of a thermoelectrical problem in cylindrical induction heating furnaces*, Adv. Comput. Math., 26 (2007), pp. 1–24.
- [11] A. BERMÚDEZ, D. GÓMEZ, M.C. MUÑIZ, AND P. SALGADO. *A FEM/BEM for axisymmetric electromagnetic and thermal modelling of induction furnaces*, Internat. J. Numer. Methods Engrg., 71 (2007), pp. 856–878.
- [12] A. BERMÚDEZ, D. GÓMEZ, M. C. MUÑIZ, P. SALGADO, AND R. VÁZQUEZ, *Numerical simulation of a thermo-electromagneto-hydrodynamic problem in an induction heating furnace*, Appl. Numer. Math., 59 (2009), pp. 2082–2104.
- [13] A. BERMÚDEZ, C. REALES, R. RODRÍGUEZ, AND P. SALGADO, *Numerical analysis of a finite element method to solve the axisymmetric eddy current model of an induction furnace*. IMA Journal of Numerical Analysis (doi:10.1093/imanum/drn063).
- [14] A. BERMÚDEZ, C. REALES, R. RODRÍGUEZ, AND P. SALGADO, *Mathematical and numerical analysis of a transient eddy current axisymmetric problem involving velocity terms*. Preprint del Departamento de Ingeniería Matemática de la Universidad de Concepción.
- [15] A. BERMÚDEZ, R. RODRÍGUEZ, AND P. SALGADO, *FEM for 3D eddy current problems in bounded domains subject to realistic boundary conditions. An application to metallurgical electrodes*, Arch. Comput. Methods Eng., 12 (2005), pp. 67–114.
- [16] C. BERNARDI, M. DAUGE, AND Y. MADAY, *Spectral Methods for Axisymmetric Problems*. Springer 1994.
- [17] A. BOSSAVIT, *Computational Electromagnetism*, Academic Press Inc., San Diego, CA, 1998.
- [18] K. E. BRENAN, S.L. CAMPBELL, AND L.R. PETZOLD *Numerical solution of initial-value problems in differential-algebraic equations*, Philadelphia: SIAM 1996.

- [19] S. L. CAMPBELL AND L. R. PETZOLD, *Canonical forms and solvable singular systems of differential equations*, SIAM J. Algebraic Discrete Methods , 4 (1983), pp. 517–521.
- [20] C. CHABOUEZ AND S. CLAIN. *Numerical modeling in induction heating for axisymmetric geometries*, IEEE Trans. Magn., 33 (1997), pp. 739–745.
- [21] CIARLET, P. *The Finite Element Method for Elliptic Problems*. New York: SIAM 2002.
- [22] S. CLAIN, J. RAPPAZ, M. SWIERKOSZ, AND R. TOUZANI., *Numerical modelling of induction heating for two- dimensional geometries*, Math. Models Appl. Sci. 3 (1993) pp. 805-822.
- [23] J.W. DEMMEL, S.C. EISENSTAT, J.R. GILBERT, X. LI, AND J. LIU, *A supernodal approach to sparse partial pivoting*,SIAM J. Matrix Anal. Appl., 20 (1999) pp. 720-755.
- [24] A. EL-AZAB, M. GARNICH, AND A. KAPOOR, *Modeling of the electromagnetic forming of sheet metals: state-of-art an future needs*, J. Mat. Process. Tech., 142 (2003), pp. 744–754.
- [25] A. ERN AND J. GUERMOND. *Theory and Practice of Finite Elements*. New York: Springer 2004.
- [26] G. FENTON AND G. DAEHN, *Modeling of electromagnetically formed sheet metal*,J. of Materials Proc. Tech. 75 (1998) pp. 6–16.
- [27] J. GERBAEAU, C. LE BRIS, AND T. LELIEVRE, *Methods for the Magnetohydrodynamics of Liquid Metals* , Oxford University Press 2006.
- [28] E.A. GONZÁLEZ-VELASCO. *Fourier Analysis and Boundary Value Problems*. San Diego, CA: Academic Press 1996.
- [29] J. GOPALAKRISHNAN AND J. PASCIAK. *The convergence of V-cycle multigrid algorithms for axisymmetric Laplace and Maxwell equations*, Math. Comp., 75 (2006), pp. 1697–1719.

- [30] H. HOCHSTADT. *The mean convergence of Fourier-Bessel series*, SIAM Rev., 9(1967), pp. 211–218.
- [31] J. JIN, *The Finite Element in Electromagnetics*, Wiley, New York, 1993.
- [32] M. KLEINER, A. BROSIUS, H. BLUM, F. SUTTMEIER, M. STIEMER, SVENDSEN, J. UNGER, AND S. REESE., *Benchmark simulation for coupled electromagnetic-mechanical metal forming processes*, University of Dortmund, Chair of Forming Technology.
- [33] A. KUFNER. *Weighted Sobolev Spaces*. New York: Wiley 1983.
- [34] P. LACOSTE. *Solution of Maxwell equation in axisymmetric geometry by Fourier series decomposition and by use of $H(\text{rot})$ conforming finite element*, Numer. Math., 84 (2000), pp. 577–609.
- [35] J. D. LAVERS, *State of the art of numerical modeling for induction processes*, COMPEL, 27 (2008) , pp. 335–349.
- [36] B. MERCIER AND G. RAUGEL. *Resolution d'un problème aux limites dans un ouvert axisymétrique par éléments finis en r , z et séries de Fourier en θ* , RAIRO, Anal. Numér., 16 (1982), pp. 405–461.
- [37] P. MONK, *Finite Element Methods for Maxwell's Equations*, Oxford Clarendon Press, 2003.
- [38] I. PÉREZ, I. ARANGUREN, B. GONZÁLEZ, AND I. EGUIA. *Electromagnetic Forming: A new coupling method*, Technical Report Labein-Tecnalia (Spain).
- [39] A. QUARTERONI AND A. VALLI, *Numerical Approximation of Partial Differential Equations*. Springer 1994.
- [40] J. RAPPAZ AND M. SWIERKOSZ. *Mathematical modelling and numerical simulation of induction heating processes*, Appl. Math. Comput. Sci. 6 (2), (1996), pp. 207-221.
- [41] A. B. J. REECE AND T. W. PRESTON , *Finite Element Methods in Electrical Power Engineering*, Oxford University Press, New York, 2000.

- [42] R. RIEBEN, B. WALLIN, AND D. WHITE, *Arbitrary Lagrangian Eulerian Electromechanics in 3D*, Progress In Electromagnetics Research Symposium 2006, pp. 265–269.
- [43] A.A. SHCHEGLOVA, *Study and solution of degenerate systems of ordinary differential equations by means of a change of variables*, Siberian Mathematical Journal, Springer New York, 36 (1995), pp. 1247–1256.
- [44] R. SHOWALTER, *Monotone Operators in Banach Space and Nonlinear Partial Differential Equations*, American Mathematical Society 1997.
- [45] P. P. SILVESTER AND R. L. FERRARI, *Finite Elements for Electrical Engineers*, Cambridge University Press, Cambridge, 1996.
- [46] M. STIEMER, O. J. UNGER, B. SVENDSEN AND H. BLUM, *Algorithmic formulation and numerical implementation of coupled electromagnetic-inelastic continuum models for electromagnetic metal forming*, Internat. J. Numer. Methods Engrg., 68 (2006), pp. 1697–1719.
- [47] B. SVENDSEN AND T. CHANDA *Continuum thermodynamic formulation of models for electromagnetic thermoelastic solids with application in electromagnetic metal forming*, Continuum Mech. Thermodyn., 17 (2005), pp. 1-16.
- [48] N. TAKATA, M. KATO, K SATO, AND T. TOBE. *High-speed forming of metal sheets by electromagnetic forces*, Japan Soc. Mech. Eng. Int. J., 31 (1988), pp. 142–150.
- [49] V. THOMÉE, *Galerkin Finite Element Methods for Parabolic Problems*. Springer-Verlag, Berlin, 2006.
- [50] J.D. THOMAS AND N. TRIANTAFYLLOIDIS, *On electromagnetic forming processes in finitely strained solids: Theory and examples*, Journal of the Mechanics and Physics of Solids 57 (2009), pp. 1391-1416.
- [51] J. UNGER, M. STIEMER, B. SVENDSEN, AND H. BLUM, *Multifield modeling of electromagnetic metal forming processes*, J. Mat. Process. Tech., 177 (2006), pp. 270–273.
- [52] J. UNGER, M. STIEMER, M. SCHWARZE, B. SVENDSEN, H. BLUM, AND S. REESE, *Strategies for 3D simulation of electromagnetic forming processes*, J. Mat. Process. Tech.

- [53] S. WANSER, L. KRÄHENBÄUHL, AND A. NICOLAS. *Computation of 3D induction hardening problems by combined finite and boundary elements methods*, IEEE Trans. Magn., 30 (1994), pp. 3320–3323.
- [54] R. VÁZQUEZ HERNÁNDEZ, *Contributions to the mathematical study of some problems in magnetohydrodynamics and induction heating*, PhD thesis, Universidade de Santiago de Compostela, 2008.
- [55] A. ŽENÍŽEK, *Nonlinear Elliptic and Evolution Problems and Their Finite Element Approximations*. Academic Press, London, 1990.
- [56] M. ZLÁMAL, *Finite element solution of quasistationary nonlinear magnetic field*, RAIRO, Anal. Numér., 16 (1982), pp. 161–191.
- [57] M. ZLÁMAL, *Addendum to the paper “Finite element solution of quasistationary nonlinear magnetic field”*, RAIRO Anal. Numér., 17 (1983) pp. 407–415.